The Pennsylvania State University

The Graduate School

College of Earth and Mineral Sciences

COAL COMBUSTION IN O_2/CO_2 MEDIUM FOR POWER GENERATION: NUMERICAL MODELING OF CHAR BURNOUT, NO_X AND CO EMISSIONS

A Dissertation in

Energy and Geo-Environmental Engineering

by

Prabhat Naredi

Submitted in Partial Fulfillment
of the Requirements
for the Degree of

Doctor of Philosophy

May 2009

The dissertation of Prabhat Naredi was reviewed and approved* by the following:

Sarma V. Pisupati
Associate Professor of Energy and Mineral Engineering
Dissertation Advisor
Chair of Committee

Alan W. Scaroni
Professor of Energy and Mineral Engineering
Associate Dean for Graduate Education and Research, College of Earth and Mineral Sciences

Ljubisa R. Radovic
Professor of Energy and Mineral Engineering

Semih Eser
Professor of Energy and Mineral Engineering

Daniel Haworth
Professor of Mechanical Engineering

Yaw D. Yeboah
Head of the Department of Energy and Mineral Engineering

*Signatures are on file in the Graduate School

ABSTRACT

Oxy-fuel combustion is a promising technique to achieve significant reduction of carbon dioxide (CO_2) emissions into the atmosphere from coal-fired power plants. In this approach, coal particles are burned in a medium of oxygen (O_2) and recycled flue gas (RFG) consisting primarily of CO_2 and/or H_2O so that the product is a near-pure stream of CO_2. The CO_2 rich flue gas obtained using this approach, as compared to flue gas from existing conventional power plants, can be more readily sequestered or utilized for oil recovery because of lesser amount of impurities. One of the significant barriers for implementing this approach is the need for an expensive oxygen generation unit. Currently, the RFG approach is being evaluated for its feasibility in existing and new coal-fired power plants.

In order to realize the full potential of oxy-fuel combustion, researchers are applying commercially available computational fluid dynamics (CFD) tools to predict the carbon burnout, CO and NO_x emissions, flame stability and heat transfer to boiler walls. However, in numerical studies, the effect of higher concentrations of CO_2 on heat transfer is typically accounted for, but its effect on coal pyrolysis behavior and char burnout is usually neglected. In experimental studies, conflicting results have been published and the discrepancies remain unresolved. The overall objective of this thesis is to modify the existing char-oxidation kinetics sub-model in a commercially available CFD tool FLUENT^{TM} by including user defined functions (UDFs) and more appropriate intrinsic activation energy values to capture the effect of elevated levels of CO_2 on char burnout and CO emissions. This study's experimental investigation attempts to identify coals that

are more suitable for oxy-coal combustion for further reducing un-burnt carbon and NO_x emissions compared to combustion in air.

In order to achieve these objectives, pyrolysis and combustion tests were conducted in a lab-scale drop tube reactor (DTR) at furnace wall temperatures of 1,173-1673 K using high-volatile (hvCb) and low-volatile (lvb) bituminous coal samples. The results show that pyrolyzing the coal particles in CO_2 changes the physical properties of resultant chars and the split of coal-N between the volatile and char fractions. However, these changes appear to be caused by the contribution from char-CO_2 reaction and not due to a change in gas phase chemistry.

The modified char-oxidation model uses a more appropriate intrinsic approach to account for the transition in rate controlling regime based on differences in char reactivity towards O_2 and CO_2. In the model, activation energy for the char-O_2 and char-CO_2 reactions is taken as an average of activation energies estimated from the onset of maximum to 80% conversion. Model calculations at lower heating rates and temperature condition in TGA using intrinsic rate parameters and physical properties of char accurately capture the transition from a kinetically controlled regime (Zone I) to an intra-particle diffusion controlled regime (Zone II). However, at higher heating rates and temperature condition in DTR, char burnouts are predicted to be ~5 times lower than the measured values. This under-prediction of the char burnout is attributed to the uncertainty in measured activation energy value (by about 13 kJ/mol) which was not reflected in TGA condition due to lower operating temperature.

During combustion tests, a higher CO, lower NO_x, and lower char burnout are observed for combustion in a 21% O_2/79% CO_2 mixture, as compared to combustion in air. The computational prediction showed that the majority of the differences in NO_x emissions between the two combustion media are the result of a decrease in gas temperature due to higher specific heat of CO_2 compared to N_2 and not due to coal-N retention in char in a CO_2-rich environment. As expected, burnout measurements in the DTR showed a rapid increase in char burnout with temperature for the lvb coal compared to that of the hvCb coal during combustion in a 21% O_2/79% CO_2 mixture in contrast to combustion in air. Reactivity and activation energy measurement of the two coal chars towards O_2 and CO_2 in the TGA showed that the observed increase in char burnout in DTR during combustion in a 21% O_2/79% CO_2 mixture arises from higher activation energy and reactivity of lvb coal char toward CO_2, as compared to hvCb coal.

Model prediction from a pilot-scale facility shows that a higher char burnout during oxy-coal combustion occurs because of higher O_2 partial pressure (30%) compared to combustion in air. A significant increase in char burnout due to contribution from char-CO_2 reaction is predicted only for lvb coal. A higher reduction in NO_x emissions is predicted for hvCb coal, as opposed to lvb coal because of differences in flame temperatures during oxy-coal combustion, as compared to combustion in air.

Overall, the results obtained in this study indicate that for oxy-coal combustion approach, a high-volatile coal is more suitable to achieve lower NO_x emissions and a low-volatile coal is beneficial to achieve lower un-burnt carbon.

TABLE OF CONTENTS

LIST OF FIGURES

LIST OF TABLES

ACKNOWLEDGEMENTS

I express my heartfelt gratitude to my supervisor Dr. Sarma Pisupati for his continuous support throughout the research program. I am indebted to my committee members Dr. Ljubisa Radovic, Dr. Alan Scaroni, Dr. Semih Eser and Dr. Dan Haworth for their valuable feedback. My special thanks to Dr. Radovic for his ideas and comments provided to me on my research work during his class (FSC 506) which has taught me a lot about technical writing and reading. I am sincerely thankful to Dr. Scaroni for guiding me throughout my research work by asking thought-provoking questions.

I acknowledge the support and cooperation from Ron Winceck, Ron Wasco and Dave Johnson from Energy Institute. I am sincerely thankful to the Energy Institute for allowing me to use the lab facilities and equipments, and Department of Energy and Mineral Engineering for supporting me during the PhD through teaching assistantship. I appreciate my officemates Prasanna, Nari, Pradeep, Denis for providing such an amazing atmosphere. I am thankful to my friends Ram and Chris from Department of Chemical Engineering for helping me in conducting a few experiments in their lab. I am also grateful to my roommates Manodeep and Krishna for maintaining such a homely environment that I never felt away from home. I would also like to acknowledge my other dear friends, Ramya, Vasudha, Samrudhdhi, Awnish, Nitin, Ravi and Raja for making my stay at State College memorable one. Finally, I would like to dedicate this thesis to my wife Sonal for her understanding, support and care through most of my years in graduate school.

Chapter 1

Introduction

Motivation

In the past decade, a near consensus has developed within the scientific community that the increasing rate of greenhouse gas emissions (CO_2, CH_4, N_2O) will result in climate change [1, 2]. Although some of the effects are not fully understood, a number of countries, under the Kyoto Protocol, agreed to limit their emissions of greenhouse gases. Among these gases, CO_2, emitted into the atmosphere from burning fossil fuels, contributes about 82% to "global warming" [3].

The main end-users of fossil fuels are transportation, residential, industrial and electric generation sectors. Recently, the Intergovernmental Panel on Climate Change (IPCC) prepared a full report evaluating the options, economics and challenges to mitigate CO_2 emissions [4]. Three options being explored to stabilize atmospheric levels of greenhouse gases are: (1) Reducing energy use through improving energy efficiency, (2) switching to different fuels for power generation by either using a lower carbon fuel or nuclear power or any available renewable energy sources, and (3) capturing CO_2 and employing carbon sequestration. Since power plants account for ~40% of CO_2 emissions [5], removal of the gas from this source can be more easily implemented and requires the least expenditure of energy. The major options to reduce CO_2 emissions from existing power plants are either to switch to less carbon-intensive fuels such as natural

gas and non-fossil energy sources or to capture the CO_2 from flue gases and either utilize it or dispose it for long-term storage. In the short term, switching from coal to natural gas can contribute to lower CO_2 emissions per unit of electricity produced. However, this option is not a permanent solution due to limited reserves of natural gas and other economic considerations. The options for CO_2 storage include injection into the deep ocean, and/or into depleted gas/oil fields. Alternatively, CO_2 can be used for methane recovery from un-minable coal seams or for enhanced oil recovery (EOR) from oil wells.

Unfortunately, capturing CO_2 from conventional power plants on a large scale, using post-combustion separation techniques such as absorption, pressure swing adsorption or membrane separation methods, are in development and seem very costly because of dilute concentration (15-18%) of CO_2 in the flue gases and presence of other process harming gases like SO_2 and NO_x [6]. A more advanced method is to adopt "oxy-fuel" combustion, which reduces the cost of flue gas separation by increasing CO_2 concentration in the flue gases [7]. As shown in Figure **1-1**, this method utilizes O_2/CO_2 mixture at the boiler inlet instead of air and involves recycling flue gases (RFG) to the boiler inlet to control flame temperature [8]. The CO_2 concentration in the flue gas can be enriched up to 95% (dry, volume basis), and then either sequestered or utilized for production of other chemicals.

At present no regulatory CO_2 emissions requirement exists for power generating utility companies in United States (US); however, the existence of global pressure anticipates some kind of regulation or credit system based on CO_2 reduction may arise in future. In that scenario, oxy-coal combustion based power plants (new or retrofitted) are expected to have a role in global reduction of CO_2 emissions into the atmosphere. Since

very few studies have been conducted for the oxy-coal combustion approach, as summarized in a review paper [9], a more thorough understanding of this technology is motivation behind the current research.

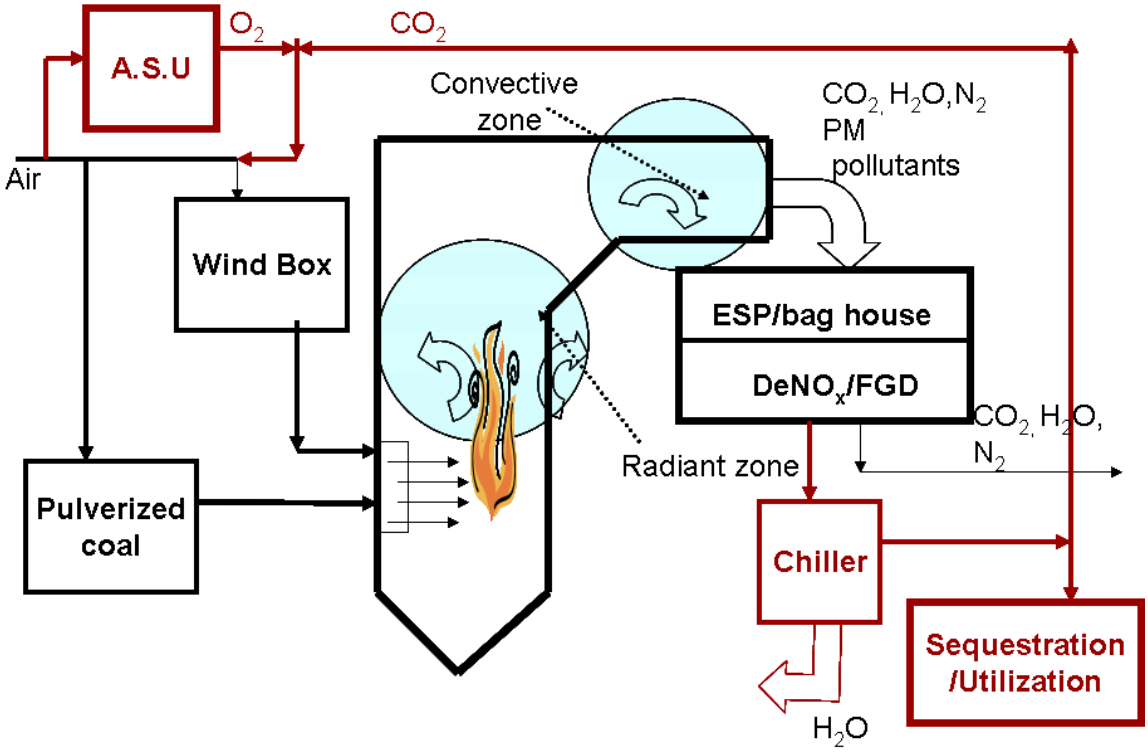

Figure **1-1**: Schematic representation of existing coal fired unit (shown in black) and additional modification needed for oxy-coal combustion (shown in red)

Literature Review

The first evaluation of the economical feasibility of oxy-coal combustion occurred in 1982 [7] and technical evaluation for retrofitting existing boilers was the focus of study in the Department of Energy (DOE)'s Argonne National Lab in 1985 [10]. In the mid- to late 1990s, a few pilot scale studies by Japanese [11, 12] and Canadian research groups [13]

demonstrated the potential of oxy-coal combustion for retrofitting or newer designs, based on the detailed characterization of boiler and other flue gas processing steps. In the early 2000s, various technical [14, 15] and economic studies [16, 17] have bridged the uncertainty gap in oxy-coal combustion, and have highlighted some of the technical issues which require more attention from research. So far, lab-scale and pilot-scale evaluation in the 20 kW_{th} – 1.5 MW_{th} range have been conducted and a demonstration plant with a capacity of of 50 MW_e [18] is in progress.

Economic Feasibility Studies

Various conceptual designs have been proposed in the literature for oxy-coal combustion and the efficiencies and economics of these design concepts with contemporary technologies for obtaining CO_2 rich stream from power plants have been estimated [7, 16, 17]. Several inter-connected process variables determine the applicability of this approach. These include:

- What is the extent to which flue gas must be cleaned of particulate matter, NO_x and SO_x components?
- Is this approach to be applied for a new or a existing plant?
- Is this approach to be for combustion of coal plant or for a gas fired plant?

The major additional cost associated with this approach is in obtaining oxygen from air (30% of total electricity cost) [17]. Separating oxygen *plus* argon from nitrogen can be accomplished easily by existing technologies: cryogenic or membrane separation,

but that result in only ~95 to 96% pure oxygen. If the purity requirement of CO_2 for the downstream application is very high, then only an expensive cryogenic approach is possible to obtain near pure oxygen from air [19]. A trial study conducted to evaluate the feasibility of combustion in O_2/RFG medium has found that, as the purity of O_2 becomes higher than 95%, the power requirement for oxygen generation increases significantly with a marginal reduction in the power requirement for compression of flue gas [20]. It has also been shown in that trial study that 97% oxygen purity is optimal if the CO_2 rich gas were to be sequestered or utilized for methane recovery from coal mines or oil recovery from near-by depleted oil fields. Non-cryogenic processes are most likely to be economical when producing a very high purity product (e.g. when oxygen of 90 to 95% purity is acceptable) is unnecessary. The existing individual non-cryogenic units rarely produce more than 200 tons per day oxygen [19] whereas oxygen demand of a 500-MW_{th} coal-fired is about 3,500 ton/day. Thus an economical integration of such non-cryogenic units with existing coal-fired boilers seems unlikely. Since the technology exists to design and construct large scale absorption columns [21], the oxy-fuel combustion system has often been compared with the absorption method to capture CO_2 [7, 16, 22, 23]. The comparisons vary significantly in projected costs, as expenditures vary between countries and whether or not CO_2 sequestration is a consideration at all.

Absorbers have capacities to treat up to 1,000 tons/day of flue gas; this capability is suitable to treat flue gas from only a 100-MW_{th} coal-fired unit [24]. The absorber column based on methyl-ethyl amine (MEA) can achieve 85% to 95% recovery of flue gas, with CO_2 purities over 99% by volume [25]. However, the MEA process requires a significant

amount of energy to operate pumps and blowers for gas and solvent circulation [26]. In this process, the greatest energy requirement arises from production of the steam used for solvent regeneration. An additional concern of the MEA process is avoiding the equipment corrosion and solvent degradation which requires SO_2 and NO_x concentrations to be below 10 ppm and 400 ppm, respectively [25, 24]. Thus, De-NO_x and De-SO_x units will be required to remove these pollutants prior to treatment in an absorber column. For the purpose of illustration, a brief summary of the differences in energy and cost requirements is provided in Table **1-1** (compiled from ref [16]).

Table **1-1**: Energy and cost comparison of oxy-coal combustion and MEA* scrubbing (compiled from ref [9])

Energy	**MEA**	**Oxy-coal combustion**
CO_2 separation and compression (MW_e)	40	53
Reboiler duty (MW_{th})	340	
Cooling requirement (MW_{th})	430	142
ASU power (MW_e)		86
Designed gross power (MW_e) (estimated)	600	600
Cost		
Amortized capital cost ($/yr)	27,775,116	29,855,736
Operating cost ($/yr)	28,246,531	13,599,325
Annual NG cost ($/yr)	50,258,989	32,978,153
Total annual cost ($/yr)	106,280,636	76,433,214
Capture cost ($/ton CO_2 avoided)	55	34

* MEA, methyl ethyl amine, appears to be most suitable solvent for CO_2 absorption

For retrofitting of plants, a few studies have indicated that combustion in an O_2/RFG medium is more economical as compared to MEA scrubbing of flue gases [16]. Studies have shown about 20% reduction in efficiency due to CO_2 capture and sequestration in coal [7] or gas fired [27] power plants using oxy-fuel combustion. This means

that, for a 35% efficient coal-fired plant, the overall efficiency is reduced to 27-28% in an O_2/RFG medium as compared to 25-26% for the MEA scrubbing method [16, 22]. This efficiency loss can receive partial compensation from saleable Ar, N_2 products and by virtue that plant is free of NO_x and SO_2. Overall, CO_2 capture and sequestration from existing coal-fired boiler represent an approximate increase of 50-60% in current electricity prices [17].

Most studies on oxy-fuel combustion concerned themselves with application to coal-fired power plants [8, 14, 15, 28, 29] because of larger amounts of CO_2 emissions from coal-fired units compared to other fossil fuels-fired units . Some studies have also considered application to *on-site* oil and gas fired power plants [30] when considering the possibility of using the produced CO_2 stream for enhanced recovery of oil/gas from the field. However, for *off-site* natural gas-fired plants, the oxy-fuel combustion approach may not be very beneficial considering natural gas-fired plants do not require a de-NO_x unit because of relatively low NO_x emissions (<50 ppmv) [31]. Stoichiometric calculation suggests that every one mole of methane requires 2 moles of oxygen, as compared to the requirement of ~1.25 mole oxygen for combustion of coal. Since obtaining oxygen is an expensive process, applying this approach to the natural gas-fired system may not be as economical as it is for coal-fired units. The current research, therefore, considers further technical evaluation of oxy-fuel technology with respect to **only** coal-fired plants.

Technical Feasibility Studies

In the oxy-coal combustion approach, coal particles are burned in a medium of O_2 and recycled flue gas (RFG) comprising CO_2 and/or H_2O. For retrofitting an existing boiler with oxy-coal combustion technology, coal combustion characteristics in a boiler differ because of differences in thermal and chemical properties of the two combustion media. Analysis shown in **Table 1-2** highlights the following differences between the two combustion systems:

- Due to the difference in specific heat of CO_2/H_2O gas as compared to that of nitrogen, about 30% O_2 in the feed gas (remaining CO_2/H_2O) is required to achieve similar flame temperatures [22]. This causes a ~30% reduction in gas volume in the boiler.
- To maintain the same flame temperature, about ~75-80% of the flue gas needs to be recycled [8]; therefore the volume of gases in the exhaust stream is reduced by about 75-80%
- The higher proportion of CO_2 and H_2O in the furnace and the reduced flow of gases in the convective section of the boiler is expected to alter the heat transfer profile [9]
- These differences coupled with CO_2 and H_2O being reactive gases, as compared to that of nitrogen, are expected to change pyrolysis/ignition/combustion behavior in coal-fired power plants [32, 33]

- Gaseous pollutant formation (NO_x and CO) is expected to differ because of the absence of nitrogen and elevated levels of CO_2 in the gas medium during oxy-coal combustion [34]
- Recycling the flue gas stream into the boiler is expected to increase the concentration of SO_x which may lead to corrosion inside the boiler [35].

Table **1-2**: Comparative analysis of combustion in Air and O_2/RFG medium*

	Air	O_2/CO_2
Moles	210 O_2 + 790 N_2	210 O_2 + 790/1.6 CO_2*
Total no. of moles	1000	703
Partial pressure of O_2	0.21	0.298
Mass	210*32 O_2 + 790*28 N_2	210*32 O_2 + 790/1.6*44 CO_2*
Total mass in kg	28,840	28,445

* Calculation is done to maintain same flame temperature assuming Cp CO_2 = 1.6 Cp N_2

As can be seen from the listed differences, some of apparent advantages of this approach are: an increase in thermal efficiency due to lower inert gas volume, a reduction in unburned carbon due to higher partial pressure of O_2 and CO_2, reduction of NO_x emissions due to an absence of nitrogen, and better operational advantage [14, 15, 30] due to flexibility from injecting the recycled gas stream into a boiler at a desired location. Despite these claimed advantages, this approach is not commercially used primarily due to the expensive oxygen production process, and to a certain extent, due to the uncertainties associated with the modifications that may be needed for retrofitting an existing power generation unit [36]. One of these concerns is whether or not CO emissions or a heat transfer aspect will change. At present, no full-scale plant operates with oxy-fuel

combustion; however, a few theoretical, lab-scale and pilot-scale studies, mainly by researchers at Canadian Centre for Mineral & Energy Technology (CANMET), Argonne National Lab (ANL), and companies such as Babcock & Wilcox, Air Liquide and Praxair, have identified the feasibility, design and operational issues. Recently, a comprehensive summary and current status review of the approach is reported in the literature [9].

Since theoretical heat transfer analysis (shown in Appendix 1.1) for the convective and radiative section conducted for the current research shows that boiler heat transfer imbalance will not be a major issue, the literature survey, here, is limited to only char reactivity, CO, and NO_x emissions. However, it can be expected that for the newer boiler design (based on oxy-coal combustion), flame temperature, and oxidizer composition (O_2/CO_2 ratio) will differ from that currently used for retrofitting purposes [37]. These changes will require detailed investigation of heat transfer. A brief summary of findings from previous studies with respect to char reactivity, CO and NO_x emissions is provided in the following section. Literature studies with respect to some of the other issues: SO_2, heat transfer and submicron particle formation appear in a journal article [9]. These issues are considered outside the scope of this research and are not discussed here.

Char Reactivity

Studies are carried out at both pilot-scale and lab-scale to understand char burnout behavior during combustion at higher O_2 and CO_2 concentrations. Initial feasibility

investigation study of oxy-coal combustion [10] measured char burnout and gas temperature in a bench scale facility (117 kW_{th}) using 21% O_2/79%CO_2 or 30% O_2/70%CO_2, mixture with recycled flue gas and compared with combustion in air. The improved char burnout in a 30% O_2/70%CO_2 mixture was attributed to the higher oxygen partial pressure; whereas, the poor char burnout in a 21% O_2/79%CO_2 mixture was attributed to the reduction in gas temperature. This observation was also found during a pilot-scale testing in which dry/wet flue gas was recycled to the inlet to maintain an oxidizer of 30% O_2 and 70% (CO_2+H_2O). Beyond these studies, subsequent research that addressed char reactivity in oxy-coal combustion has simulated O_2-CO_2 mixtures.

Among such studies, Wang et al. [38] predicted ~10% faster rate of char burnout and measured between 0 to 1% increase in overall char burnout in a down-fired combustor (100 kW_{th}) during combustion in a 30% O_2/70% CO_2 mixture as compared to combustion in air. Their results also indicated that the combustion rate in a 21% O_2/79% CO_2 mixture was lower compared to that of combustion in air. Liu et al.[39] conducted experiments in a down-fired combustor (20 kW_{th}) to measure gaseous emissions and char burnout during combustion in air and in O_2/CO_2 media. That study also showed that when air, as a combustion medium, was replaced by a 30% O_2/70% CO_2 mixture, the carbon in ash decreased from 13.2% to 5.1%, and in a 21% O_2/79% CO_2 mixture, it increased to ~19%. In other words, their result indicated that char burnout (calculated using ash tracer technique) increased from 79% to 92% during combustion in a 30% O_2/70% CO_2 mixture and decreased to 71% during combustion in a 21% O_2/79% CO_2 mixture compared to that of combustion in air. In a subsequent paper, these researchers reported higher coal burnout efficiency during combustion in a 30% O_2/70% CO_2 mixture

compared to that of combustion in air during experimental testing on seven bituminous coals taken from different regions [28]. Apart from the higher O_2 partial pressure, gasification of carbon with CO_2 and longer residence time of char particles in a combustor were suggested as possible reasons for the better char burnout observed during combustion in a 30% O_2/70% CO_2 mixture.

In a recent entrained flow reactor (EFR) study, char burnout of various ranks of coal was measured at 1,373 K in air and in gas mixtures consisting of -21%, -30%, and -35% O_2 in CO_2 [40]. For all the coal samples tested, char burnout in a 21% O_2/79% CO_2 mixture appeared to be lower than that of combustion in air. A higher char burnout was measured in the gas medium consisting of 30% and 35% O_2. A lower char burnout in a 21% O_2/79% CO_2 medium compared to that of combustion in air correlated to an increase in ignition temperature, and, thus, delays in ignition due to a higher specific heat of CO_2. A larger increase in char burnout was observed for higher ranks of coal than lower ranks of coal during combustion in a 30% O_2/70% CO_2 mixture compared to that of combustion in air. A relatively smaller increase in char burnout during combustion in a 30% O_2/70% CO_2 mixture was observed for lower rank of coal and was attributed to the small improvement margin.

To study the effect of ambient CO_2 levels on char burnout, Mitchell and Madsen [41] measured the rate of char burnout and particle temperatures in a 2.1% and 8% CO_2 in a 3% or 6% O_2 gas environment at gas temperatures between 1,340 and 1,520 K . From their theoretical analysis, the conclusion was that the double-film model of a burning carbon particle is not applicable for particles less than about 130 μm. This result, in other words, suggested that particle size plays a significant role in determining whether

or not CO_2 content of the ambient gas affects the rate of char burnout. However, the study simulated conditions typical in intermediate and late stages of coal combustion in air, in which CO_2 concentrations are lower (8-10%) and may not be directly applicable for gas environments consisting of elevated levels of CO_2 and O_2.

Saastamoinen et al. [42] studied the effects of CO_2 concentration on the combustion rate for coal particles sizes between 140 and 180 μm in an Entrained Flow Reactor (EFR) operating at gas temperatures of 1,073-1,473 K, O_2 partial pressure of 0.025-0.1 MPa, and CO_2 partial pressure of 0.05-0.2 MPa. Both the measured and calculated results consistently demonstrated a decrease in the particle temperatures and an increase in combustion rate with an increase in CO_2 partial pressure. Surprisingly, a negligible change in overall rate of char burnout was concluded, based on the proposition that the lower particle temperatures caused by an increase in CO_2 level offsets the contribution from char-CO_2 reaction, despite the fact that overall combustion rate increases with an increase in CO_2 partial pressure.

A recent experimental study, conducted using 90-106 μm sized coal particles and O_2 concentration ranging from 6% to 36% (remaining being N_2 and water vapor) at gas temperature of ~1,700 K, proposed that elevated levels of O_2 in the gas medium causes an increase in the rate of CO oxidation within the boundary layer near char particles[43]. Theoretically, it was expected that the increase in rate of CO oxidation would cause an increase in char particle temperatures much higher than the measured particle temperatures. Therefore, it was suggested that in an oxygen rich environment, endothermic char-CO_2 reaction also takes place on particle surfaces. Overall, the study

implies the need to consider a double-, or a continuous-film kinetic model for the case of gas medium consisting of higher O_2 and CO_2 levels.

Hampartsoumian et al. [44] studied the effect of CO_2 partial pressure on the rate of char burnout in a high-temperature thermogravimetric analyzer (TGA) furnace and in a flat flame burner (FFB) for coal particle sizes between 75 and 90 μm. The TGA experiments conducted at different partial pressures of CO_2 in N_2 gas at furnace temperature of 1,233 K expectedly produced an increase in the rate of char burnout due to char-CO_2 reaction, However, the increase in rate of char burnout due to char-CO_2 reaction was negligible at ~3% O_2 in a CO_2 mixture. In the FFB, at each sampling position, gas and particle temperatures observations indicated a decrease by ~75 K with an increase of 0.1 atm for CO_2 partial pressure. A reduction in gas temperature, unsurprisingly, was attributed to the decrease in thermal diffusivity of the gas mixture caused by an increase in CO_2 concentration. A reduction in particle temperatures was attributed to the endothermic nature of char-CO_2 reaction. This proposition implies that char-CO_2 reaction takes place even for small particle sizes (mean size of 82 μm) in the gas environments consisting of elevated CO_2 concentrations.

Varhegyi et al. [45] measured rate of char burnout in varying concentrations of O_2 in Ar and CO_2 gas at temperatures between 673 and 1,173 K in a TGA. The rate of O_2 reaction with char particles was found to be proportional to the O_2 concentration in the ambient gas and was unaffected by CO_2 concentration. This result is not surprising considering the operating temperature (1,173 K) where the rate of char-CO_2 reaction is expectedly 10^3-10^4 times lower than the rate of char-O_2 reaction.

In summary, most of these studies showed expected behavior when combustion medium switches from air to O_2/CO_2. For example, observations showed a reduction in gas/particle temperature and char burnout when CO_2 replaces N_2 in combustion medium, and an increase in char burnout with an increase of O_2 and CO_2 partial pressure. However, in one study, surprisingly the difference in carbon burnout from combustion in air and in a 30% O_2/CO_2 mixture was found to depend on coal type [40]. It was also observed that the typically held proposition that the double-film model is not applicable for particle sizes <130 μm is not valid for combustion in gas mixtures consisting of higher O_2 and CO_2 concentrations [46].

CO Emissions

Curiously, for coal combustion, less attention has focused on accurately predicting CO emissions, as compared to other pollutants such as NO_x and SO_x. Perhaps this is due to the existence of high temperature and turbulent flow conditions in boilers which causes CO species to be in equilibrium with surrounding O_2 and CO_2 levels, and insignificant CO levels (<100 ppm) [47]. However, a shift from equilibrium CO levels can be expected if sufficient mixing between CO and an oxidizer is not present.

Thambimuthu and co-workers [14, 48] conducted pilot-scale (0.3 MWt) studies to compare coal's combustion behavior in air with that of O_2-CO_2 mixtures. In an experimental test using a simulated O_2-CO_2 mixture, they reported that CO emission was: combustion in air < 35% O_2/65% CO_2 < 28% O_2/72% CO_2 [4]. Since the exact cause for the observation of this trend is not explained in their study, a simplified equilibrium

calculation is conducted (shown in Appendix 1.2). This calculation shows that the CO emission depends upon both the prevailing temperature and O_2/CO_2 condition as shown in Figure **1-2.** Considering the exit temperatures during the pilot-scale study was on the order of: air (1,423 K) ~ 35% O_2/65% CO_2 (1,423 K) < with 28% O_2/72% CO_2 (1,323 K), based on the equilibrium (see Figure **1-2**) the expected CO emission would be on the order of: air < 28% O_2/65% CO_2 < 35% O_2/72% CO_2. This suggests that the lower CO emission observed during combustion in 35% O_2/65% CO_2 compared to combustion in the 28% O_2/72% CO_2 mixture is probably due to faster oxidation kinetics at higher O_2 partial pressure.

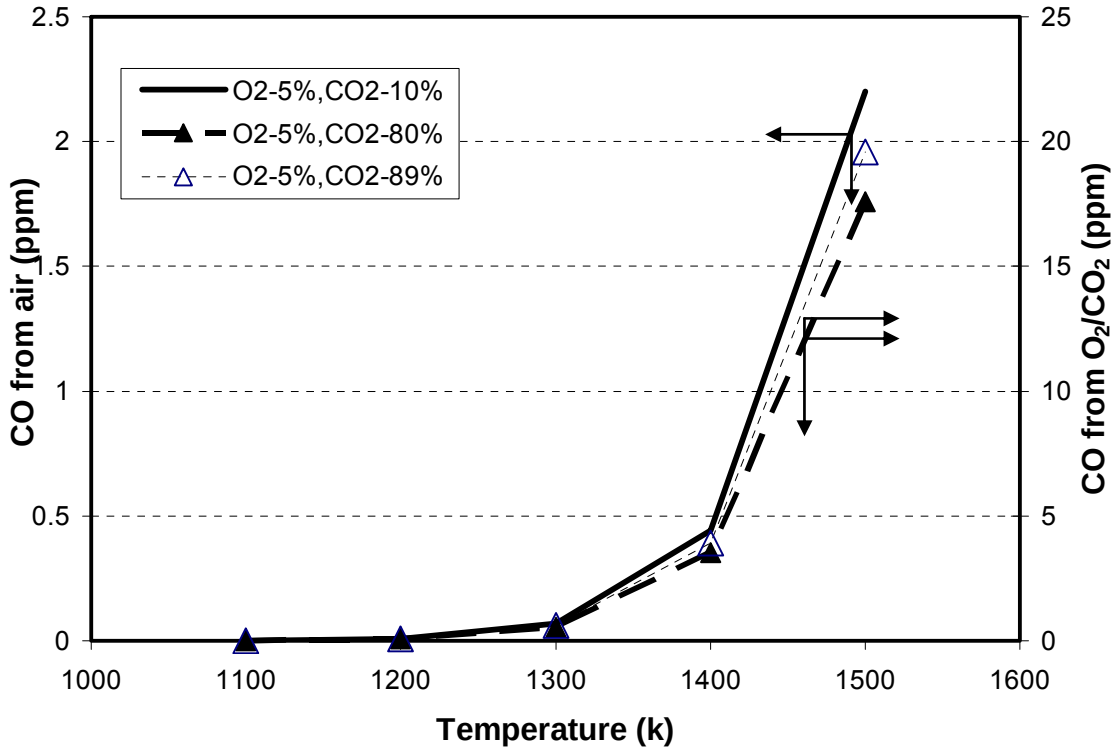

Figure **1-2**: Predicted equilibrium concentration in different gas mixtures: (—) concentration of combustion in air. (---) concentration during combustion in O_2/CO_2

A subsequent paper reported higher CO emission during combustion in 35% O_2 and recycled flue gas (RFG) medium compared to the baseline air tests [49]. The reported exit CO emission values for eastern bituminous, sub-bituminous and lignite coals were 51, 9, and 1 ppmv, respectively during combustion in air compared to 85, 75 and 14 ppmv, respectively, during combustion in O_2/RFG. A recent pilot-scale (5 MMBTU/hr) evaluation conducted by Babcock & Wilcox also showed higher CO emission during combustion in 30-35% O_2 with RFG medium (70-90 ppmv) compared to that of combustion in air (12-15 ppmv) [47]. Surprisingly, both of these studies reported CO emission on a volume basis while the difference in exit flue gas volume in the two combustion systems (air and O_2/RFG) is well known. The difference in CO emission from the two combustion approaches is expected to be reduced if the comparison is to be done on a mass basis. In a smaller level, pilot-scale testing (20 kW_{th}), conducted using a simulated O_2/CO_2 mixture, Liu et al. [39] observed that coal combustion in a 30% O_2/70% CO_2 mixture emitted lower (34 ppmv) CO emissions compared to that of combustion in air (50 ppmv). When a 21% O_2/79% CO_2 mixture replaced air, CO concentration increased to more than 200 ppmv. Both of these results appear to be surprising based on equilibrium analysis, as the expectation is lower CO emission in a 30% O_2/70% CO_2 mixture and about same CO during combustion in a 21% O_2/79% CO_2 mixture, as compared to that of combustion in air. However, the research offered no rationalization to explain the observation.

Wang et al. [38] measured higher CO concentrations during combustion in a 30% O_2/70% CO_2 mixture and lower CO concentrations in a 21% O_2/79% CO_2 mixture along the combustor length compared to that of combustion in air during bench-scale (~200

kW_{th}) testing conducted using simulated O_2/CO_2 mixtures. Lower CO concentration in flame during combustion in a 21% O_2/79% CO_2 mixture was observed compared to combustion in air and was attributed to the reduction in gas temperature caused by the higher specific heat of CO_2. An observation of higher CO concentration in flame during combustion in a 30% O_2/70% CO_2 mixture was attributed to the elevated levels of CO_2 during combustion in the O_2/CO_2 medium.

In summary, notably, no attention has been paid to explain the observed CO emission during oxy-coal combustion, presumably because CO emission was lower (200 ppm) [14]. While a majority of these studies indicated that CO emission is higher during oxy-coal combustion, trends of CO emission between lab-scale and pilot-scale studies are inconsistent. As mentioned in the char reactivity section, an increase in CO concentration in the ambient gas surrounding coal particles affects the O_2 availability to the particle surface. Therefore, it is essential that accurate accounting of CO formation and destruction reaction is considered in the model for oxy-coal combustion conditions.

NO_x Emissions

During coal combustion in air, NO_x formation takes place through oxidation of N_2 present in air at higher temperatures (>1,800 K) [50] and oxidation of fuel bound nitrogen. However, in oxy-coal combustion, NO_x formation through only conversion of fuel-N will takes place due to an absence of an N_2 in oxidizer. This apparent advantage has led various researchers to investigate the potential for NO_x reduction by using oxy-coal combustion [29, 51, 52]. These studies conducted at lab-scale and at pilot-scale levels, use

simulated O_2/CO_2 mixtures and 30-35% O_2 with recycled flue gas (RFG) mixture. In the case of combustion in O_2/RFG medium, NO_x emissions (lb/MMBTU produced on a lb/lb basis) have been reported to be lower than those during combustion in air primarily because of a reduction of recycled NO_x by char [8, 12, 49] and not just because of an absence of nitrogen in the oxidizer. These bases for comparison were the choice in place of ppmv because of lower volumetric flow rate but similar mass flow rate of combustion gases from oxy-coal combustion as compared to combustion in air. A summary of experimentally observed NO_x emissions from these two approaches appears in Table **1-3**. Form this table, it can be observed that studies have consistently shown ~70% reduction in NO_x emissions during combustion in O_2/RFG medium compared to combustion in air.

Table **1-3**: Summary of the literature's reported NO_x emission values

Study	Air	O_2/RFG	O_2/CO_2 (28%)	O_2/CO_2 (35%)	NO_x reduction
1. Payne et al.[5]	1.31 lb/MMBTU	0.38 lb/MMBTU			71%
2. Kiga and co-workers[16,23] Upon oxidizer stagging	30% fuel-N 8% fuel-N	5% fuel-N 3% fuel-N			90%
3. Thambimuthu and co-workers[15, 25]	320 ng/J	100-150 ng/J	210 ng/J	270 ng/J	68.75%
4. Liu et al.[13, 19] Upon oxidizer stagging	835 ppm (27.6% fuel-N)	 10% fuel-N	22.6% fuel-N 7.5% fuel-N		72.82%
5. B&W[30] Upon oxidizer stagging	.4 lb/MMBTU .22 lb/MMBTU	0.1 lb/MMBTU 0.065 lb/MMBTU			75%
Year	2000	2008	2018		
NO_x emission cap (lb/MMBTU) [12]*	0.4	0.17	0.14	*Clear Skies Act	

In one of the classic lab-scale studies conducted to separate formation of thermal-NO_x from fuel-NO_x a synthetic mixture of Ar, CO_2, O_2 gas was used as an oxidizer for combustion of a bituminous coal [53]. A change in CO_2 content of the gas, keeping the same flame temperature, resulted in a negligible change in NO_x emissions. This result

implies that elevated levels of CO_2 during oxy-coal combustion do not alter the chemistry of NO_x formation.

In one of the earlier studies conducted for oxy-coal combustion, Payne et al. reported up to 70% reduction in NO_x emissions during combustion in an O_2/RFG medium compared to that of combustion in air during pilot-scale tests [8]. A similar amount of reduction in NO_x emissions was observed in an industrial scale testing [15]. Upon staging oxidizer, from their respective baseline values, NO_x emissions reduced to ~25% during air-blown combustion and to 50% during combustion in O_2/RFG medium.

Okazaki and Ando [54] reported that more than 50% of the recycled NO_x converts to N_2 in the combustion chamber during use of O_2/RFG medium. A pilot-scale combustion study, conducted using a eastern bituminous and a sub-bituminous coal in air and in simulated O_2/CO_2 mixture as an oxidizer, showed that both the NO_x emissions (ppmw) and flame temperatures were in the order of: combustion in air > 35% O_2/65% CO_2> 28% O_2/72% CO_2 [14]. Observation of lower NO_x formation in a 35% O_2/65% CO_2 medium compared to that of combustion in air was attributed, naturally, to the absence of thermal-NO_x formation. However, this result appears to be unexpected because maximum measured temperature during combustion in air was ≤ 1,773 K. At such temperatures, the consensus is that formation of thermal-NO_x is negligible [50, 53] which has also been verified during the DTR tests in the current investigation. A higher NO_x formation during combustion in the 35% O_2/65% CO_2 mixture compared to combustion in the 28% O_2/72% CO_2 mixture was attributed to higher temperature (by ~100 K) and O_2 availability in the 35% O_2/65% CO_2 mixture than in the 28% O_2/72% CO_2 mixture. The results showed a further reduction of 40-50% in NO_x emissions when the combustion

tests were conducted in O_2/RFG media compared to the simulated O_2/CO_2 mixtures [48]. This reduction has generally been accepted to be due to additional reaction of recycled NO_x with -CH radicals present in the flame or with char particles. A subsequent paper compared NO_x emissions for three different ranks of coal during combustion in air and in O_2/RFG media [49]. Observations indicated that exit NO_x concentration (ng/J) was lower for both sub-bituminous (SB) and lignite coal during combustion in O_2/RFG medium compared to that of combustion in air. Surprisingly, higher NO_x emission was observed for O_2/RFG medium compared to combustion in air for an eastern bituminous coal. This result is extremely unexpected because various studies have observed significant reduction in NO_x (as discussed in this section) during combustion in a 30% O_2/RFG mixture as compared to combustion in air. However, the research proposed no explanation to elucidate the reason for the lower NO_x formation during combustion of an eastern bituminous coal in an O_2/RFG medium as compared to that in air.

Liu et al. [28] studied the effect of oxidizer staging on NO_x formation from a high volatile UK bituminous coal in a 20 kW_{th} lab-scale combustor using air and O_2-CO_2 mixtures as oxidizers. According to observation, staging reduced conversion of coal-N to NO_x from 27.6 % to 10% during combustion in air, and from 22.6% to 7.5% during combustion in a 30% O_2/70% CO_2 medium. In other words, NO_x emissions (ppmv) were 25% lower during combustion in a 30% O_2/CO_2 medium than in an un-staged combustion in air. In a subsequent paper, such conversion of coal-N to NO_x in these two combustion approaches depended upon coal type [28]. The highest difference (~50%) in NO_x formation during the two combustion media was observed for a South African bituminous coal; whereas, a UK bituminous coal produced only a ~10% reduction during combustion in a

30% O_2/70% CO_2 mixture compared to combustion in air. Although no clear dependency of coal rank, volatile matter, and coal-N contents on the NO_x reduction appeared, a general trend was that the coal with lower combustion efficiencies achieved higher NO_x reduction.

In summary, pilot-scale studies conducted using a simulated 30% O_2/70% CO_2 mixture reported lower NO_x emissions compared to combustion in air. Surprisingly, in these studies, gas temperature during combustion in air was ≤ 1,773 K [14], and therefore formation of thermal-NO_x was least expected [53]. Despite this fact, higher NO_x emissions were observed during combustion in air compared to combustion in a 30% O_2/70% CO_2 mixture. In a few studies, the reduction in NO_x emissions from oxy-coal combustion was also found to depend upon the coal type [28, 49].

Numerical Modeling

Very few studies exist to model the combustion [38], heat transfer [55] and pollution formation [56] characteristics that exist in oxy-coal combustion. Initially, simple one-dimensional model was applied to model the heat transfer and char burnout behavior from oxy-coal combustion [8, 38]. Later, a 3-D model of a pilot-scale boiler using CFD code (FLUENT™) illustrated the effect of various burner configurations and oxygen management schemes on NO_x emissions [56]. The modified design reportedly resulted in a 30% reduction in NO_x emissions compared to a baseline design [57]. Recently, a study using FLUENT™, showed the effect of difference in jet aerodynamics of combustion in air and oxy-coal combustion on flame shape and flame type [58]. However, all of the

studies used the existing knowledge of coal combustion in air to predict the considered parameters and recognized that accurate parameters for devolatilization in a medium of elevated O_2 and CO_2 should be determined [56]. Also, char-oxidation was modeled using a global combustion model which neglects the effect of char-CO_2 reaction [59]. Traditionally, global combustion model to account for char-oxidation is considered in the CFD models because of lower CO_2 levels (~8-10%) during combustion in air; however indications from recent experimental studies suggest that char-CO_2 reaction does play a role in the char particle conversion process during oxy-coal combustion [46].

Hypothesis

In the literature, two surprising results are without satisfactory explanation. First, in an EFR study, NO_x emissions from oxy-coal combustion compared to combustion in air was found to depend upon coal type [28]. A known factor is that flame temperature and ignition behavior of coal particles depends on the coal's volatile matter [60, 61]. Thus, a different amount of NO_x formation through thermal route, which is absent in oxy-coal combustion, is expected to occur for the different ranks of coal during combustion in air.

Second, in an EFR study, difference in weight loss from combustion in a 30% O_2/CO_2 mixture and combustion in air was greater for higher ranks of coal than for relatively lower ranks of coal [40]. One of the reasons behind this difference may be that the reactivity of coal-char towards CO_2 and O_2 is different for different types of coal [62]. Recent literature of char reactivity studies for oxy-coal combustion has indicated, in contrast to combustion in air, that char-CO_2 reaction does play a role in the overall rate of

char burnout [42, 63]. The exact contribution of char-CO_2 reaction in overall burnout is expected to depend upon the prevailing temperature, O_2 and CO_2 partial pressures and activation energy of char-O_2 and char-CO_2 reactions [64].

Thus, the main hypothesis of this thesis is: Some coal types are more suitable for oxy-coal combustion in reducing un-burnt carbon because of differences in their reactivity towards O_2/CO_2, and reduction of NO_x emissions because of differences in flame temperatures.

Problem Statement

Theoretical analysis for heat transfer (shown in Appendix 1.1) and literature studies regarding CO emission suggest that heat transfer imbalance and a slight increase in overall CO emission will not be a concern when retrofitting existing boilers with oxy-coal combustion technology. However, the cost associated with oxygen generation remains a major challenge in the use of oxy-coal combustion. This additional cost can, in part, be compensated by a reduction in NO_x emissions and an increase in char burnout from this technology. An improvement in char burnout will be useful for the existing coal-fired utilities where ash instead of being a liability can be a saleable product [65]. Although, the majority of literature suggested lower NO_x emission during combustion in a O_2 and recycled flue gas (O_2/RFG) mixtures [12] than combustion in air, uncertainty remains regarding the magnitude of NO_x reduction which appears to depend on coal type or burner design [49]. One of the additional advantages of oxy-coal combustion is flexibility for injecting the recycled stream in a boiler at the desired location [59]. The recycled stream

can be injected through the burner or within the boiler to achieve the desired temperature and Stoichiometric condition which favors NO_x reduction [66].

In order to exploit the full potential of oxy-coal combustion technology, a necessary development is a reliable computational fluid dynamics (CFD) model, which can be used to simulate various aspects of coal combustion such as heat transfer, particle ignition, ash formation, char burnout and pollutant emissions during O_2/CO_2 rich environment in a boiler. The overall objective of the current research is to modify the existing char-oxidation kinetic sub-model in a commercially available CFD tool, FLUENT^{TM}, and use more appropriate intrinsic rate paameter to accurately account for the contribution from char-CO_2 reaction for the prediction of char burnout and CO emissions. Development of this tool has the potential to exploit the operational flexibility in oxy-coal combustion to minimize NO_x emissions or oxygen consumption requirements, or to reduce the furnace size for newer boiler designs. On the technical side, development of such a tool, coupled with experimental results, would provide an explanation of why and how much reduction in char burnout and NO_x emissions is possible if this technology is employed in retrofitting existing coal-fired systems.

Research Objectives

Specific objectives of the present investigation are to:

1. Determine if pyrolysis in elevated levels of CO_2 causes any change in resultant char reactivity or coal-N distribution between volatile-N and char-N. A change in the reactivity of char is expected to change the overall char burnout. A change in

the rate of coal-N release and distribution between volatile and char phase is expected to affect NO_x emissions [67]. Prior knowledge of both of these parameters is necessary for accurate prediction of char burnout and NO_x emission from oxy-coal combustion.

2. Determine the intrinsic rate parameters for char-O_2 and char-CO_2 reaction and demonstrate that the intrinsic char-oxidation model accurately predicts char burnout and CO emissions for oxy-coal combustion.
3. Compare CO, NO_x and char burnout from combustion in air with combustion in O_2/CO_2 using a lab-scale experimental facility for two ranks of coal. These experimental data will be used to test the hypothesis and also serve as a basis to test the accuracy of sub-models for char burnout, and CO and NO_x emission predictions.
4. Compare the CFD predictions against measurements of temperature and CO, NO_x species profile inside a pilot-scale boiler for combustion in air, and extend the prediction for oxy-coal combustion conditions.

Thesis Organization

In order to achieve these objectives, pyrolysis and combustion tests were conducted in a lab-scale Drop Tube Reactor (DTR) for two ranks of coal. A combustion test in air in a pilot-scale research boiler measured axial profiles of gaseous species and temperatures and exit char burnouts. A Thermogravimetric Analyzer (TGA) measured

char reactivity and intrinsic rate parameters. A commercially available Computational Fluid Dynamics (CFD) tool, FLUENT^{TM} simulated the interaction of gas and particle phases. A detailed description of these facilities, experimental procedure and chosen sub-models is provided in Chapter 2.

To address the first objective, it was necessary to determine a priori, is whether or not elevated levels of CO_2 concentration during coal pyrolysis cause any change in the reactivity of resultant char particles, and coal-N distribution between volatile and char phase. This concern formed from the published literature, in which a change in gas medium apparently affected the NO_x precursor species [68] and physical properties of char [69]. A change in the reactivity of char is expected to affect the overall char burnout. A change in the rate of coal-N release and distribution between volatile and char phase is expected to affect the NO_x emission [67]. The relevant literature on this aspect and the approach used is provided in Chapter 3.

In order to accurately capture the effect of char-CO_2 reaction on the char burnout and CO emission predictions and transition from a kinetically controlled (Zone I) to intra-particle diffusion controlled (Zone II) regime, use of a more appropriate intrinsic model is necessary. Accuracy of these predictions depends upon the activation energy value used for char-O_2 and char-CO_2 reaction [64] which is widely scattered in the literature [70] even for a given coal char. Relevant background about why such a scatter in activation energy value exists, and the approach used in the present research for estimation of rate parameters are discussed in Chapter 4.

Although, intrinsic rate parameters [71, 72] and physical properties [73] of char samples have been measured by various studies, use of these values in an intrinsic model for char

burnout prediction has rarely been demonstrated [74]. Relevant literature background, primary challenges in the use of this approach, and the current methodology to predict char burnout using the intrinsic model are discussed in Chapter 5.

To test the hypothesis that some coal types are more suitable for oxy fuel combustion in terms of overall NO_x emissions and char burnout, lab-scale combustion tests were conducted in air and in O_2/CO_2 media at different furnace temperatures, using two ranks of bituminous coal, and exit CO, NO_x emissions and char burnout were measured. Detailed measurements, conducted inside a pilot-scale boiler for combustion in air assess the accuracy of model predictions and are discussed in Chapter 6.

Chapter 2

Experimental and Computational Details

This chapter describes details of the Computational Fluid Dynamics (CFD) code and experimental facility used for the current research. A brief description of sub-models used, selection criteria of chosen sub-models, the model parameters, and boundary conditions is also included. Chapters 3 to 6 discuss actual experimental and computational results.

Lab Scale Testing

An entrained flow reactor [75], termed in this research as a "drop tube reactor" (DTR), is a laminar flow furnace with controlled wall temperatures and particle residence time. This reactor simulates the typical flow configuration, high heating rate and temperature conditions that exist in an actual, pulverized coal (PC) boiler [76]. In this reactor, pulverized coal particles are fed along with a primary gas in a dilute suspension through a water-cooled injection probe. Typically, a preheated secondary gas stream is used to achieve rapid heating of the coal particles. A water-cooled collection probe collects the entire gaseous and particle flow and quenches the char reaction. Char particles are collected iso-kinetically from the gas stream using either a filter paper or in a cyclone chamber. Subsequent analysis of the gases uses a continuous emission monitoring (CEM) system or, if not analyzed the gases are vented. The particle residence

time in the furnace depends on the inlet gas flow rates, wall temperatures, particle size, and insertion length of the collection probe in the furnace.

Description of DTR

The DTR for this research is used in this work for both pyrolysis and combustion studies, and a schematic diagram is shown in Figure **2-1**. The DTR consists of a single zone, electrically heated furnace operated at a maximum temperature of 1,873-1,973 K [77]. The reactor is a high purity alumina refractory tube, positioned vertically. Six U-shape Kanthal-super heating elements are attached on the wall. Acrison GMC-60, a rotary type, feeder supplies coal in an entrained flow of a primary gas through a water-cooled injection tube. A ceramic sheath provides additional thermal protection. The position of the tip of the injector is in level with the bottom of a mullite™ flow-straightener. Secondary gas from two inlets enters the furnace through the top of the preheater. Secondary gas exits the flow straightener with the coal-laden primary gas. A vacuum pump applies suction and iso-kinetically* collects char particles from the gas stream using a water cooled collection probe. These particles are collected on a filter paper, and sucked gas is passed through a condenser to remove water vapor to prevent corrosion in the vacuum pump and CEM system. During all tests, the preheater temperature is fixed at 873 K to maintain the durability of the heating element.

* For iso-kinetic collection, a suction rate of 8 l/min was applied based on the opening diameter of collection probe and used gas flow rates.

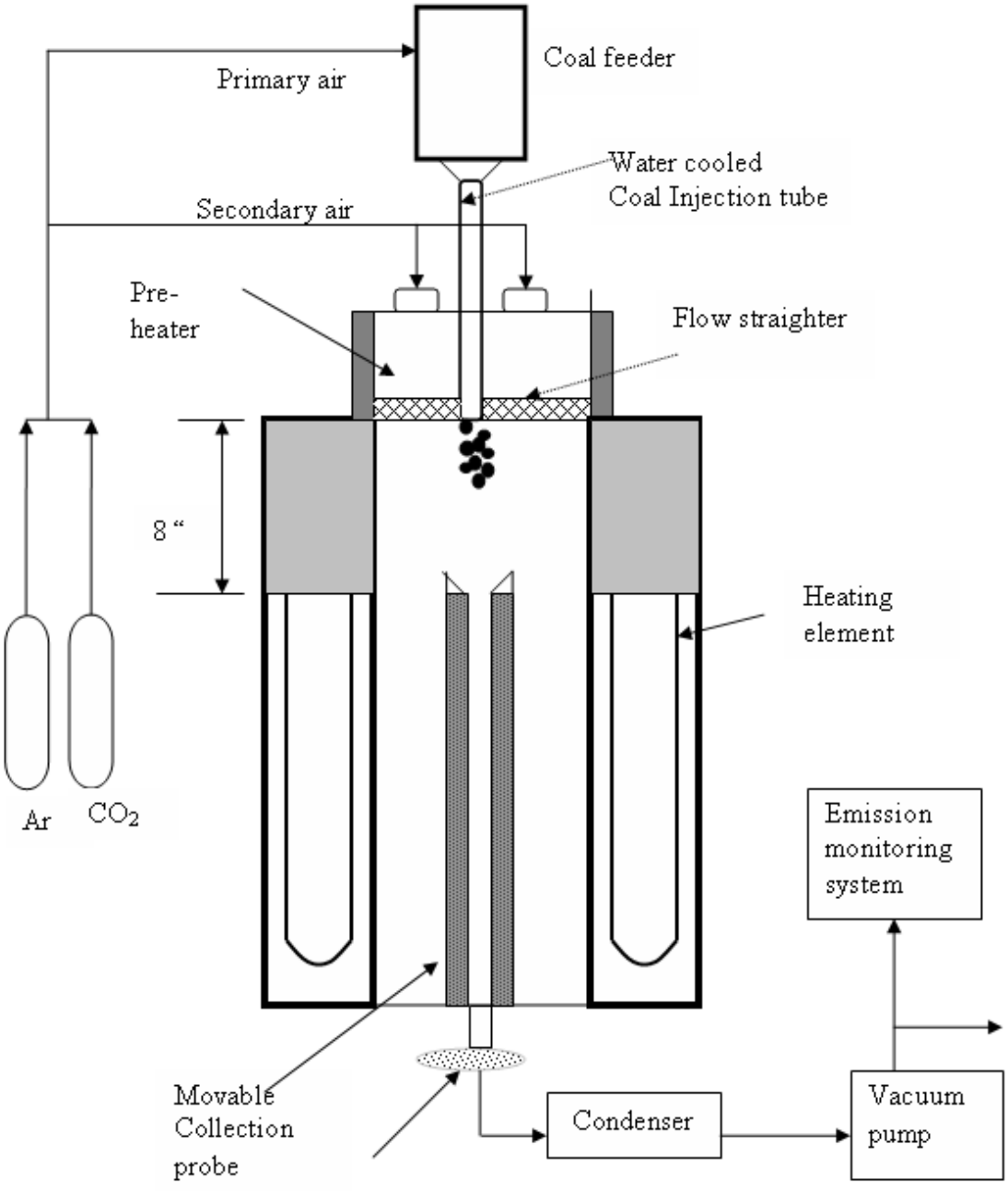

Figure **2-1**: Schematic representation of drop tube reactor

Test Conditions

During pyrolysis, coal particles at the rate of ~0.33 (±0.02) g/min are entrained in a primary gas (Ar or CO_2) stream flow of ~1 L/min[†] (STP). A secondary gas (Ar or CO_2) flow rate of 15 L/min (STP)[‡] is used to maintain the oxygen free environment during these tests. The same gas flow rates are used during combustion tests, but the coal feed rate is increased to ~1.33 (±0.02) g/min to maintain ~30% excess air, typical of industrial combustion systems. During all tests (unless specified otherwise) a collection probe is situated 20 inches from the injector. Typical pyrolysis tests for ~30 minutes and combustion tests for ~15 minutes are done to collect sufficient amounts of char samples for further analysis. Two coals, differing in rank, a high volatile (hvCb) (DECS-5) and a low volatile (lvb) (DECS-19), obtained from the Pennsylvania State University (PSU) Coal Sample Bank were used during pyrolysis and combustion tests. These two coal types were chosen to represent the extreme sub-ranks of bituminous coal and have been well studied in literature [78]. The coal particles were wet sieved into two particle size classes (-100+140 mesh) and (-140+200 mesh). Their particle size distributions and the proximate and ultimate analyses are shown in Table **2-1**. The D(v, 0.1), D(v,0.5), and D(v,0.9) values are the particle sizes where, respectively, 10, 50, and 90% of the particles, by volume, are less than the respective indicated size. Heating values and inorganic element analyses for these two coal types are obtained from the PSU Coal

---

[†] This primary gas flow rate was chosen as a compromise that maintains a uniform coal flow and desired higher coal particle residence time during the tests.

[‡] Actually, 11 Lpm was observed to be sufficient to avoid any air contamination. But since 30% O_2CO_2 combustion tests needed lower (by 1.4 times) flow rate than air for same stoicheomtery, ~15 Lpm (11*1.4) was used throughout the pyrolysis and air combustion tests for consistency in conditions.

Sample Database. Inorganic elements and ash mineral oxide analyses for these two ranks of coal is provided in Table **2-2**.

Table **2-1**: Chemical composition of coal used during DTR tests

	hvCb		**lvb**	
US mesh	(+140-100)	(+200-140)	(+140-100)	(+200-140)
Proximate Analysis (Wt %)				
Moisture	5.23	5.71	0.88	0.83
Volatile Matter	38.51	37.01	18.70	17.16
Fixed Carbon	8.09	7.39	6.81	5.44
Ash	48.16	49.88	73.61	76.57
Ultimate Analysis (Wt %)				
Carbon	69.93	69.85	83.24	85.19
Hydrogen	5.16	5.01	3.71	3.77
Nitrogen	1.25	1.07	1.03	0.96
Sulfur	0.83	0.83	0.74	0.74
Oxygen (by difference)	9.51	10.14	3.59	3.07
Particle Size Distribution (μm)				
D(v,0.9)	100	75	115	71
D(v,0.5)	138	110	145	105
D(v,0.1)	174	142	188	138
Heating Value (BTU/lb)	13917		12551	

Table **2-2**: Mineral element analysis of studied coal

(Oxide %) in ash			**Element (% of dry coal)**		
	lvb	hvCb		lvb	hvCb
SiO_2	28.60	44.10	Si	0.70	1.80
Al_2O_3	19.60	11.00	Al	0.60	0.50
TiO_2	0.95	0.84	Ti	0.03	0.04
Fe_2O_3	17.00	8.10	Fe	0.70	0.49
MgO	2.49	1.73	Mg	0.08	0.09
CaO	15.20	8.40	Ca	0.60	0.52
Na_2O	1.14	4.29	Na	0.05	0.27
K_2O	0.83	0.18	K	0.04	0.01
P_2O_5	0.04	0.41	P	0.001	0.02
SO_3	13.00	10.20			
Other	1.15	10.75			

Characterization

Proximate analyses for coal and char particles were obtained in a commercially available instrument (Mac-400) according to ASTM method. Surface area of the samples was determined using a Quantachrome Absorb-1. For CO_2 and N_2 surface area, approximately 0.2-0.3 g of sample was outgassed for a minimum of 24 hours at 383 K and a pressure of 10 millitorr. The CO_2 surface area was calculated using Dubinin-Polanyi(DP) method, which assumes a cross sectional area of a single CO_2 molecule to be 25.3 $A^{o\ 2}$ at 273 K[79]. The N_2 surface area and pore size distribution was determined using adsorption branch of isotherm at 77 K[80]. Particle size distribution was determined by laser light scattering (Malvern Instruments). About 5-10 mg of the sample was placed in a transparent cell containing an ethanol medium, and a spinning magnetic bar provided the necessary agitation to keep particles in suspension. Laser light scattering from the particles depended upon their size which is analyzed by the 31 concentric annular sector rings yielding a particle size histogram. Helium density determination was performed using a Qunatachrome pycnometer. Ultimate analyses are performed according to ASTM Method D-5373 using a LECO Tru-Spec Carbon, Hydrogen, Nitrogen Determinator. Products of combustion from the lab-scale or a pilot-scale reactor are analyzed by a complete analytical package, continuous emission monitoring (CEM) system, consisting of a set of on-line O_2, CO_2, CO, NO_x, and SO_x analyzers. The flue gas analyzers included: a Beckman Industrial Model 755 paramagnetic O_2 analyzer, two Beckman Industrial Model 864 infrared analyzers for CO and CO_2, a Rosemount Analytical Model

890 SO_2 analyzer, and a Thermo Electron Model 10 chemiluminescent NO-NO_2-NO_x analyzer.

Weight loss of coal samples during pyrolysis, is calculated using an ash tracer technique [76] which resulted in the equation:

$$\% \text{ weight loss} = \left[1 - \frac{A_c(100 - A_r)}{A_r(100 - A_c)}\right] \times 100 , \qquad \textbf{2.1}$$

Where, A_c = Ash (% dry) in the feed coal, and

A_r = Ash (% dry) in the residual char.

For char burnout calculation, the assumption is made that char particles consist of ash and char fractions only. The initial ash content of char particles is calculated assuming that all the volatile matter content of the coal sample is removed. This was necessary for convenience purposes because, in CFD predictions, a direct value of char burnout in this way is readily available. The char burnout during combustion is calculated using the equation:

$$\% \text{ char burnout} = \left[1 - \frac{A_c}{A_r}\right] * 100 , \qquad \textbf{2.2}$$

where, A_c is the initial ash content of char, and

A_r, is the residual ash content of char.

Since weight loss during combustion is typically calculated using the ash tracer technique (Equations **2.1)**, a sample calculation is shown in Appendix 2.1 to illustrate the relative comparison of burnout calculated by the two approaches (Equations **2.1** and **2.2**).

Although the ash tracer technique has wide acceptance [76, 81], accuracy is sometimes questioned because of inherent assumptions involved[82]. For example, the technique assumes that mineral matter transformations in DTR and proximate analyzer are similar. The error in weight loss estimation arises for coal containing significant amounts of carbonates or sulfur. Alternate approaches using Ti, Al, Si have shown that weight loss calculated using ash as a tracer technique are within 5% of that obtained using the Ti as a tracer technique[83].

Temperature Profile

Since the heating elements are attached only in the lower 12 inches of the DTR furnace (Figure **2-1**) and the preheater temperature is at a much lower than the typical furnace temperature, coal particle residence time and temperatures are calculated using a computational fluid dynamics (CFD) tool FLUENT^{TM} (described later in this chapter). A suction pyrometer is used to measure the temperature profile within the hot zone of the furnace to determine more reasonable thermal wall boundary conditions [84].

The suction pyrometer is water-cooled and is inserted through the bottom of the reactor. The S-Type thermocouple, shielded with a ceramic tip, is positioned several centimeters above the water-cooled section of the pyrometer. A separate radiative shield extends ~3 cm above the thermocouple. Typically, a suction pyrometer's position is perpendicular to the direction of flow, when high suction rates are necessary to ensure reasonable heat transfer efficiency. However, in the DTR, suction above the total flow of 8 L/min will mis-represent the actual fluid residence time and temperature conditions of

the DTR. Thus, for this research, the flow rate in the suction pyrometer is set equal to 8 L/min. Centerline gas temperatures were measured at intervals of every 2-inch at furnace wall temperatures of 1,673 K in a CO_2 medium and in air. The measured values are shown in Figure **2-2,** and the DTR wall boundary condition in CFD code is set accordingly.

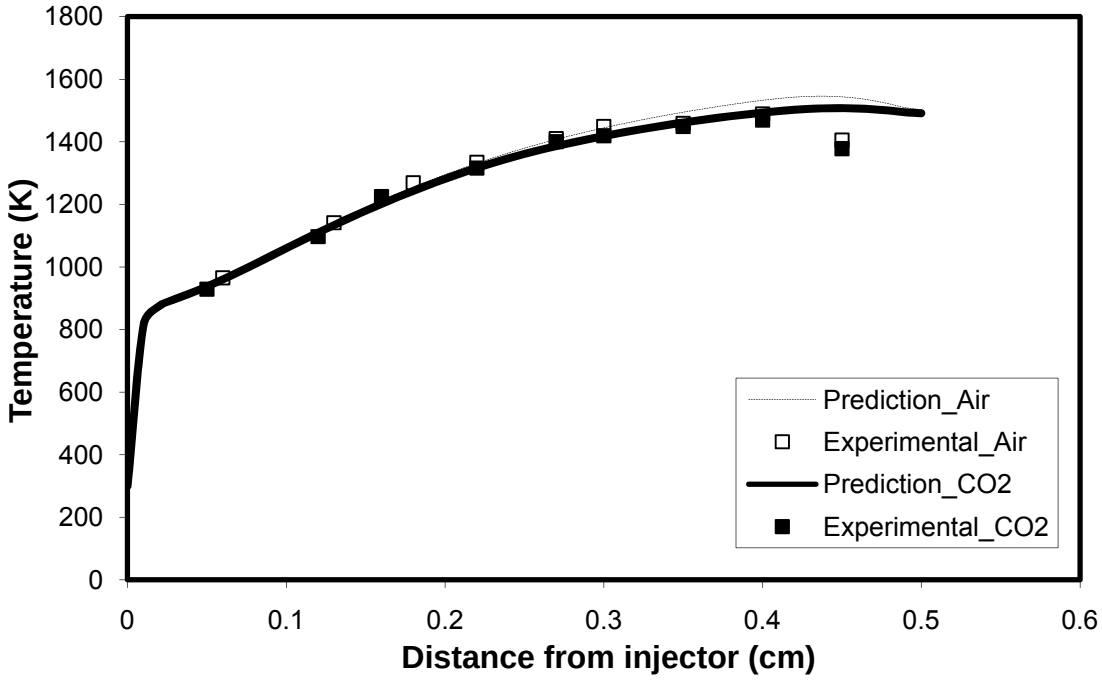

Figure **2-2**: Gas temperature profile in the drop tube reactor at 1,673 K

Pilot Scale Testing

A pilot-scale test was conducted in air, and detailed species and temperatures inside the boiler were measured to validate the CFD model predictions. The baseline coal used for the testing is a bituminous (mvb) coal from a Middle Kittanning seam, in

Pennsylvania. The pulverized particles are obtained from a large chunk by passing the coal through a milling circuit. This is done in a three step process. First, the coal particles are passed through a Denver Jaw Crusher to reduce the size to a 1-inch top size. These particles are then fed through an American Pulverizer Company Roll Crusher to reduce the size to a $1/8^{th}$-inch top size. These coal particles are then passed through a Hosokawa Micron Powder Systems Micro-ACM air swept mill to generate utility-sized pulverized coal. The speed for this mill is maintained such that the coal particles are in the PC range (70% passing through a 200 mesh). Table **2-3** shows the compositional analysis of the coal and particle size distribution.

Table **2-3**: Composition analysis of Middle Kittanning (mvb) bituminous coal used in the Research boiler (70% passing through 200 mesh)

Proximate Analysis (Wt %) as received	
Moisture	2.20
Volatile Matter	30.10
Fixed Carbon	63.00
Ash	4.70
Ultimate Analysis (Wt %) as received	
Carbon	80.10
Hydrogen	4.70
Nitrogen	1.30
Sulfur	0.70
Oxygen (by difference)	6.20
Particle Size Distribution (µm)	
D(v,0.9)	140.7
D(v,0.5)	45.6
D(v,0.1)	10.4
Heating Value (BTU/lb) as received	13,917

Description of the Research Boiler

The pilot-scale combustion test is performed in the PSU commercial-scale A-Frame water tube boiler [85]. The combustion chamber (shown in Figure **2-3)** is 3 ft by 3 ft by 7 ft with a maximum heat release rate of 42,000 BTU/ ft^3-h. The boiler contains 288 ft^2 of heating surface and the maximum firing rate is 2 MMBTU/hr. The boiler, originally designed to burn oil, has 18 side ports for gaseous and particulate sampling.

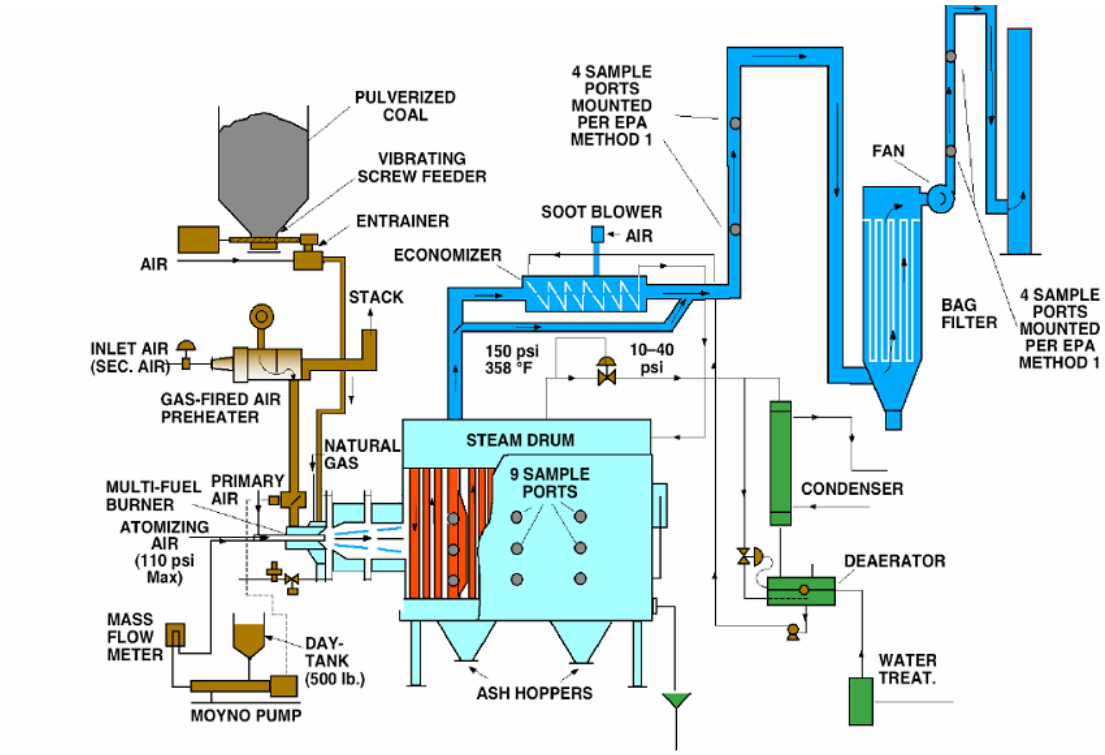

Figure **2-3**: Schematic diagram of a pilot-scale watertube research boiler (adapted from [85])

To promote and enhance combustion of coal and coal-water droplets, a ceramic burner throat extends 29-inches into the combustion chamber. This ceramic section, termed a quarl, is preheated by a natural gas flame prior to introducing the coal. The quarl aids in the ignition of hard to burn fuels by storing some of the radiant heat energy

released by the flame. The combustion gases split into two convective sections, one on each side of the radiant combustion chamber. Two ash hoppers are under each convective section, and a doorway provides access to the radiant combustion chamber.

Test Conditions

The preheated combustion air (secondary air) is passed through a conventional swirl ring several inches before encountering the gas distribution ring, both of which are 8 inches in diameter. A small portion of unheated primary air feeds with coal particles through an annular gap surrounding the nozzle. A schematic diagram of the swirler used in this research is shown in Figure **2-4**. Combustion air feeds through the outer annulus of swirler, and a small portion of combustion air is introduced in the quarl tangentially through two headers that were balanced for uniform flow. The coal feed rate used during the test is calculated from the calorific value of the coal to meet a predetermined firing rate, which, in this case, is ≈1.5 million Btu/h. Ash samples, are collected from the bag-house hopper and all four boiler convective pass hoppers for carbon burnout analysis.

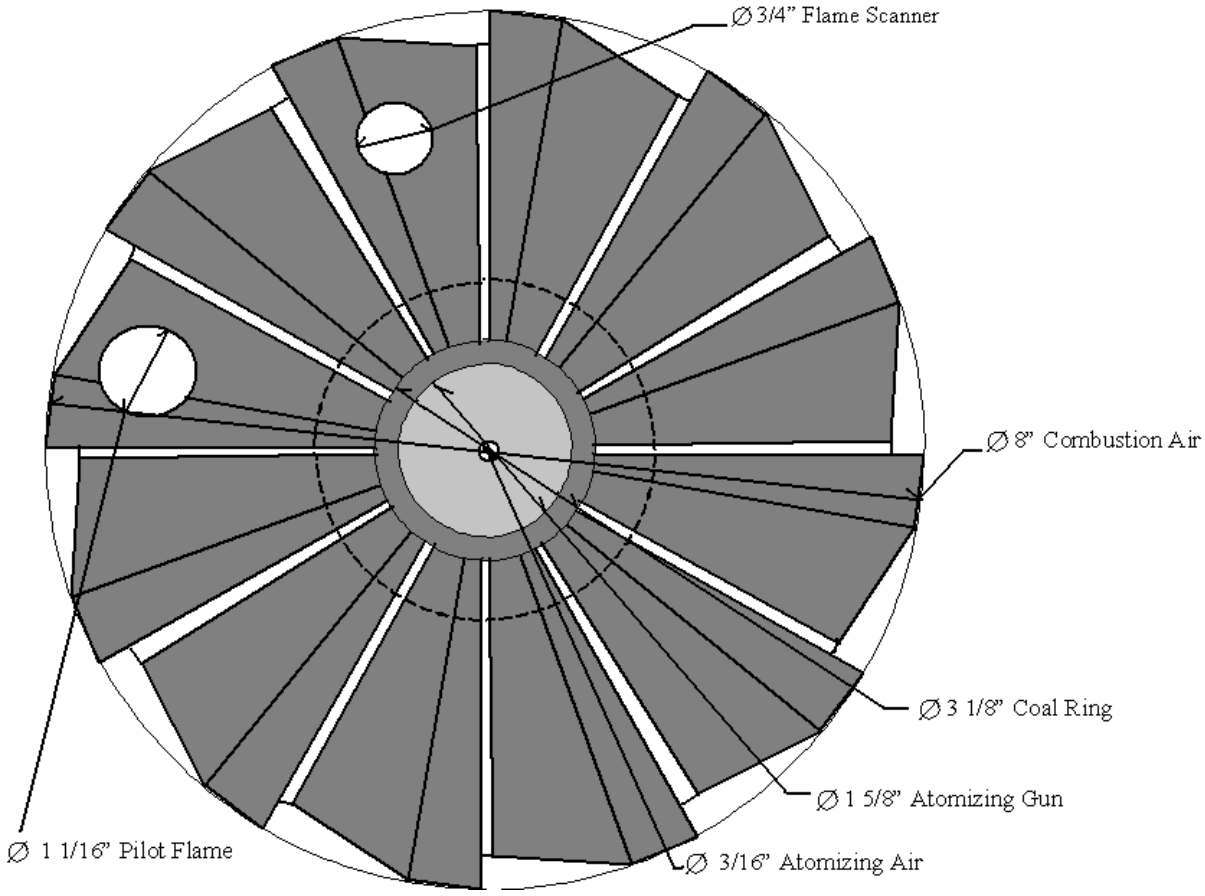

Figure **2-4**: Schematic diagram of swirler used during pilot-scale testing

Table **2-4** reports the average operating conditions and flue gas composition at the outlet of the boiler. A suction pyrometer, previously described, is used to measure the concentration of gaseous species and gas temperatures through ports located on each side of the boiler. Typically, a steady state reading is observed after 10 minutes of operation.

Table **2-4**: Operating conditions during pilot-scale testing performed in air using a Middle Kittanning coal

Flowrate		
Fuel feed rate	109	lb/h
Firing feed rate	1.46	MMBTU/hr
Transport air	27	SCFM
Primary air	163	lb/h
Secondary air	1119	lb/h
Temperature		
Primary air	350	ºF
Combustion air	623	ºF
Quarl top	1612	ºF
Quarl bottom	1405	ºF
Flue gas composition		
O_2	3.9	%
CO	187	ppm
CO_2	14.4	%
SO_2	512	ppm
NO_x	801	ppm

Computational Modeling

Calculating the general features of a coal fired flame requires the simulation of a two-phase, reacting, swirling, turbulent flow. Many commercial tools such as PCGC™, CFX™, Star-CD™, FLUENT™, etc. are available to model these features [86]. These tools differ more in grid generation and data post-processing than in the sub-model available to simulate turbulence and combustion behavior [87]. The current research uses FLUENT™ because it has wide acceptance in modeling coal combustion behavior [84, 88] and is more economical than the other CFD tools. FLUENT™ is a flexible CFD package that supports customized grid generation, applies a finite difference solver to the governing fluid dynamics equation, and handles basic data and post-processing tasks [89].

Model Details

The equations governing fluid dynamics behavior are founded on the assumption that fluid is a continuum, i.e. the fluid and its properties have continuous distribution in space. The computational frame work for simulating a continuous medium is a discretized representation of the space occupied by the fluid.

Gas Flow

The dynamics of the continuous phase fluid flow, characterized from a Eularian frame of reference by a system of partial differential equations, describe the conservation of mass, momentum, energy, turbulence quantities and chemical species. Turbulent diffusivity is handled by an effective viscosity obtained from the well known k -ε model and involves two additional equations for k and ε. The gas phase conservation equations in three dimensions can be cast as:

$$\frac{\partial \rho u_i \phi}{\partial x_i} = \frac{\partial\left(\left(T_\phi\right)\frac{\partial(\phi)}{\partial x_i}\right)}{\partial x_i} + S_\phi + S_{p\phi} \qquad \textbf{2.3}$$

Here, ϕ represents any of the above variables (mass, momentum etc); T_ϕ relates to turbulent diffusivity; S_ϕ is the source or sink term in the gas phase, and $S_{p\phi}$ is the term representing the particle phase.

To create a system of algebraic relations describing the interdependence of the cells, these equations are discretized for each cell in the computational domain according to the finite difference method. A solution, obtained through an iterative procedure,

solves for the different properties of each cell until meeting convergence criteria. The pressure, velocity, turbulence quantities, enthalpies, and species concentration data are computed directly using the discretized partial differential equations.

Particle Flow

The trajectory of the second phase in a two-phase flow is evaluated from a Langrangian frame of reference. The equation for motion and trajectory of particles are solved for multiple incremental time steps for each cell through which the second phase travels. The equation for motion includes drag, virtual mass, and pressure gradient related forces. In the model, the assumption is made that the second phase is dispersed; i.e. neglecting the interaction between the droplets and interaction with the gaseous phase is continuous over the whole trajectory. Turbulence in the flow requires that a stochastic particle tracking method be used to determine the effect of turbulent velocity fluctuations on the motion of the droplets. The fluctuating velocity components are calculated based on the kinetic energy of turbulence and the characteristic lifetime of the turbulent eddy.

Energy Transport

In a furnace environment, coal particles experience a thermal and mass exchange with the gas phase due to pyrolysis, char-oxidation and char-gasification reaction. The heat and mass transfer from the particle to the gas phase changes the species concentration and enthalpies of the gas in the cells that lie along the particle's trajectory.

Representations of these interactions are by the source and sink term in the energy and the species conservation equation. The computational solution is obtained by alternating between the Eularian gas phase calculations and Langrangian solid phase calculation until meeting the convergence criteria (described later in this chapter)

Heat transfer between the particles and gas phase is governed by an energy balance. Standardized enthalpies are used for all species including the coal particles. The gas phase enthalpy equation contains only two source terms: the cell radiation and that due to the enthalpy of fuel transferred from the solid phase to the gas phase. The thermal radiation transfer between the dispersed and continuous phases is modeled by a P1 radiation model with the domain–based, weighted sum of gray-gases model (WSGGM). The WSGGM-domain-base is a variable coefficient that uses a length scale from the geometry of the model. This is preferred because the WSGGM cell-based model available in FLUENT^{TM} uses a characteristic cell length and can be more grid dependent.

Turbulence

The jets in the research boiler have a Reynolds number ~ 25,000, indicating that flow is fully turbulent. A two-equation k-ε turbulent model calculates the Reynolds stress with the assumption that turbulent viscosity is isotropic. In strongly swirling flows the turbulent viscosity is likely to vary with the direction. The Reynolds stress model is able to simulate this behavior but at the expense of computational time. In the current model, therefore, a Re-normalization Group (RNG) k-ε model was used to capture the general characteristics of the flow.

Coal Combustion Model

Coal particles are considered to consist of combustible and ash fractions. Devolatilization and combustion of the volatiles takes place in the gas phase through rapid heating of the particle. The remaining char particle subsequently burns to ash at a chemical or diffusion controlled rate depending upon the particle temperatures and surrounding gas species concentration.

i) Pyrolysis

Devolatilization modeling uses a first-order, Arrhenius-type reaction. It is considered that coal particles upon entering the furnace release the volatile according to:

Combustible –> Volatile + Char.

In the present model, a single reaction model is used. The literature reports a wide scatter (as much as by 3 orders of magnitude) in the rate parameters for this process [90]. This has been attributed to the difficulty in measuring accurate particle temperature, assumption of negligible pyrolysis in the initial heat-up period, and rapidity of the devolatilization process [91]. Therefore pyrolysis rate parameters for both the coal samples (lvb and hvCb ranks) are estimated from the weight loss at different furnace wall temperatures (973-1673 K) in the DTR (shown in Appendix 2-2). These estimated rate parameters, employed in CFD model and modified using an iterative procedure such that the measured weight loss equal the CFD calculated weight loss. This accounts for weight loss of the sample in the initial, non-isothermal zone.

ii) Char Oxidation

Char combustion modeling uses a parallel process of surface kinetics and oxygen diffusion.

The particle mass change due to char burnout is:

$$\frac{d(m_p)}{dt} = -\pi \rho_p d_p^2 X_{O2} . K_t . \qquad \textbf{2.4}$$

Here, K_t is the combination of surface kinetics rate, K_c, and gas diffusion rate coefficients, K_d according to:

$$K_t = 1/(1/K_c + 1/K_d)) . \qquad \textbf{2.5}$$

Oxidation of char produces CO/CO_2 at the particle surface, and then the CO oxidizes to CO_2 in the bulk gas [92]. Accurate knowledge of this product ratio determines the amount of heat transferred to the coal particles. For example, CO, as a char-oxidation product, produces ~30% heat on the particle's surface than if CO_2 is a char-oxidation product. Because of the difficulties in measuring the boundary layer surrounding small particles, no definitive experimental data exists for high temperatures (~1,800 K) to establish the ratio of CO_2 formation at the surface of particles and CO_2 formation in the boundary layer surrounding in the pulverized-coal [93]. Relevant studies that estimated the CO/CO_2 ratio have a long history [94], with a clear initial outcome in the beginning but with major complexities following. For CO/CO_2 production in the primary heterogeneous reaction at the solid surface, the most accepted conclusion, from the original studies, is that the CO/CO_2 ratio has an Arrhenius-type temperature dependence [95, 96]. This dependence ratio also predicts, with support from related measurements, that at a

temperature above 1,000 K, the reaction product is nearly all CO [97]. Mitchell and co-workers [98], on the basis of particle temperatures and weight loss measurement argued that as much as 15% of carbon converts to CO_2. In the present case, therefore, CO is chosen as the char-oxidation product.

Two approaches typically model the surface kinetics of char oxidation step [99]: Field's model assumed the particles to be non-porous, and considers reactions to take place at the external boundary of particles [92]. On the other hand, the intrinsic model accounts for the pore structure of particles and considers reaction occur on the entire internal surface of particles [71]. In the intrinsic model, the rate measured at low temperature is extrapolated to high temperature by accounting for the effectiveness factor [100]. Although, this model considers a more realistic representation of the char oxidation stages, the most significant disadvantage of this approach is the large uncertainty in the intrinsic rate parameters and effective diffusivity of particles [101]. Chapter 5 extensively discusses use of this approach and its challenges.

The present study uses the intrinsic method to model the char oxidation step. This is done to account for the change in rate controlling regime at different temperatures. Accounting for the transition in the rate controlling regime is a most important feature to accurately capture the effect of CO_2 on rate of char burnout. Since the existing intrinsic model in FLUENT^{TM} does not incorporate multiple gas-solid reaction, a user defined function (UDF) is written for char-O_2 and char-CO_2 reactions [89].

iii) Gas Phase Combustion

The particle mass loss rate to the gas phase during devolatilization and char burnout processes provide source terms for the gas–phase species concentration and enthalpy equations. A finite rate/eddy dissipation model is adopted to model the gas phase oxidation reactions. This model considers that the overall reaction rates between the reactants are governed by the minimum of chemical kinetics and mixing rates[102]. In turbulent flows, this mixing time is dominated by the eddy properties, and therefore the rate is proportional to a mixing time as defined by the turbulent kinetic energy (*k*) and dissipation (ε). The CO oxidation and volatile combustion are modeled using the following reaction scheme:

$$CO + 0.5\ O_2 – CO_2$$

$$C_xH_yO_z + (x/2+y/4-z/2)\ O_2 \text{ --- } x\ CO + y/2\ H_2O.$$

Rate parameter for this reaction is taken from published literature [103]. Composition (x, y, z) and heating value of the volatiles is calculated from the proximate and ultimate analysis of the coal sample (shown in Appendix 2.3). Moisture is considered a component of the volatiles, and enthalpy of the volatiles is adjusted accordingly.

NO_x Model

NO_x formation and destruction processes in combustion systems are very complex. Hill et al. [104] provided a recent review of the reaction processes involved in NO_x formation in pulverized coal combustion systems, including work in laboratory-scale, pilot-scale, and full-scale furnaces. During combustion, nitrogen from the

combustion air or fuel converts to nitrogen-containing pollutants such as NO, NO_2, N_2O, NH_3, and HCN. The formation of pollutant species depends principally on the temperature, fuel/ oxygen ratio in the combustion zone and swirl settings [105]. NO_x from combustion systems results from three main processes: thermal NO, prompt NO, and fuel NO.

i) Thermal NO_x:

Thermal NO_x forms from oxidation of atmospheric nitrogen at relatively high temperatures in fuel-lean environments, and is strongly temperature-dependent. This process is described by the widely-accepted, extended Zeldovich three-step mechanism:

$$N_2 + O \underset{K_{-1}}{\overset{K_1}{\Leftrightarrow}} NO + N \,,$$

$$N + O_2 \underset{K_{-2}}{\overset{K_2}{\Leftrightarrow}} NO + O \text{, and}$$

$$N + OH \underset{K_{-3}}{\overset{K_3}{\Leftrightarrow}} NO + H \,.$$

The overall rate for thermal NO_x formation is:

$$\frac{d[NO]}{dt} = 2[O]\left\{\frac{K_1 N_2 - K_{-1}K_{-2}[NO]^2 \Big/ K_2[O_2]}{1 + K_{-1}[NO] \Big/ K_2[O_2] + K_3[OH]}\right\}. \qquad \textbf{2.6}$$

A simplified expression is obtained by assuming the initial concentrations of NO and OH is low so that only the forward rates of the Zeldovich mechanism are significant. The simplified production rate of thermal NO_x becomes:

$$\frac{d[NO]}{dt} = 2K_1[O][N_2], \qquad \textbf{2.7}$$

where concentration of oxygen atoms [O] is assumed to be in equilibrium with O_2 according to the correlation:

$$[O] = K'[O_2].$$

Thus, overall, rate expression becomes:

$$\frac{d[NO]}{dt} = 2K_1K'[O_2][N_2] \quad \text{or} \quad \frac{d[NO]}{dt} = K[O_2][N_2]. \qquad \textbf{2.8}$$

This is the expression used in the current model, and the rate parameter for this reaction is taken from Miller and Bowman [106].

ii) Prompt NO_x:

Prompt NO_x formation occurs from the reaction of atmospheric nitrogen with hydrocarbon radicals in fuel-rich regions of flames. Many NO_x models neglect Prompt NO_x reactions due to the increased complexity of the nitrogen chemistry and also due to the intimate coupling of these reactions with the fuel oxidation steps [107]. In addition, prompt NO_x is only significant in very fuel-rich systems, and is a small portion of the total NO_x formed in most combustion systems [104]. Therefore, contributions from this route are neglected in the current model.

iii) Fuel NO_x:

Although the route leading to fuel NO_x formation and destruction is still not completely understood, various investigators seem to agree on a simplified model as shown in Figure **2-5** [108-110].

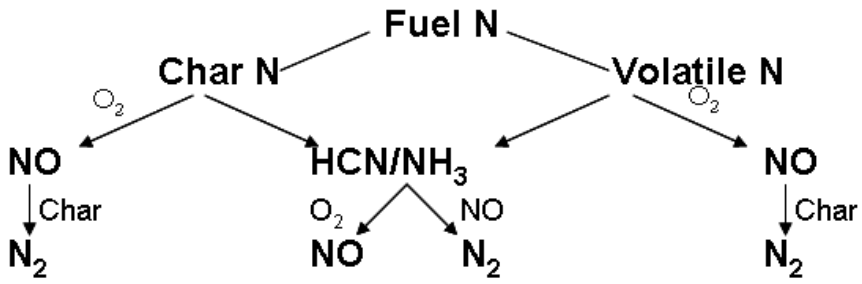

Figure **2-5**: Coal-N conversion mechanism available in FLUENT^{TM} to model NO_x

A realistic assumption used in the model is proportionality between the release rate of fuel nitrogen into the gas phase and the devolatilization rate. Distribution of coal-N between char and volatile matter is approximated in the ratio of volatile and char fractions. Coal-N was assumed to evolve as HCN during the pyrolysis. Char-N is assumed to evolve as NO on the basis that most of the char-N will be evolving in the oxidizing environment. Fuel NO_x forms through the reaction of HCN with O_2 and reduces from the reaction of HCN with NO. These assumptions are made to simplify the overall NOx formation from fuel-N and have been used by many numerical studies [111, 112]. The reaction mechanism is based on the global reaction proposed by De Soete. Sometimes the NO_x formed (regardless of its source) is partly reduced by the char reaction in later stages of combustion. The heterogeneous reaction of NO reduction on the char surface has been modeled according to:

$$R = KA_g P_{NO}, \qquad \textbf{2.9}$$

where, *K* is the rate coefficient for the char-NO reaction, taken from the FLUENT™ default database. A_g is surface area, taken as 100,000 m^2/kg (average measured value on char samples during the experiments) and P_{NO} is the mean NO partial pressure (atm).

Thermal and prompt NO_x formation mechanisms automatically de-activate in the absence of molecular nitrogen for oxy-coal combustion. Calculation of NO_x formation occurs in a “post-processing" mode, with the flow field, temperature and hydrocarbon combustion species concentrations fixed. Prediction of NO_x in this mode is justified on the grounds that the NO concentrations are very low and have negligible impact on the hydrocarbon combustion prediction.

Discretization Scheme

Sometimes, existence of strong gradients, especially at an angle to the computational grid, can lead to numerical errors in the discrete representation of the continuous phase. Truncation errors can be introduced into the calculations due to the inability of the grid to accurately represent the string gradients that may exist in some regions of the solution. Instead of using a power-law differencing scheme, a higher order quadratic upwind interpolation scheme, QUICK, was used in the furnace model to reduce the errors of this sort. By using QUICK, computational time increased, but the gradients in the flow had better resolutions.

Convergence Criteria

No universal metrics for judging convergence exist. Residual definitions that are useful for one class of problem are sometimes misleading for other classes of problems. Therefore, judging the convergence occurs not only by examining residual levels, but also by monitoring relevant integrated quantities and checking for mass and energy balances. To evaluate whether convergence has been reached, the indicators used during the current simulation are:

1) *The residuals have decreased to a sufficient degree as established in the model set-up.* The criterion employed in the present study is that each residual should be reduced to a value of less than 10^{-3}, except the energy and the P_1 (used in the radiation model) residual for which the criterion is 10^{-6}.

2) *The solution no longer changes with further iterations.* Sometimes the residuals may not fall below the convergence criterion set in the case set-up. However, monitoring the representative flow variables through iterations may show that the residuals have stagnated and do not change with further iterations. In the present study, temperature and oxygen mass fraction on a mass weighted area average basis at the exit of the boiler or DTR were chosen as a monitoring points for better indication of convergence. A difference of (+/-) 5K in temperature and (+/-) 0.05% in oxygen mass fraction was the criteria employed to ensure convergence between successive runs. To ensure acceptable reproducibility in char burnout, large numbers of particle streams were tracked. Also, an established assurance verified that NO_x and CO exit values did not change by more than 5 ppm between successive runs.

3) *The overall mass, momentum, energy, and scalar balances are obtained.* This examination occurs in the overall mass and energy balances in the "Flux Reports" panel of FLUENT^{TM}. Typically, net heat and mass imbalance should be less than 0.2% of the net flux through the domain when the solution has converged. Both of these imbalances were ensured by comparing the net flux in the gas domain with the flux coming from particle domain.

Reactor Grid

For the pilot-scale boiler, areas of primary and secondary inlets of the burner are projected onto the input boundary plane of the burner, with primary and secondary outlet diameters of 2.5 inches and 8 inches, respectively. A central oil gun of 1-inch diameter is located inside the primary inlet. Three-dimensional furnace geometry was created using a GAMBIT 2.2 version and is shown in Figure **2-6**. The selected mesh is finer near the burner and also near the furnace wall. The meshed geometry consists of ~15326 cells and 32688 faces. Largest volume of a cell in the grid is ~ 137 mm^3 representing cell dimension of ~5 mm. Only a quarter section of the boiler was modeled using an axi-symmetry assumption. This was necessary to reduce the computational time so that the sensitivity analysis of various parameters involved in the model could be completed.

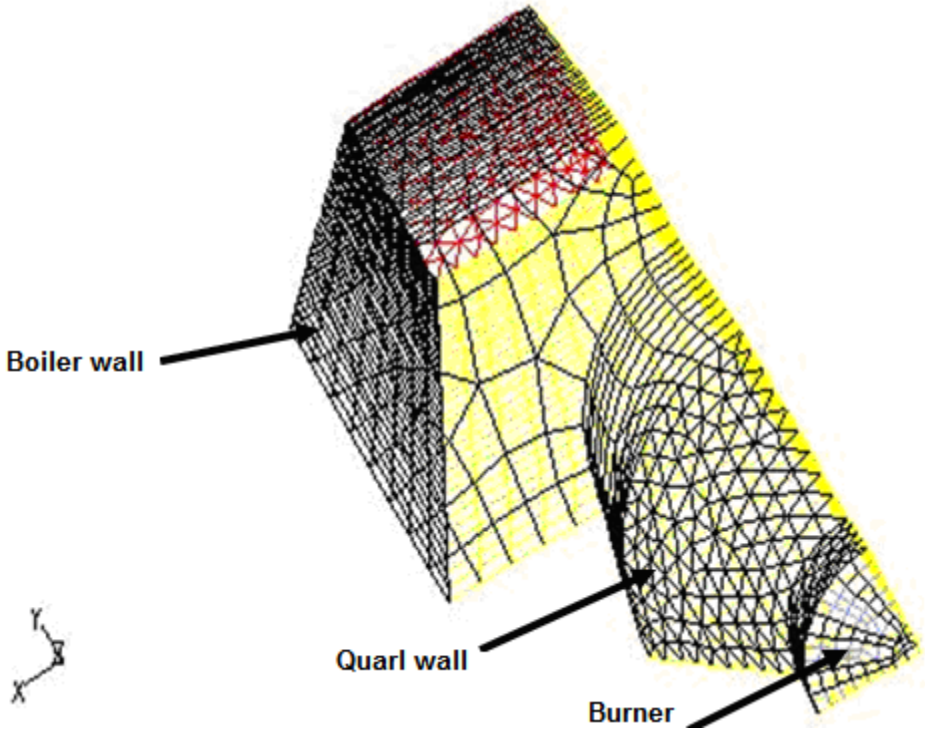

Figure **2-6**: Grid geometry of research boiler

The DTR furnace was modeled with 2-D coordinates using axi-symmetry around the centerline as shown in Figure **2-7**. The DTR grid consists of 50 cells in length and 10 cells in radius. This grid involves two inlets: one for coal laden primary gas (3 mm dia) and another for secondary gas. A furnace length of 50 cm and diameter of 6.3 cm was used.

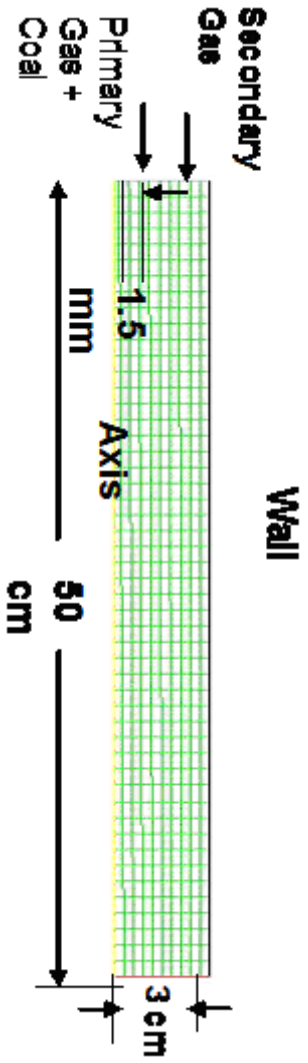

Figure **2-7**: Grid geometry of drop tube reactor

Boundary Conditions

In the model, coal particles are injected with primary air. The poly-disperse distribution of coal is segmented into discrete particle groups, assuming a Rosin–Rammler distribution. The parameters used for the coal pyrolysis and char combustion

model are derived from the experimental measurement in the DTR and in a TGA, respectively. FLUENT^{TM} provides an option for addition of extra species for the oxidizer stream, which is useful in case of oxy-combustion, which includes CO_2 and H_2O along with O_2. The model naturally adjusts to give the proper radiative properties for the gas medium consisting of O_2/CO_2 based on the concentrations of CO, H_2O and CO_2.

For the pilot-scale boiler, the input boundary conditions are the furnace wall temperature, set at 600 K, and a wall emissivity of 0.7. Quarl wall temperature, set at 1,300 K, is an average measured value during the experiment (refer to Table **2-4**). Input mass flow rate and temperature at each inlet was taken from the operating conditions of the test as shown in Table **2-4**. Due to the absence of flow measurement, a velocity component at burner inlet was calculated from the geometry of the swirler. In the boiler, swirl is imparted at the burner inlet using an axial vane type swirler. These vanes are at an angle (Φ) of 60 degrees. Approximate swirl number (SN) for this type of swirler is calculated using [113]:

$$SN = \frac{2}{3}\tan\Phi\left|\frac{1-\left(R_i/R_o\right)^3}{1-\left(R_i/R_o\right)^2}\right|, \qquad \textbf{2.10}$$

where, R_i is inner radius of the swirler, and R_o is outer radius of the swirler. It must be noted that, both primary and secondary air is fed through the swirler. Based on the above equation, the swirl number for primary and secondary air is estimated to be 1.46 and 1.27 respectively. Also, a portion of the swirler completely blocks the flow (as shown in Figure **2-4**) which was modeled as part of the wall of the burner face. In this study,

tangential and axial component of velocity was provided at the burner inlet according to 60 degree vane angle.

For the DTR, the temperature boundary condition on the furnace wall is determined by an iterative procedure such that the measured gas temperatures using suction pyrometer along the DTR length matched with the predicted gas temperature. Particle and gas flow conditions are chosen as described in the testing section. The predicted gas temperature is shown in Figure **2-2** along with experimental measurements. The empirical equation for the wall boundary condition in the non-isothermal zone, derived using an iterative procedure, is:

$$T_w(x) = (T_w\text{-}873)*X /(0.2). \qquad \textbf{2.11}$$

where, T_w = furnace wall temperature, and X = the distance from the injector in a non-isothermal zone, (m).

Chapter 3

Comparison of Coal Pyrolysis in a Reactive CO_2 and Inert Gas Medium

Introduction

In modeling studies related to oxy-coal combustion, the frequent assumption is that coal pyrolysis behavior in an O_2/CO_2 gas environment is the same as combustion in air and has been recognized as one of the area where research efforts are needed [56]. So far, experimental studies in oxy-coal combustion have addressed issues such as CO, NO_x emissions and char burnout, but very few studies determine whether or not pyrolyzing the coal particles in CO_2 is different from pyrolyzing in an inert gas medium. Few studies have been published over the years which addressed the effects of gas atmosphere on coal's pyrolysis behavior and are described below.

Banerjee et al. [114] reported higher concentration of olefins and higher yields of gas products during pyrolysis in Ar and N_2 atmospheres for three different coal samples as compared to *in vacuo* pyrolysis. The proposal was that the presence of an inert gas during pyrolysis promotes the fragmentation of primary free radicals and prevents collision between primary free radicals. Apparently, no clear distinction can be made from the reported data on yields and gas composition about the role of inert (Ar versus N_2) pyrolysis atmospheres.

Eltawil et al. [115] observed differences in physical properties of a sub-bituminous char (prepared in He gas) upon reheating in He and N_2 gases. The authors reported an

unexpectedly large increase in macropore volume for the sample reheated in He compared to sample reheated in N_2. These researchers were surprised by this result because no difference in additional weight loss appeared from use of the two media, and the changes in physical properties were largely in helium but not in N_2. In a follow-up study, they also observed that the inert environment employed during reheating affected adsorptive capacity, surface area, porous volume, and gasification reactivity of the reheated char samples. These measured values were in the order of He > Ar > N_2 atmospheres [69]. The authors suspected that the difference in trace amounts of O_2 impurities in the He gas cylinder (used in initial char preparation step) caused the changes. Dugwell and co-workers [116] also observed that a char prepared in N_2 had lower reactivity than the corresponding char produced under He. However, that study proposed no explanation.

Walker et al. [117] investigated the role of "inert" diluents on the rate of C-CO_2 at 1,373 K and C-O_2 reactions at 889 K. Rate of reaction for both of these reactions followed in the order of medium containing Xe > N_2 > Ar > He > no diluents. These researchers suggested that heavier diluents of gases might have interacted with the active complex such that the activation energy for desorption decreased. Another proposed explanation was that the heavier gases might have slowed the re-hybridization of nascent carbon sites, and thus the char was more reactive.

However, a change from an inert gas to a reactive medium can alter coal pyrolysis behavior because of reaction of reactive gas medium with the pyrolyzing coal or evolved volatile radical species. The effect of reactive H_2 gas in comparison to inert gas during coal pyrolysis in enhancing the volatile yield is well documented [118]. Jenkins and

Morgan [119] found an increase in weight loss from a lignite coal during pyrolysis in a drop tube reactor (DTR) at 1,173 K in atmospheres of wet nitrogen, and CO_2 compared to that of dry N_2. The increase in weight loss was attributed to the reaction of released volatile matter with the reactive pyrolysis medium, and thus, a reduction in secondary condensation and re-deposition of evolved volatile species. Reaction between pyrolysis gas with coal particles was considered to be negligible for the two reasons: First, the rate of C-H_2O or C-CO_2 reaction measured in a Thermogravimetric Analyzer (TGA) at a temperature of 1,173 K was much lower (5 g/g-h) than the rate of additional weight loss observed in DTR (860 g/g-h). Second, the ultimate weight loss values for the acid washed coal samples were the same for the three media employed.

In some of the studies where chars from pyrolysis were gasified *in-situ* with H_2O or CO_2, the suggestion was that the gasification reaction contributed to the gas evolution in the early period of temperature holding time [120-122]. Peng et al. [123] compared reactivity of in-situ gasified coals (lignite, sub-bituminous and bituminous rank coal) with those of chars from the same coals, prepared in N_2 under similar reaction conditions. The research was carried out at atmospheric pressure in a thermogravimetric balance, operated under steam and N_2 mixtures (76 % mol steam), at temperatures between 1,273 K and 1,673 K. Measurement of initial reactivity of the chars generated during direct gasification experiments were higher (~ six times) than those of corresponding chars prepared in nitrogen. The observed higher reactivity for *in-situ* char samples was proposed to be due to differences in microstructural rearrangements caused by steam interaction with the pyrolyzing coal particles.

Recently, Messenbock et al. [124] studied flash pyrolysis of a bituminous coal in three different atmospheres (He, steam, and CO_2) at 1 MPa. The peak temperature, heating rates, and holding times were 1,273 K, 1,000 K/s and 0–60 s, respectively. A negligible increase in total volatile yield during the initial heating period occurred when the gas atmosphere changed from either He to CO_2 or from He to steam. But afterwards, the reactive gases caused weight loss at a much higher rate (10-20 g/g-h) than the expected rates (5-10 g/g-h) based on the previous reports of char gasification [125].

Hayashi and co-workers [126-129] extensively studied the role of reactive gas atmosphere (steam/CO_2) on the nascent char reactivity, and the interaction of the gas medium with evolved volatile species from a brown coal. In a DTR study conducted at a temperature of 1,173 K, an additional weight loss of ~17% was measured within 4.3 sec during steam pyrolysis of coal as compared to an inert pyrolysis in N_2. Reports indicated similar high reactivity of a nascent char in the case of a pyrolysis medium consisting of a CO_2 atmosphere [128]. Such a significantly higher conversion rate (~120 g/g-h) was attributed to the catalytic char gasification reaction caused by inherent alkali species such as Na, Ca in the coal [126]. One of the Hayashi, et al. [68] studies attempted to understand the effect of a gas atmosphere surrounding coal/char particles on formation of NO_x precursor species such as HCN/NH_3. Three ranks of coal with different petrographic compositions were gasified in H_2O/CO_2 and pyrolyzed in Ar in a DTR at temperatures up to 1,173 K. One of the significant conclusions was the proposition that the chemisorption of CO_2 on the N-sites of nascent char surface may block access to N-sites for the -H radicals to form HCN and NH_3 [127]. On the other hand, a significant enhancement in NH_3 concentration

occurred during steam gasification, caused by the observed increase in -H radicals.. This implies that the char generated in CO_2 medium retains more coal-N.

Recently, Senneca and Salatino [130], addressed the influence of oxidizing versus inert atmosphere on the rate and extent of thermal annealing. They proposed that the presence of oxygen during heat-treatment of carbon hinders the development of structural anisotropy in carbon, and thus causes an increase in char combustion reactivity. This result suggested the cause to be the formation of a stable oxide complex on the carbon's surface during oxidative heat treatment. However, such effects appeared to diminish above 1,473 K.

In a very recent research report, Borrego and Alvarez [131] prepared chars from a highly volatile and a low volatile bituminous coal in O_2/CO_2 and O_2/N_2 environments in a DTR operating at 1,573 K. They observed that the chars from both coal types were similar in terms of subsequent reactivity and micropore surface area (determined by Dubinin-Radushkevitch [DR] method using CO_2 adsorption). However, an increase in mesopore surface area (determined by Brunauer-Emmett-Teller [BET] method using N_2 adsorption) appeared for the char prepared in O_2/CO_2 media as compared to the O_2/N_2 char. The difference in BET surface area for the char prepared in the two media was suggested to have an important implication for the diffusion controlled rate regime of carbon oxidation. These researchers also observed lower weight loss during pyrolysis in CO_2 gas than for pyrolysis in an N_2 gas medium. This was suggested to be caused by participation of CO_2 participating in cross-linking reaction which prevents coalescence of aromatic clusters. This result appears to be in contradiction to several published studies (as described earlier in the chapter) which reports a higher weight loss in a CO_2 medium.

Also, based on the reasoning of Borrego and Alvarez [131], the expectation would be that the reactivity of the resultant disordered char sample (prepared in CO_2) is higher than the corresponding char prepared in N_2 [132]. To the contrary of the expectation, the authors measured the same reactivity for the two char samples.

In summary, some studies observed that the char prepared in He had higher reactivity than the char prepared in N_2 [69, 116]. Unfortunately, no explanation was forthcoming from these studies to clarify the plausible reasons behind such an observation. Most of the studies have recorded higher weight loss during pyrolysis in a CO_2 medium as compared to pyrolysis in an inert gas [119, 128, 133]. However, disagreement exists over the magnitude and mechanism (secondary [119] versus direct gasification [129]) by which CO_2 causes an additional weight loss during coal pyrolysis. The role of CO_2 during pyrolysis on the split of coal-N into volatile and char fractions, and surface areas and reactivities of resultant char samples remain uncertain. Knowledge of all of these factors is essential for accurate prediction of NO_x and char burnout from oxy-coal combustion.

Objectives

The specific objectives of this part of the study are to:

1. Quantify the effect of CO_2 during coal pyrolysis on weight loss, and
2. Compare the effect of pyrolysis in CO_2 *versus* inert medium on properties of resultant char and distribution of coal-N into volatile and char fractions.

Methodology

In the present work, char particles are produced in a drop tube reactor (DTR) at different furnace temperatures (1,173 K-1,673 K) in Ar gas or CO_2 gas atmospheres. Details of the DTR test facility and operating conditions are provided in Chapter 2. A high volatile (hvCb) coal and a low volatile (lvb) coal are the selected samples (to represent bituminous coal range) used in this study. The hvCb coal with particle sizes between (74-90 μm), and the lvb coal with particle sizes between (74-112 μm) were obtained by wet sieving. Proximate analysis of the coal and the resultant char particles is presented in Table 3-1. The gas medium-temperature (K) denotes the resultant char samples For example; a char sample produced in Ar medium at 1,373 K is denoted as, Ar-1373.

Table **3-1**: Proximate analysis of a hvCb coal (-170+200 mesh) and char samples

	Moisture (%)	Fixed Carbon (%dry)	Vol. Matter (%dry)	Ash (%dry)	C (%)	H (%)	N (%)
Coal	3.36	51.84	39.68	8.48	69.93	5.16	1.25
Ar_1173	1.37	61.45	27.89	10.66	72.20	3.57	1.25
CO_2_1173	1.37	62.31	26.99	10.70	72.20	3.50	1.28
Ar_1373	1.82	73.57	14.75	11.68	76.85	2.37	1.31
CO_2_1373	1.33	70.34	16.47	13.19	76.20	2.32	1.32
Ar_1573	1.59	81.03	6.48	12.49	79.55	1.35	1.19
CO_2_1573	0.71	77.10	7.22	14.68	76.50	1.36	1.19
Ar_1673	1.06	82.38	4.09	13.53	79.73	1.00	1.12
CO2_1673	0.90	79.24	5.20	15.49	73.60	1.18	1.13

Since the collection efficiency of the probe was less than 100% in the DTR tests, a direct measurement of weight loss was not possible. Therefore, weight loss is calculated using ash as a tracer technique [76]. The use of the technique involves various

assumptions; for example the mineral matter transformations occurring in the high heating rate of DTR and the low heating rate of the proximate analyzer are similar. However, the use of this approach is justifiable on the basis that comparison is made at a single temperature in two gas media where transformations of the mineral matter should be similar. Table 3-1 also includes the ultimate analysis of the coal and the resultant char samples tested in the two gas media. Surface area calculation uses the BET method by N_2 adsorption experiments at 77 K. Reactivity measurement occurs by a thermogravimetric analysis (TGA) using a Perkin-Elmer TGA-7 instrument to compare the relative reactivity of DTR produced char samples from the two pyrolysis media.

Char Reactivity Measurement Procedure

Typically, reactivity measurement uses a sample mass of about ~2-3 mg and an operating temperature of 673 K. Purging the TGA system with N_2 at 100 mL/min at room temperature for about 30 minutes removes any air contamination in the system. The reactor is then heated to the reaction temperature at 20 K/ min increments. The sample is held at the reaction temperature for ~5 minutes to establish a thermal equilibrium before switching to an air flow of 100 mL/min. Weight change is monitored as a function of time, and ash yield of the sample is measured for each run by raising the temperature to 1,123 K. The measured data are converted on a dry ash free (daf) basis, and rate, as a function of conversion, is calculated for each sample.

Results and Discussion

Since a few studies have found that the physical properties of the produced char samples depend on the pyrolysis medium employed [69, 131], a theoretical analysis is conducted to understand the difference in coal particle heat-up rate caused by the changes in thermal properties of pyrolysis media. The analysis indicated that coal particle heat-up rate in the DTR depends upon the thermal conductivity of the pyrolysis medium and the gas temperature (shown in Appendix 3-1). Also well known is that CO_2 gas emits and absorbs radiation [134]; whereas, Ar gas does not, and this difference may cause different surrounding gas temperatures in the vicinity of coal particles. The thermal properties of some of the gases as a function of temperature are taken from the literature [135] (shown in Table **3-2**). Thermal conductivity data shows that coal particle heat-up rate in CO_2 can be higher by a factor of ~2 compared to that in Ar gas.

Table **3-2**: Data of physical properties of gases as a function of temperature [135]

Temperature (K)		573	873	1173	1473	1873	2073
	ρ (gm/cc)	1.177	0.588	0.392	0.294	0.235	0.196
Air	Cp (J/KgK)	1.006	1.051	1.121	1.179	1.231	1.288
	K (W/mK)	0.026	0.047	0.063			
	ρ (gm/cc)	1.623	0.811	0.54	0.405	0.324	0.27
Ar	Cp (J/KgK)	0.521	0.52	0.52	0.52	0.52	0.52
	K (W/cmK)	0.018	0.03	0.04	0.048	0.055	0.064
	ρ (gm/cc)	1.797	0.894	0.596	0.446	0.357	0.304
CO_2	Cp (J/KgK)	0.853	1.077	1.205	1.281	1.327	1.355
	K (W/cmK)	0.017	0.043	0.063	0.079	0.095	0.103

In order to understand the influence of radiation, particle temperature profiles during the pyrolysis in the two gas media are predicted using a computational fluid dynamics (CFD) tool FLUENT^{TM} (details of which appear in Chapter 2). Figure **3-1** shows the comparison of computed particle temperatures in the two media at a furnace wall temperature of 1,673 K. These profiles in Figure **3-1** show that the particle heat-up rate in CO_2 is slightly faster compared to that of Ar medium, and the final particle temperature attained by coal particles in CO_2 medium is ~20 K higher than that in Ar gas. The radiative property of CO_2 apparently has negligible effect on particle temperatures.

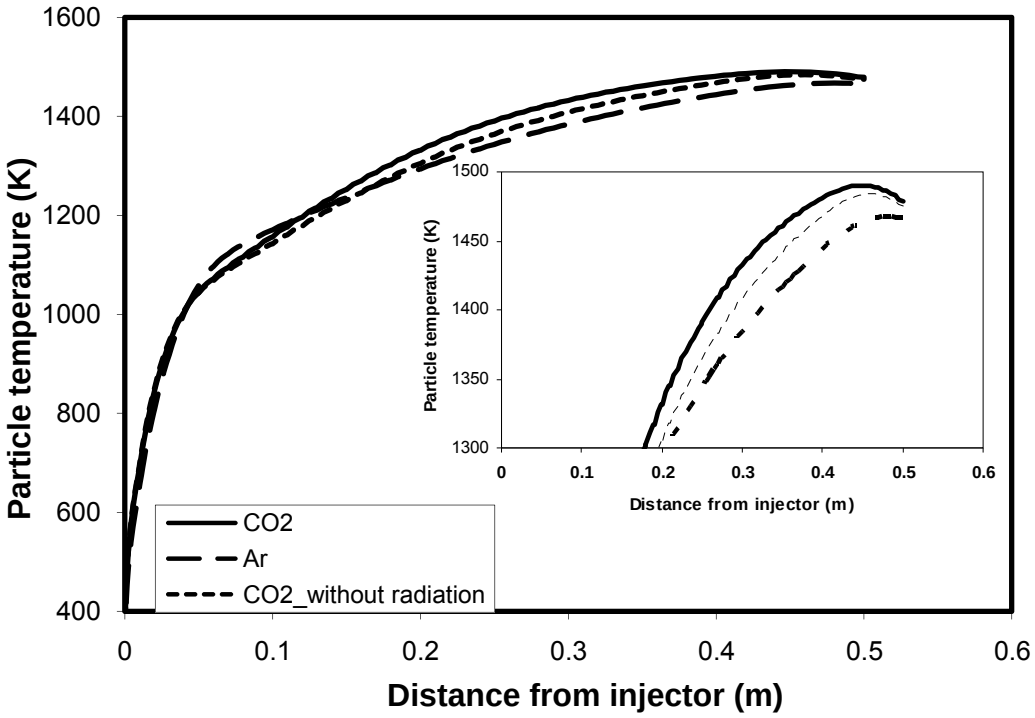

Figure **3-1**: Effect of pyrolysis gas medium on particle temperature profile at 1,673 K

Therefore, predicted minimal increase in particle heat-up rate and final particle temperature in CO_2 medium compared to that of inert Ar medium is expected to cause

negligible change in char properties. The weight loss is plotted against ASTM volatile matter loss in these two pyrolysis gas media and is shown in Figure **3-2**. Similar weight loss (22.57%) at 1,173 K in the two gas media suggests that switching the gas from an inert Ar to a reactive CO_2 does not affect the pyrolysis at such lower temperatures. However, at higher temperatures (for example at 1,673 K), a higher weight loss does occur in a CO_2 medium (49.18%) as compared to an Ar medium (40.22%).

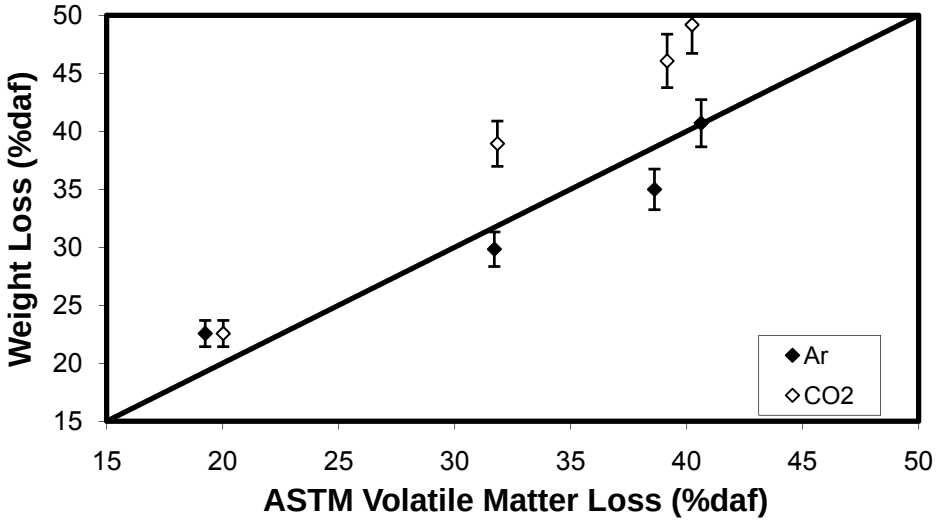

Figure **3-2**: Comparison of the weight loss in Ar and CO_2 medium during pyrolysis

In order to investigate whether the additional weight loss is the result of C-CO_2 reaction or due to changes in the gas phase chemistry, weight loss value is calculated by employing the intrinsic rate parameter of char-CO_2 reaction. The intrinsic rate parameter of char-CO_2 reaction for both coal types is determined in a TGA (details appear in Chapter 4). Table **3-3** shows the measured and predicted weight loss values. The data indicates that the observed additional weight loss for hvCb rank coal particles at 1,673 K in a CO_2 medium compared to that in an Ar medium is marginally higher (9.24%) than

the calculated weight loss (2.78%) caused by C-CO_2 reaction. An increase in rate by a factor of 2 in prediction yields about the same weight loss as measured in the experiment. For the lvb coal, predicted and measured weight loss at 1,673 K is nearly the same. Since various studies have suggested that a nascent char in the DTR is more reactive than a thermally stabilized char [136], the additional weight loss observed during pyrolysis in CO_2 can be considered to be caused by char-CO_2 reaction. This result is in agreement with the observation of Messenbock et al. [124] and is in contrast to the proposition in which observed additional weight loss in reactive CO_2/H_2O medium was attributed to the reduction in secondary gas phase reactions [119].

Table **3-3**: Additional weight loss during coal pyrolysis due to char-CO_2 reaction

	Temperature (K)	**1573**	**1673**
hvCb coal	ΔW (%) Measured	4.23(±2.5)	9.24(±2.5)
	ΔW (%) Predicted using R	1.1	2.78
	ΔW (%) Predicted using R*2	4.59	7.98
lvb coal	ΔW (%) Measured	4.56(±2.5)	8.45 (±2.5)
	ΔW (%) Predicted using R	3.2	7.45

R is rate measured in TGA for char gasification reaction

It is important to distinguish the effect of pyrolysis gas medium on the coal-N distribution between the volatile and char fraction for NO_x modeling purpose. Therefore, the N/C ratio and weight loss of the samples is plotted against furnace temperature and is shown in Figure **3-3** for both ranks of coal. A lower N/C ratio of the char sample (0.015) compared to that of the coal sample (0.018) shows that the fraction of coal-N released in the gas phase is higher as compared to the volatile yield. This result is observed for both the pyrolyzing gas media. Also seen is that for both ranks of coal, a significant increase (by 20%) in N/C ratio occur at higher temperatures (1,673 K) in CO_2 as compared to pyrolysis in Ar.

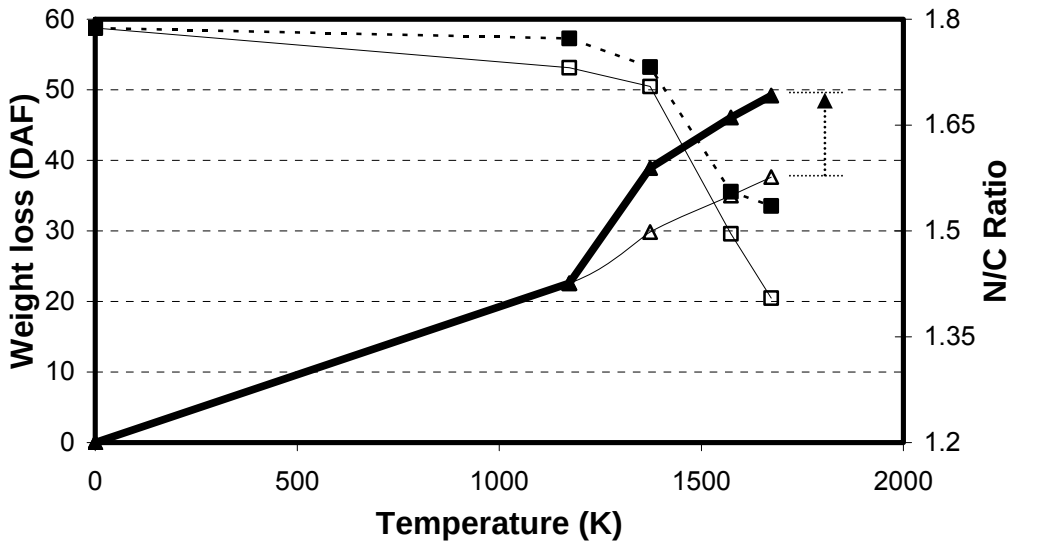

(a)

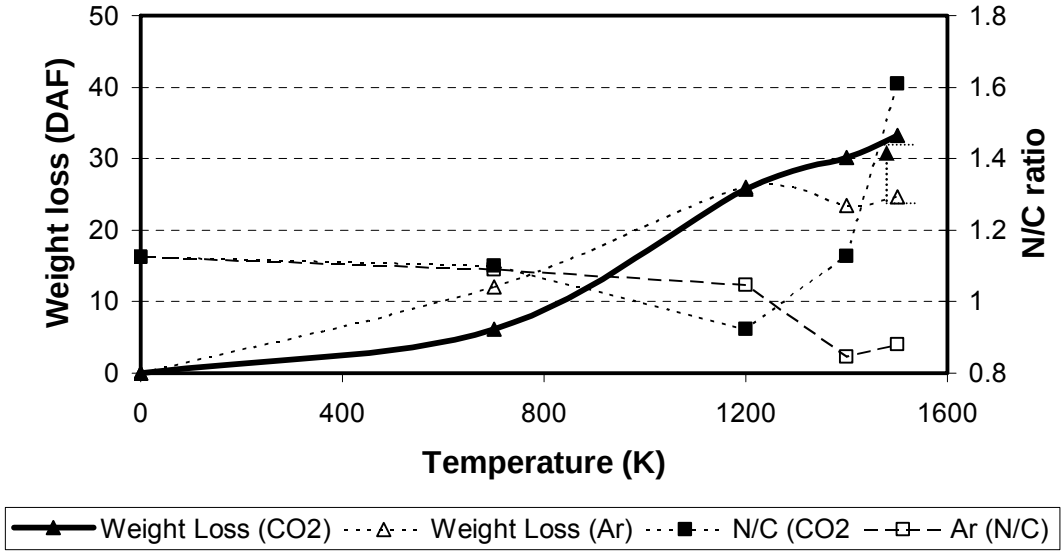

(b)

Figure **3-3**: Effect of pyrolysis gas medium on split of coal-N into volatile and char fraction (a) hvCb coal; (b) lvb coal

This increase may occur because of higher carbon loss due to gasification reaction. A partial support for this reasoning is also found from the CHN analysis where the C value of char pyrolyzed in CO_2 is less (73.6%) than that of char prepared in Ar

(79.55%) at higher a temperature (1,673 K) but is similar at a lower temperature (up to 1,373 K). Rate versus conversion profiles of these char samples, obtained from the TGA are shown in Figure **3-4**.

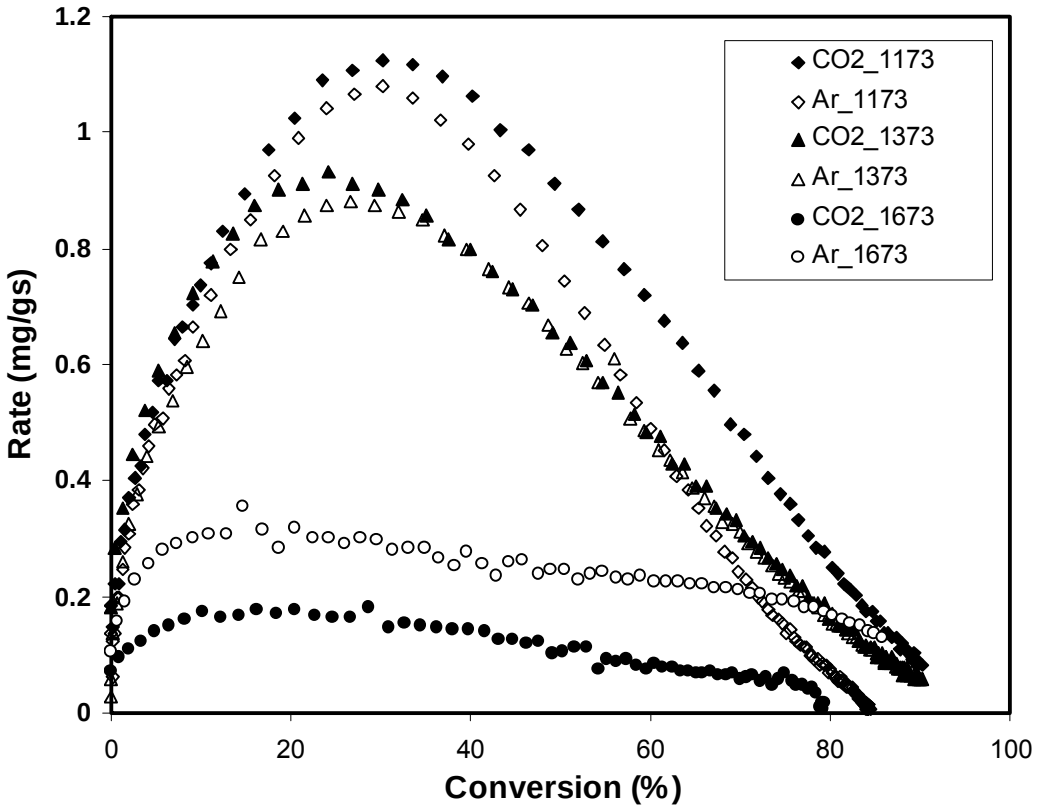

Figure **3-4**: Reactivity profiles measured in air at 673 K for DTR pyrolyzed chars generated at different temperature

An excellent match of the reactivity profile for the char generated at the same temperatures in two gas media indicates that the chars have similar combustion characteristics. Slight differences observed in the rate profile for the chars generated at 1,673 K are likely due to additional weight loss of the CO_2-1673 sample. Similar observations of a decrease in char reactivity with an increase in prior mass loss have been

reported in the literature [137]. In order to further investigate this possibility, the coal particles are pyrolyzed at 1,373 K in the DTR for two different residence times (0.55 sec and 0.4 sec) in Ar gas medium which had prior weight loss (daf) of 43% and 38%, respectively. Reactivity profiles of the resultant char samples show that the char sample whose prior weight loss was more, had 15% lower reactivity than the other char sample, as shown in Figure **3-5.**

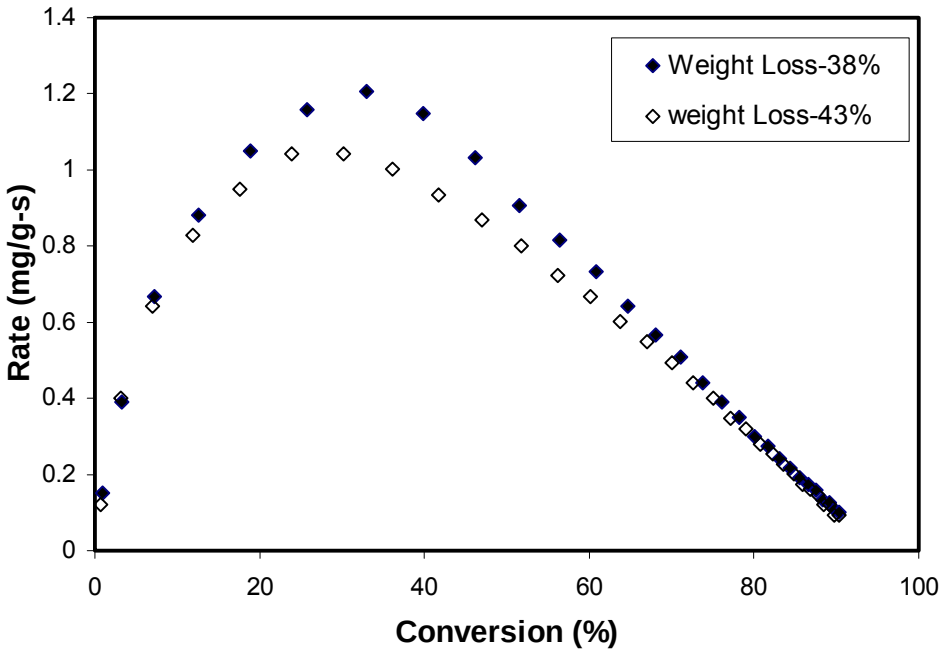

Figure **3-5**: Effect of prior weight loss on reactivity of char sample generated at 1,373 K in Ar

Overall these results suggest that char reactivity of the sample generated in CO_2 is similar to those of char generated in an Ar gas medium. It has been proposed that despite the same reactivity in a kinetically controlled regime (Zone I) conditions, a different physical structure might lead to a change in combustion rate in actual combustion conditions [131]. Therefore, physical properties (BET surface area, and pore volumes) of the

char samples are measured, and are provided in Table **3-4**. The data show that the BET surface area and pore volume of the char samples generated at lower temperatures (up to 1,373 K) in CO_2 medium (5 m^2/g and 0.01 cm^3/g) are similar to the chars generated in Ar medium (5 m^2/g and 0.004 cm^3/g). However, larger BET surface areas and pore volumes occur for the chars generated at higher temperatures (1,673 K) in CO_2 medium (181 m^2/g and 0.125 cm^3/g), as compared to the corresponding chars prepared in Ar medium (11 m^2/g and 0.019 cm^3/g).

Table **3-4**: Comparison of physical properties of hvCb char generated in Ar and CO_2 gas

		BET Analysis		Crystallite Size	
	Helium Density (cm^3/g)	Average Pore Volume (cm^3/g)	Surface Area (m^2/g)	L_a (*A*º)	L_c (*A*º)
Coal	1.37				
Ar_ 1173	1.19	0.00132	0.77	8	8
CO_2 1173	1.25	Not detectable	Not detectable	8	9
Ar_ 1373	1.36	0.0043	5		
CO_2 1373	1.45	0.0102	5		
Ar_ 1573	1.46	0.0137	9		
CO_2 1573	1.65	0.0627	160		
Ar_ 1673	1.59	0.0196	11	11	16
CO_2_ 1673	1.78	0.125	181	13	18

These results show a higher surface area for the sample prepared in CO_2,; this result is in agreement with Borrego and Alvarez [131], but the reason is due to additional C-CO_2 reaction. Notably, for both char series, the reactivity of the char samples decreases as the pyrolysis Heat Treatment Temperature (HTT) increases, despite an increase in surface area (shown in Figure **3-6)**.

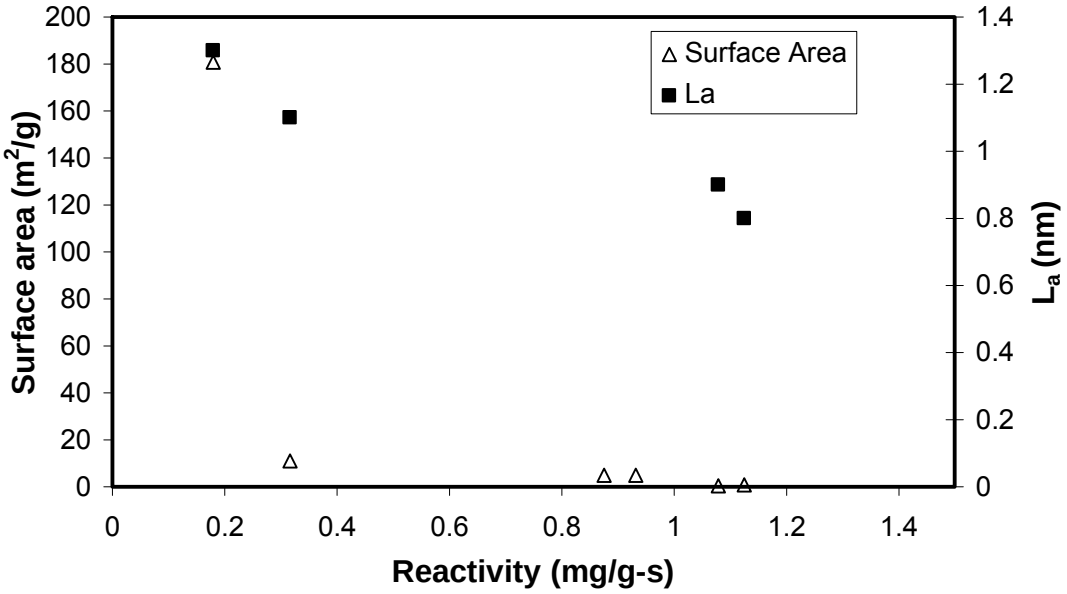

Figure **3-6**: Correlation of reactivity with physical properties of char

The decrease of reactivity with temperature is consistent with the observed increase in structural order, as indicated by both the increase in helium density and crystallite size (L_a and L_c) values. This result is in direct contrast to many studies in which a positive correlation between surface area and reactivity has been found [138, 139] and is in agreement with studies where no generic correlation has been found [140-142].

Summary and Conclusions

The main objective of this research is to determine whether or not pyrolyzing coal particles in CO_2 compared to pyrolysis in Ar affects the reactivity and split of coal-N between volatile and char fractions. In the present study, coal particles, were pyrolyzed in Ar and CO_2 gas media in a drop tube reactor (DTR), operating at 1,173-1,673 K, and a

CFD analysis was conducted to determine particles' temperatures and additional weight losses due to the presence of CO_2. A minimal increase in particle heat-up rate and final particle temperature was the prediction for a CO_2 medium, as compared to Ar gas. This environment appears to cause negligible effect on the reactivity of resultant char samples. The higher weight loss observed for the coal particles in CO_2 media, as compared to that of Ar media for both ranks of coal appears to be the result of char-CO_2 reaction. The increase in prior weight loss during pyrolysis was responsible for a lower reactivity of char generated in CO_2, as compared to that of Ar. Similar surface area and pore volume occurred for both series of chars prepared at lower temperatures. However, a large increase did evolve for both the surface area and pore volume for the char generated in CO_2 than did for the corresponding char prepared in Ar at higher temperatures. This increase in surface area is attributable to the pore widening caused by the char-CO_2 reaction. Both series of chars obtained at lower temperatures had remarkably similar apparent reactivity. Apparently, the reactivity of resultant char samples decreases with an increase in structure order despite an increase in BET surface area. Overall, results obtained in the study indicate that the reactivity of resultant char or coal-N release rate during pyrolysis in CO_2 is similar to that generated in an inert medium. Therefore, existing knowledge of pyrolysis of bituminous coal ranks can be conveniently used in CFD models to predict char burnout and NO_x emissions or any other aspect of coal combustion.

Chapter 4

Determination of Intrinsic Rate Parameters for Char-O_2 and Char-CO_2 Reactions

Introduction

For the char burnout predictions in combustion conditions using an intrinsic approach, accurate knowledge of intrinsic activation energy is of utmost importance because this indicates the reaction rate's sensitivity to temperature. Sometimes, an arbitrary temperature, for example 823 K, is used to compare the relative ranking of coals [143, 144]. However, a different ranking of coal samples' reactivity will occur for samples having different activation energies for other reference temperatures. This chapter's main objective is to determine the intrinsic rate parameter for char-O_2 and char-CO_2 reaction; therefore a brief discussion of existing methods used in determining the intrinsic rate parameter follows.

A few studies have determined intrinsic rate parameters using combustion tests conducted in high temperature conditions of an entrained flow reactor (EFR) [41, 93, 145]. However, apparently small differences in experimental conditions and modeling assumptions could lead to different parameters [146], and therefore parameters deduced using this method may not be accurate. On the other hand, thermogravimetric analysis (TGA)[§] potentially offers an attractive method of monitoring char conversion rates in controlled temperature and gas environments [147]. This analysis can be carried out in standard, commercial equipment and is rapid, inexpensive, easy to use, and gives

[§]Sometimes, TGA in this thesis is also used to refer thermogravimetric analyzer.

repeatable results. Since the current research uses this method, a more detail description of the literature relating to this method follows.

For char-oxidation rate measurement purposes, the TGA instrument is operated in either an isothermal or non-isothermal manner. Typically, the non-isothermal method is used to compare the relative rank [148] whereas; the isothermal method is used to derive the intrinsic rate parameters [72]. In an isothermal method for kinetic parameter determination, experiments are performed at sufficiently low temperatures and the resulting curve of variation in the sample mass time is then represented as a rate-conversion curve (reactivity profile). However, even while operating at reasonably lower temperatures in a TGA, in most of the reactivity plots, a maximum is observed [149]. The rate (normalized to initial sample mass) apparently increases with conversion, up to a certain conversion level, and reaches a maximum, and subsequently decreases monotonically, thereafter. The initial part up to the maximum in the reactivity plot has been suggested to be due to the building gas partial pressure [138], thereby opening previously closed pores [139], or a balance between the mass gain (because of stable complex formation) and the mass loss (because of carbon reaction) [150]. Because of the presence of a maximum in the rate profile, various methods such as, average reactivity [151-153], maximum reactivity [154], and reactivity at a fixed conversion level [62, 155] have been used in the literature to obtain the rate parameters. Sometimes, rate parameters were calculated at various conversion levels in the entire reactivity plots [140, 150, 156, 157].

Table **4-1** summarizes details of the operating conditions, methods used, and the activation energy values published in the last few years of char oxidation reaction

research[**]. Apparent from Table **4-1** is that a wide range of activation energy values have been reported for oxidation of char and porous carbon samples. In fact, for a same ASTM ranks, same seam coal, different studies report a wide range of activation energy values. For example, activation energy value from 117 kJ/mol [144] to 180 kJ/mol [158] and 110 kJ/mol [153] to 140 kJ.mol [159] are reported for a Illinois No 6 bituminous coal and a North Dakota lignite coal respectively. This shows that a value from the literature cannot be directly adopted for use in the model. This point is further highlighted by the inconsistency in reported activation energy values in the literature:

- In the same study, a different activation energies are reported for similar ASTM rank coal [144]
- In a TGA plot, estimated activation energies at various conversions reportedly remain constant with conversions [140, 150, 155, 160] or increase with conversions [161], or be a function of preheat treatment [162].
- Activation energy, reportedly is independent of pyrolysis heat treatment [163, 164], or increases with the severity of pyrolysis [161, 165, 166].
- Activation energy, reportedly, increases with carbon content of the parent coal [167] or is similar for a wide rank of chars [168, 169].

[**] Detail summary of the operating conditions and reported char gasification activation energy is included in Appendix 4-1

Table **4-1**: A summary of operating conditions, methods used and reported activation energies in the literature for char-oxidation reaction

Technique	Rate parameter estimation method	Pyrolysis condition	Coal seam	ASTM rank	Further char treatment	Oxidation temp.	Activation energy	Reference
Isothermal								Zolin et al. (1998) [144]
			Cerejjen	HVB	Insitu	450-650 C	97	
			Dietz	SB			163	
			Blue	SB			136	
			Hiawatha	hvC			148	
			Illinois 6	hvC			117	
			Pittsburgh 8	HVA			112	
			Ulan	HVB			116	
	Random pore model	TGA:900 C, 15 min	Blair Athol	HVB			140	
			Lower Kitt	lvb			132	
		TGA:1273, 120 min	North Dakota	Lignite	……na….		142	Suuberg et al. (1989) [163]
	……na….	TGA:1273, 60 min	Illinois 6	hvC	……na…..	<750 K	180	Kulaots et al. (2003) [158]
					HTT:1100 K	725-875 K	147	Floess et al. (1988) [170]
	x=0.5	TGA:925 K, 60 min	Sucrose char spherocarb				135	
								Roberts and Harris (2000) [62]
	x=0.1	TGA:1100 C, 180 min		HV anthracite	……na…	<500 C	153	
							140	
	…..na……	TGA: 773-1273 K	Colorado	hvC		773-1273 K	85	Zolin et al. (2001) [171]
		TGA:1200 K, 7 min	Biomass char		250 C, 15 min	583-670 K	120	Zimbard (2000) [157]
		TGA:700 C		MVB	Insitu	<625 C	105	de la Puente et al. (2000) [160]
		TGA:900 C, 30 min	non porous char		Exsitu	593-673 K	189	Lizzio et al. (1988) [150]
		DTR:1000 C		HV	1000 C, 10 min	450-600 C	105-118	Arenillas et al. (2003) [140]
	entire range of conversion	DTR:1700 K	Dietz	SB	As it is	623-723 K	102-133	Hecker et al. (1992) [161]

						95-115	
					112-131		
20-60% averaged	EFR: 1300 C	Pitt 8	HVA	As it is	615-723	125	Zeng et al. (2005) [152]
	EFR: 1600-1700 K	Pitt 8	hvC	As it is	773-823 K	135	Hecker et al. (2003) [153]
		North Dakota	Lignite		598-713	147	
average reactivity (50%)	EFR:1200 K	Wide macerals	HVA lvb	As it is	600-825	125 130	Tsai and Scaroni (1987) [151]
t0.5		North Dakota	Lignite	1030 K, 5 min	598-700 K	140	Patel et al. (1988) [159]
	DTR:1030 K			As it is		110 120 76	
….na…..		Zap	Lignite	973 K, 30 min	600-700 K	113	Gopalakrishnan and Bartholomew (1996) [172]
	DTR:1700 K	Dietz Spherocarb	SB			113 151	
Least square	EFR:1500-1700 K	Illinois 6 Pittsburgh 8 Blue	hvC HVA SB	….na….	773-885 k	130-133	Sorensen et al. (1996) [146]
Non-isothermal	Entire conversion range	TGA:973 K, 60 min	South African high ash		<823 K	133	
	<10% <30%	TGA:500-950 C	Pittsburgh 8	HVA	750-1050 C	130 76	Everson et al. (2006) [173]

----na--- indicate information is not available
"as it is" means char were brought to reaction temperature without any treatment
"Ex-situ" means char were further heat treated to remove adsorbed/residual species
EFR is used for entrained flow reactor. DTR means drop tube reactor
In this table, data is not included from U. Leeds group because of inconsistency in their reporting
In this table, data derived from high temperature combustion conditions are not included because of extreme sensitivity in assumptions used to deduce those parameters

Various reasons are possible for the inconsistency in the observed trends, some of which are well known. For example, time-temperature history of coal particles during pyrolysis affects the resulting char structural order [174]. Development of the char structural order, which determines the measured activation energy [161], depends upon the parent ranks of coal. However, the uncertainty of a reliable method to compute these rate parameters may be one of the reasons behind apparent significant scatter in the reported activation energy data. Part of this inconsistency in activation energy may also be due to non-uniformity in char oxidation temperatures used to measure activation energy (refer to Table **4-1**). Although various studies have attempted to explain the occurrence of the maximum in the reactivity profile from surface area or active surface area points of view, surprisingly, significantly less attention has been paid to rule out the "purging effect" †† behind the occurrence of such a maximum [138].

Objectives

Specific objectives of this part of the study are to:

1. Achieve a better understanding of the factors responsible for the occurrence of a maximum in the rate profile so an accurate rate parameter can be estimated.
2. Investigate if the use of different methods and time-temperature histories of char particles lead to scatter in measured activation energy.

---

†† Typically, TGA furnace is brought to the reaction temperature in an inert gas environment and then switched to reactive gas for rate measurement. "Purging effect" is referred here for time taken in building up of reactive gas partial pressure.

Methodology

Accomplishing the objectives includes preparation of char samples at various temperatures at high heating rates in a drop tube reactor (DTR). To distinguish the effect of heat-rate condition on char reactivity, a char sample is also prepared at a low heat-rate condition using a TGA furnace. The rate parameters for all the char samples are calculated by using various methods, such as maximum, average reactivity up to 50% and 75%, and at intervals of 10 between 10-80% conversions. Various tests investigate and quantify the time taken during buildup of gas partial pressure in the TGA system ("purging effect") during the rate measurement.

The coal char primarily used in this study are produced from pyrolysis of a high volatile (hvCb), coal at different temperatures and heating rate conditions. These coal particles are injected with argon (Ar) gas into a drop tube reactor (DTR) at 1,173, 1,373, 1,673, and 1,873 K. The resultant char samples are denoted: DTR-1173, DTR-1373, DTR-1673, and DTR-1873, respectively. Preparation of low heating rate (10 K/min) char occurs by pyrolyzing the coal sample in a TGA at 1,123 K in an N_2 gas medium for 7 min, and the sample is denoted: TGA-1123. An isothermal TGA method determines the intrinsic rate parameter. In order to estimate the rate parameters, rate measurements on these char samples are conducted at 673, 698, 723, and 748 K. These conditions represent typical temperature ranges (Table **4-1**) to maintain the char-oxidation reaction in a kinetic controlled zone. Proximate analysis of the char sample in Table **4-2** shows that samples prepared in the DTR had significant amounts of residual volatile matter. To ensure measurement of activation energy for char-oxidation reaction, and not for the oxidation

of volatile residuals, the rate parameters are estimated by removing the residual volatile matter of DTR prepared char samples prior to rate measurement.

Table **4-2**: Proximate analysis of hvCb rank coal and DTR generated char samples

	Coal	DTR-1173	DTR-1373	DTR-1573	DTR-1673	DTR-1873
Moisture	3.36	1.37	1.82	1.59	1.06	0.50
Volatile (dry)	39.69	27.89	14.75	6.48	4.09	2.90
Ash (dry)	8.49	10.76	11.68	12.49	13.53	14.30
FC (dry)	51.82	61.45	73.57	81.03	82.38	82.80

Rate parameter estimation uses about 5 mg weight of a char sample. First, the TGA system is flushed with N_2 at 100 mL/min for ~45 min at room temperature to purge air from the furnace. Afterwards, heating the furnace to 1,123 K at 50 K/min in an N_2 gas atmosphere and maintaining that for 7 min at 1,123 K removes any adsorbed oxygen species and residual volatile matter left on the DTR generated char samples. Then, the system is brought to the reaction temperature and maintained for 10 min to establish the thermal equilibrium. Initiation of the char oxidation reaction occurs by replacing the inert gas with air flow at 100 mL/min. The weight of the sample is recorded every 15 sec for several minutes until achieving ~90% dry ash-free (daf) weight loss. The ash content of the sample is determined separately in an oven furnace using ASTM (D-3178) method. After each experiment, conversion-time data is converted into the rate of weight loss normalized with respect to initial mass (m_0) to construct reactivity plots and the rate is calculated based on Equation **4-1**:

$$\text{Rate} = 1/w_0\,(dw/dt) = d/dt\,[(w_0 - w_t)/w_0] = -dX/dt\,, \qquad \textbf{4-1}$$

where, w_t is weight of the sample at time, t, and X is the conversion.

Use of a lower time interval reflects the true nature of reaction rate but leads to a scatter in the rate data. For consistency purposes, in this research, a 30 sec time interval is used to construct the reactivity plot.

Results and Discussion

Presence of Maximum

Figure **4-1** shows rate profiles for the char samples exposed to different time/temperature histories. Rate profiles for the DTR-1373 char sample at different operating temperatures appear in Figure **4-2**. Several trends are apparent from Figure **4-1** and Figure **4-2**. First, as reported by many investigators [149, 150] (described earlier in the chapter), the rate for both of these cases transition through a maximum in reactivity profiles. Second, these rate profiles show that the location of a maximum shifted to a lower conversion level upon decrease in oxidation temperature. Similar trends are observed for other char samples (shown in the Appendix 4-2). Third, the location of the maximum shifted to a lower conversion value at a lower intrinsic reactivity of the char samples.

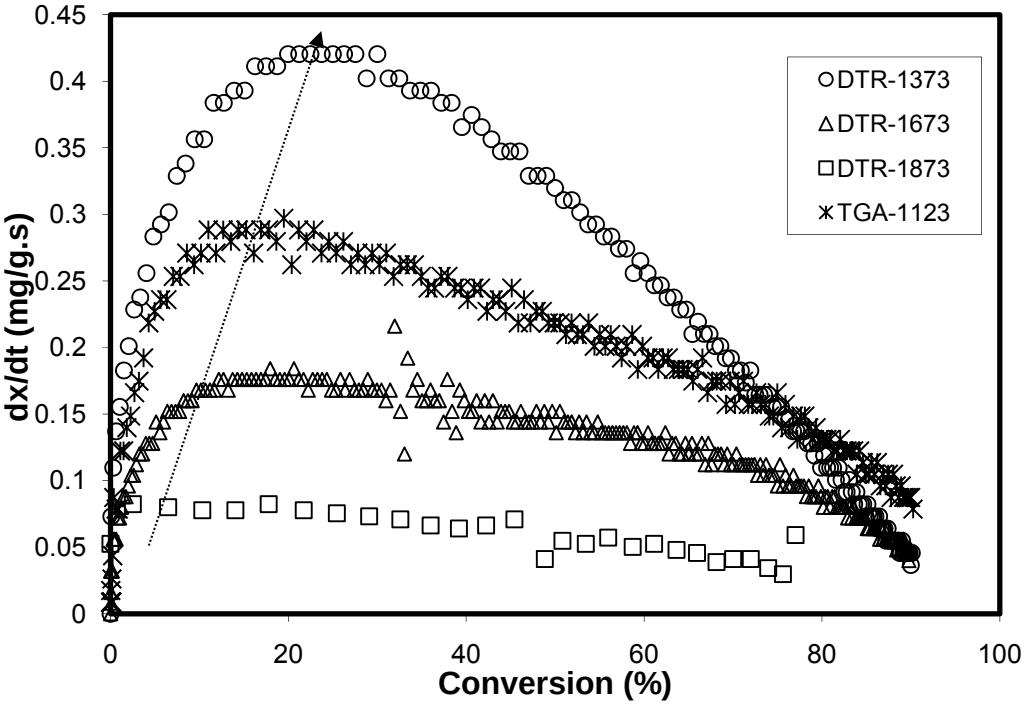

Figure **4-1**: Presence of maximum during rate measurement in air for char samples prepared in both the high and low heat rate conditions

Therefore, from the trends depicted in Figures **4-1** and **4-2**, the hypothesis is that the maximum is observed because of an intraparticle diffusion limitation in the initial part of the rate profile. This hypothesis was formed on the basis that;

A) If one char is structurally ordered i.e., has lower intrinsic reactivity than another, then the kinetics of the oxidation reaction are slower compared to gaseous diffusion at the same temperature and a maximum occurs at a lower conversion level.

B) If the temperature of the oxidation reaction increases, the rate of oxidation increases much faster than the rate of intraparticle diffusion (as evident from the

activation energies, E_{kin} ~120-140 KJ/mol [72], E_{diff} ~40-60 KJ/mol [125]), and a maximum occurs at a higher conversion level.

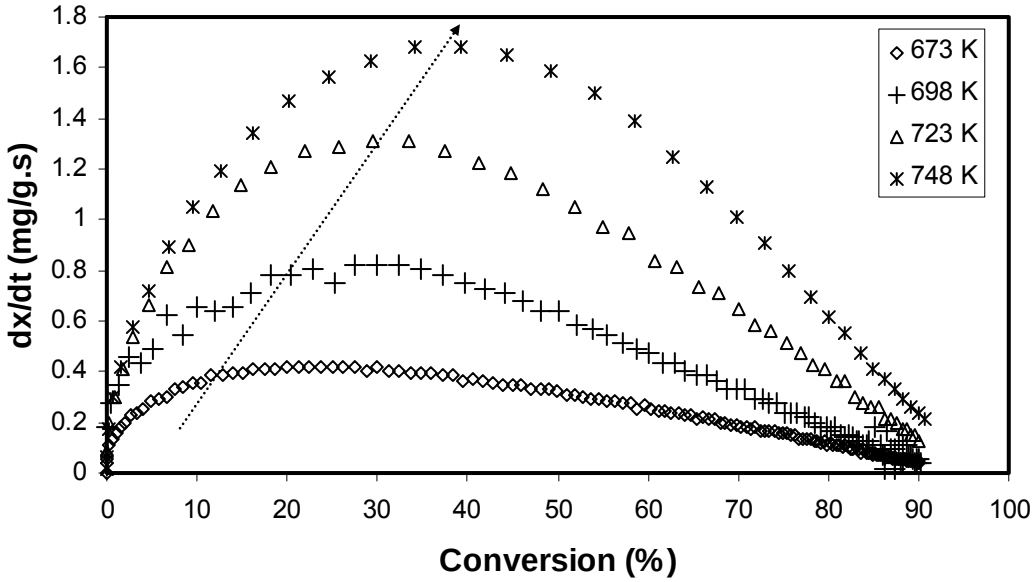

Figure **4-2**: Effect of oxidation temperature on location of maximum for DTR-1373 sample

These observations are very curious from a fundamental point of view and lead to further investigation. To test if the maximum is a result of a balance between chemisorption of oxygen and a weight loss due to char-O_2 reaction, the DTR-1673 char sample is gasified at 1,123 K, 1,148 K, and 1,173 K in CO_2 gas. At such high temperatures, the effect of chemisorption has been reported to be very negligible [150]. The rate profiles for these settings appear in Figure **4-3**. Shapes of the rate profiles are similar to those for gasification of DTR-1373 char samples (shown in the Appendix 4-3). The shape of rate profiles observed during char gasification tests are different from the ones observed during char oxidation tests. Although, no pronounced maximum is apparent during char gasification, the rate increases and becomes constant for most of the

conversion region, and then decreases. Such a prolonged maximum may be caused from the differences in the molecular size of CO_2 and O_2 gas [149]. Evidence also exists that char-O_2 reaction is generally much faster than thermal annealing; whereas, char-CO_2 reaction and annealing are likely to take place over comparable time scales [175]. This could also play a role in differences observed in the rate pattern. Therefore, the presence of a maximum during char-gasification plots suggests that chemisoprtion alone is not a factor in the occurrence of a maximum.

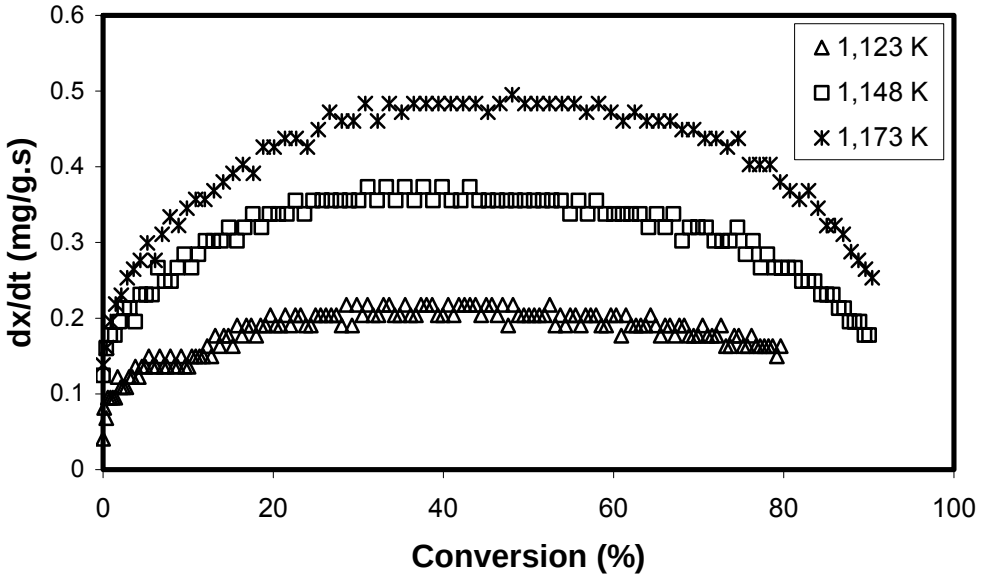

Figure **4-3**: Effect of gasification temperatures on char reactivity profile for DTR-1673 sample

In order to further test the hypothesis, oxidation rate profile of the DTR-1673 sample is compared with that of a pet coke sample and the outcome appears in Figure **4-4**.

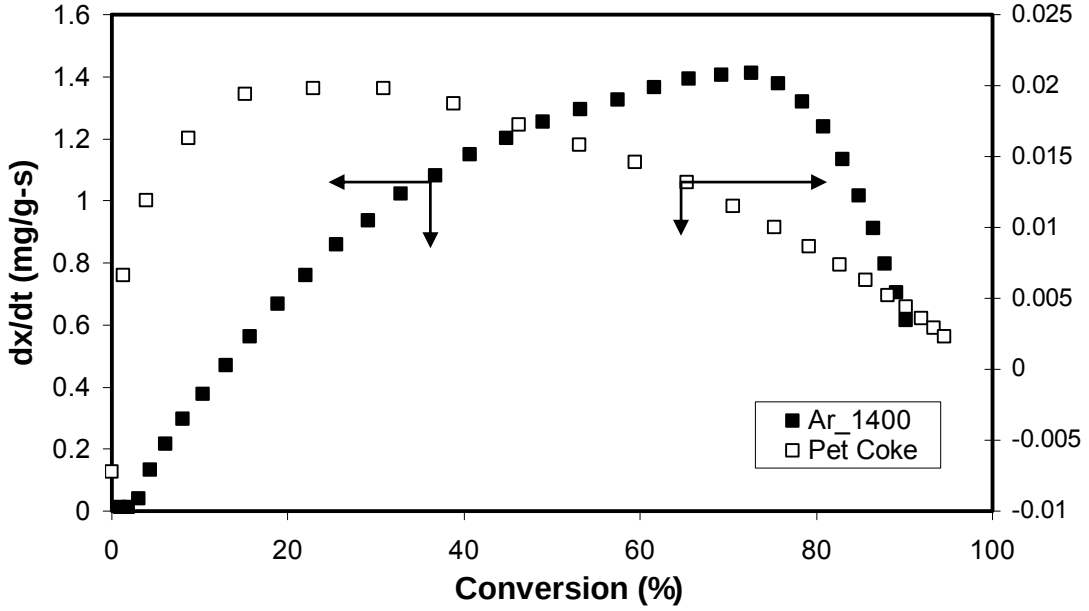

Figure **4-4**: Comparison of char reactivity profile for DTR-1673 sample and pet coke sample at 748 K in air

Crystallite size parameters of the pet coke sample (L_a=22 A^0, L_c=32 A^0), presented in Table **4-3,** clearly indicate that the pet coke sample is highly ordered compared to the DTR-1673 char sample (L_a=13 A^0, L_c=18 A^0).

Table **4-3**: Physical properties of coal, DTR generated chars and pet coke sample

	Helium	BET Analysis		Crystallite Size	
	Density (cm^3/g)	Average Pore Volume (cm^3/g)	Surface Area (m^2/g)	L_a (nm)	L_c (nm)
Coal	1.37				
Ar-1173	1.19	0.0013	1	0.8	0.8
Ar-1473	1.25	0.003	5	0.9	1.1
Ar-1673	1.59	0.0196	11	1.3	1.8
Pet Coke				2.2	3.2

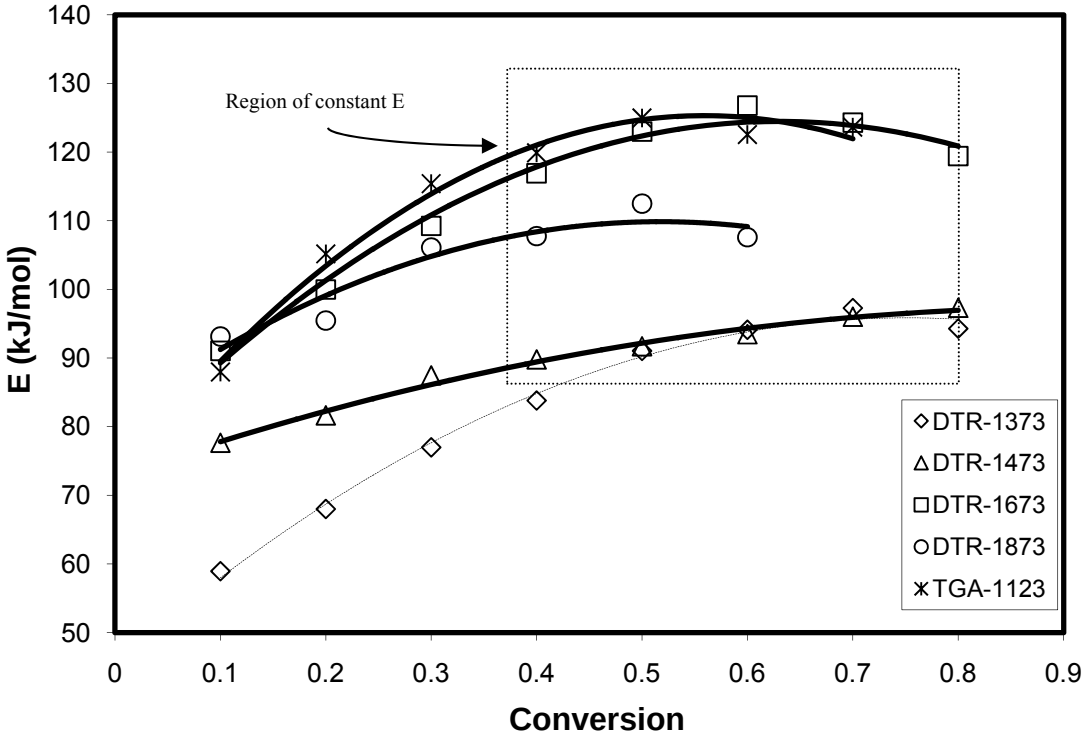

Figure **4-5**: Dependence of estimated activation energy values on chosen conversion level. Data is shown for char samples prepared from hvCb rank coal at different thermal treatment.

As expected, the reactivity of the pet coke sample is lower than the DTR-1673 char sample and a maximum is, therefore, apparent at a much lower conversion value (refer to Figure **4-4**). Further support to the proposed hypothesis is evident from the estimated activation energy values at difference conversion levels (refer to Figure **4-5)**. The data shows that the activation energy value rises to the maximum and then remains constant (within the accuracy of measurement) until reaching an 80% conversion level for a wide range of char samples. A continuous increase in the activation energy with conversion in the initial part of char conversion is presumed to be because of opening of pores, and thus, transition into a kinetically controlled zone. The onset of a maximum in

activation energy coincides with the typical location of a maximum (X≅20% for DTR-1873, and X≅40% for all other char samples) observed during the rate measurements for these char samples. These results suggest that a maximum in the rate profile occurs because of the presence of an intra-particle diffusional limitation in the initial part of reactivity profile.

Purging Effect

To determine if a "purging effect" is responsible for occurrence of a maximum in rate, the hvCb coal particles are pyrolyzed in a CO_2 and N_2 gas medium in a TGA at 1,123 K, and the rate is measured in CO_2 at 1,123 K. The rate profiles for these two cases appear in Figure **4-6**. It can be seen from Figure **4-6** that when the pyrolysis environment is N_2 (termed here as *ex-situ* because the gas is changed from N_2 to CO_2 for reactivity measurement), a maximum in rate profile occurs. However, when coal particles are pyrolyzed in CO_2 (termed here as *in-situ* because gas is not switched during the rate measurement), a maximum in rate does not occur. Remarkably, similar rates for these two char samples are observed after the appearance of a maximum.

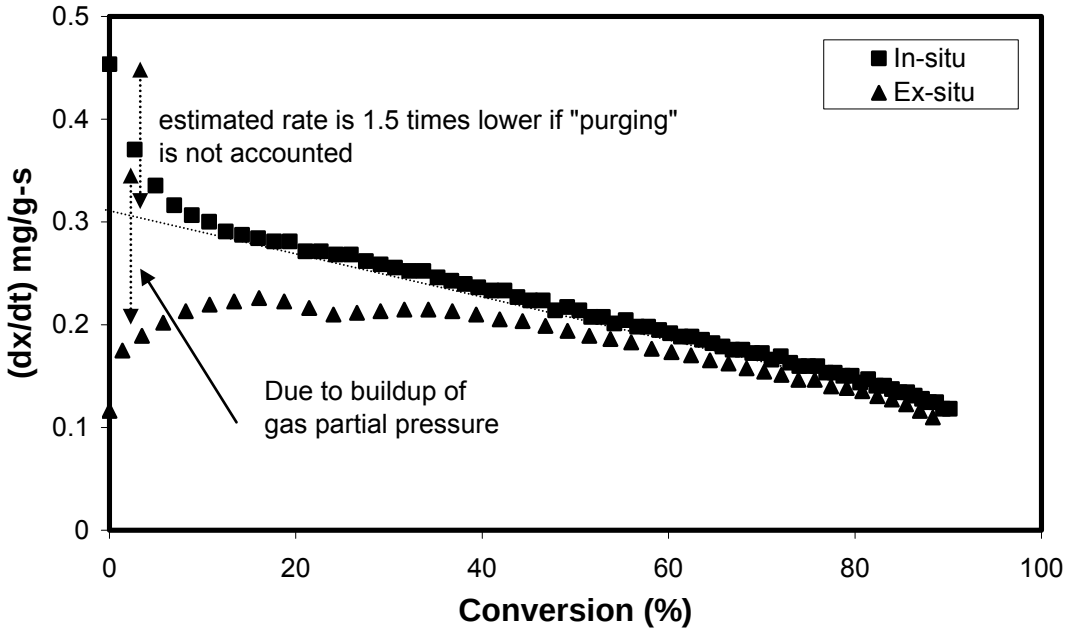

Figure **4-6**: Absence of maximum in char reactivity profile when CO_2 as a pyrolyzing gas was used

A similar result of the absence of a maximum for the "*in-situ*" char sample was also observed by Peng et al. [123] for three ranks for coal gasified in steam in the temperature range of 1,273-1,473 K. However, those authors attributed this behavior to the possibility that the presence of steam in the pyrolysis may have led into a different structural rearrangement of the *in-situ* char than for the N_2 pyrolyzed *ex-situ* char. Therefore, an additional test is done to minimize the structural rearrangements of char samples in steps prior to the rate measurement. A coal char from the exit of a pilot-scale research boiler (denoted as RB-X75) and a char from the DTR (denoted as DTR-X89) are chosen for this purpose as these samples had already undergone significant thermal

annealing and weight loss. The char samples are brought to the rate measurement temperature (673 K) in a TGA furnace in a N_2 medium and in an air medium at a rate of 25 K min^{-1}. Thus, this small exposure time (~16 min) at such a low temperature/heating rate during the pre-treatment step in the two media can be considered to cause negligible changes in the char structure. Rate profiles for these char samples appear in Figure **4-7**. A maximum is not observed for both samples pre-treated in air for which no gas switch occurred for the rate measurement. On the other hand, char samples pretreated in N_2 show a maximum in the rate profiles. All these results provide strong evidence that a "purging effect" is the possible, and indeed, may be a significant factor behind the observation of a maximum in the rate profile.

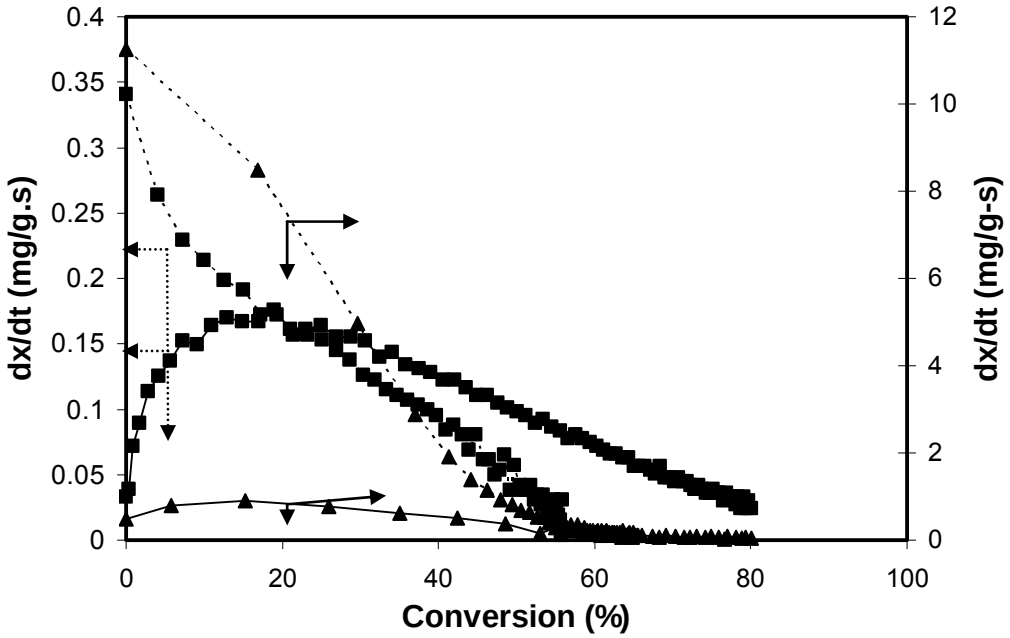

Figure **4-7**: Absence of maximum in char reactivity profile when air as a pretreatment gas was used. Solid line represents pretreatment in N_2 and dashed line represent pretreatment in air. (▲) represent DTR-X89 sample, (□) represent PSB-X75 sample

To further investigate the likelihood of a "purging effect," the reactivity tests are conducted using different air flow rates during the rate measurement step in the TGA. A higher flow rate is expected to purge the inert gas from the system faster, and therefore, a maximum is expected to occur at a lower conversion or time. During these tests, the hvCb rank coal sample is pyrolyzed in inert gas to 1,123 K in a TGA and is kept for 15 min. before bringing the system to the char oxidation temperature (673 K) for reactivity measurement. After establishment of thermal equilibrium at 673 K, different flow rates of air, such as 50 mL/min, 100 mL/min or 300 mL/min is used during the rate measurement. Rate profiles for these conditions appear in Figure **4-8**.

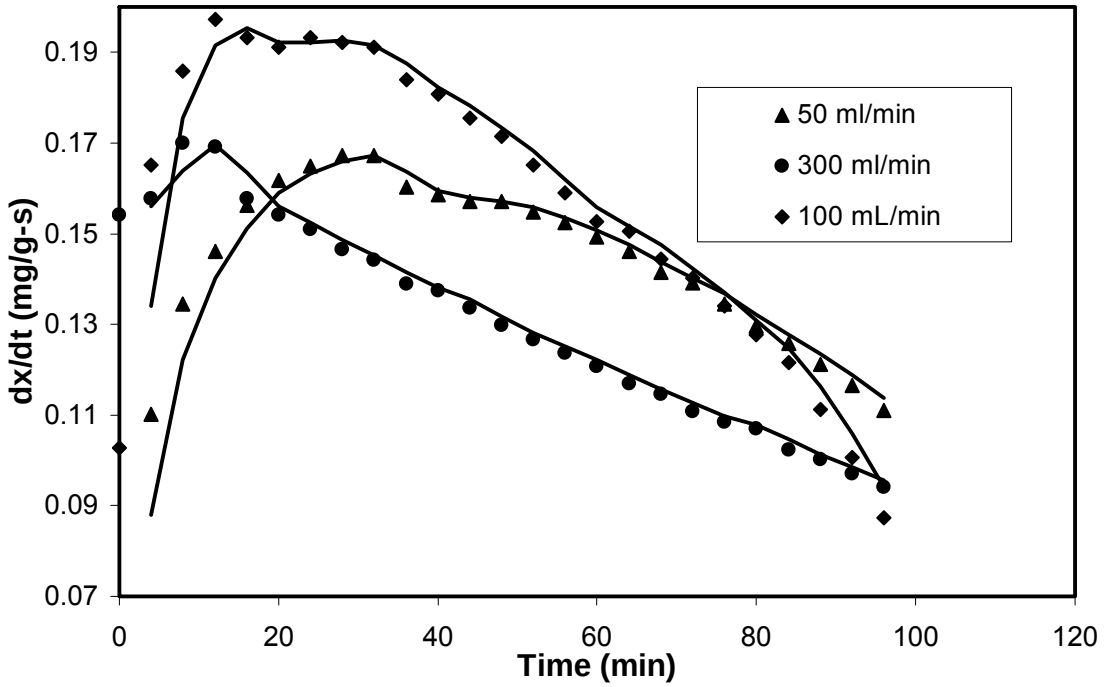

Figure **4-8**: Effect of purge flow rate during rate measurement in CO_2 at 1,123 K on location of maximum of a hvCb char prepared in TGA at 1123 K for 7 min

As expected, at a higher air flow rate, the TGA system flushes faster, and thus, a maximum appears at an earlier time. These results clearly demonstrate the presence of a "purging effect" during the rate measurement. Also noteworthy from the initial values of reactivity in Figure **4-6** and Figure **4-7** is that typically measured reactivity of a char sample is about ~1.5-2 times lower than the actual value. A theoretical calculation is done to determine how much time is necessary for the build-up of reactive gas partial pressure and is discussed below.

Purging Calculation

The rate of partial air pressure build-up in a TGA furnace (upon switching from N_2 to air during the rate measurement) can be approximated by assuming the TGA furnace to be a well mixed reactor. By applying the conservation equation of species, partial pressure of air in the the system can be estimated from:

$$[Air] = 1 - \exp(-Qt/V), \qquad \textbf{4-2}$$

where, Q is purging gas flow rate, and V is the volume of TGA furnace as shown in Figure **4-9.** Therefore, as seen from Equation **4-2,** the time taken for partial air pressure build- up depends upon the volume of the TGA furnace (V) and the flow rate (Q) used. Typically, in this research, a flow rate of 100 mL/min is used during the rate measurement. Considering that the gas in the furnace arrives through a weighing balance chamber of volume ~600 mL, the calculation from Equation **4-2** suggests that ~95% partial pressure of the gas is achieved in ~18.7 min.

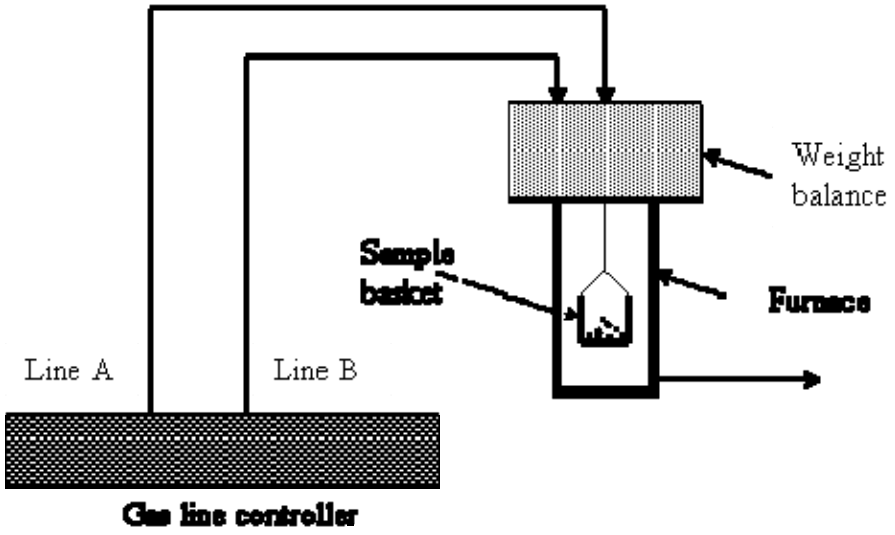

Figure **4-9**: Schematic representation of a thermogravimetric analyzer

Typically, partial pressure of air, $[Air]$, in the TGA furnace is assumed to be unity during rate parameter estimation [151]. However, if a "purging effect" is present, then the corrected rate becomes:

$$(dx/dt)_{corrected} = (dx/dt)/[Air]. \qquad \textbf{4-3}$$

The corrected plot for *in-situ* char appears in Appendix 4-4. The remarkable agreement between the *in-situ* and *ex-situ* char times suggest that purging is responsible for the observed maximum in reactivity plots. It can be seen from the initial part of the plot in Appendix 4-4, that reactivity curves for *in-situ* char become identical with that of *ex-situ* char after ~ 16 min. The presence of a purging effect also implies a conclusion

reached based on the initial rate values, for example done by Peng et al. [123], may be misleading.

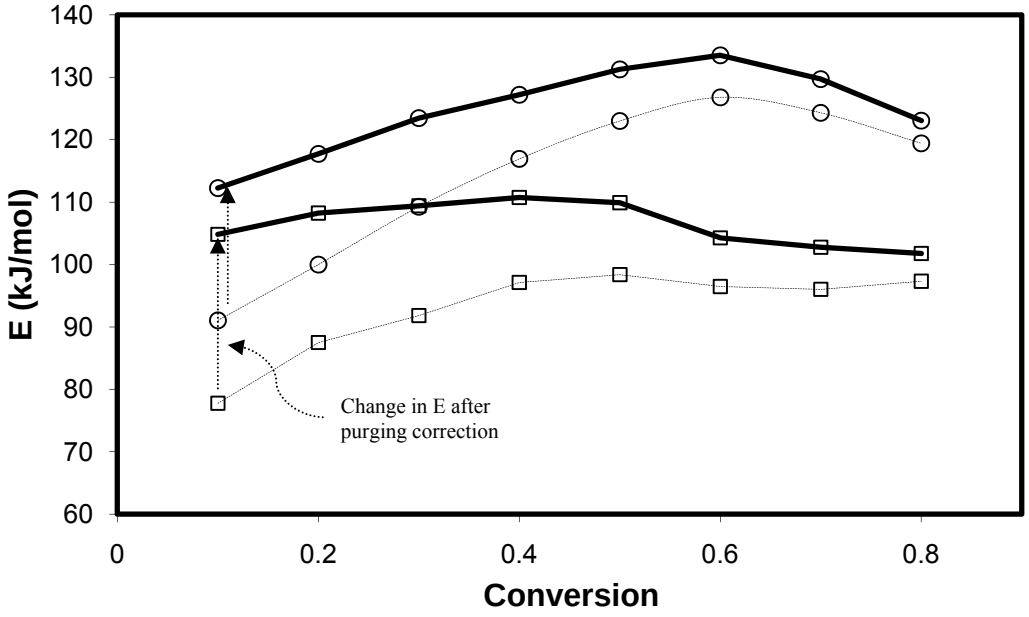

Figure **4-10**: Activation energy value with and without correction for purging. Solid line represents purging correction whereas dashed line represent without correction. (○) DTR-1673, (□) DTR-1473

This correction factor of induction time is applied to the rate of DTR-1473 and DTR-1673 char samples and the rate parameters are re-estimated at various conversion levels. Corrected activation energy and previously estimated activation energy values, plotted against the conversion levels, appear in Figure **4-10**. Figure **4-10** shows that previously estimated activation energy at lower conversion levels has increased after purging correction and falls within the range of constant activation energies observed after the onset of a maximum. Similar changes in activation energy values, after accounting for the "purging effect" correction, were also observed for other char samples,

(shown in Appendix 4-5). Therefore, the results obtained for the "purging effect" show that the char particles were always in a kinetically controlled zone and not in an intra-particle diffusion zone as suggested in the previous section.

Activation Energy Estimation Method

Several methods have been used in the literature to calculate rate parameters from such reactivity plots. For example, Jenkins and co-workers used the maximum in the rate profile to compare char reactivity [138]:

$$R_{,max} = 1/W_0\,(dW/dt)_{max} \qquad \textbf{4-4}$$

Scaroni and co-workers [176], however, felt that reactivity parameters determined using a maximum are not appropriate because of an extremely short rectilinear region. They proposed determining the rate parameters using averaged rate values during different extents of burn-off.

$$R_{a,x} = \frac{\sum (R_u . \Delta W)}{\sum \Delta W} \qquad \textbf{4-5}$$

where, $R_u = (dW/dt)/W$, is the reactivity determined based on the unburned carbon.

Fletcher et al. [137] and Dugwell et al. [177] compared the char based on the rate determined at fixed values of burn-off. In the current research, calculation of intrinsic activation energy uses these methods. The main purpose for the exercise is to determine the scatter in estimated activation energy that could arise due to use of different methods. Parameter estimation using initial conversion (X=0) value is not done because the computed rate of initial value appeared to depend upon the time interval used. A

comparison of the calculated activation energy using these methods appears in Table **4-4** for all the char samples. Since, it is demonstrated that in the initial part of the reactivity profile, partial pressure of the oxidizer is building-up, the rate parameters are also estimated using an average rate from conversion (X) where the rate is a maximum to X=80%. The data in Table **4-4** shows that different calculation methods yield different activation energy values for a char sample. An average difference of ~20 kJ/mol and the maximum difference of up to 44 kJ/mol (see for example for TGA-1123 char) can be observed when employing various methods to estimate the activation energy for a char sample. The data in Table **4-4** also indicate that the rate determined using a maximum is ~2-3 times lower than the rate calculated from other methods. This is, quite obviously, because in the $R_{,max}$ method, the rate normalizes with respect to initial sample weight, while other methods normalize with the instantaneous weight of the sample. In general, better agreement arises between the activation energy estimated using the average (X=40-80%) and the $Ra_{x,90}$ method.

Table **4-4**: Rate parameter values estimated using various methods for char samples prepared from a hvCb rank coal at various thermal treatment conditions

Method	DTR-1373		DTR-1473		DTR-1673		DTR-1873		TGA-1123	
	A*	E**	A*	E**	A*	E**	A*	E**	A*	E**
Avg (40-70)	1.00E+04	92	1.08E+04	93	1.33E+06	123	3.50E+04	108	1.70E+06	123
$Ra_{,X}50$	9.00E+02	79	4.00E+03	88	6.00E+06	135	2.00E+04	106	4.00E+05	116
$Ra_{,X}90$	2.00E+04	97	1.00E+03	81	5.00E+05	117	8.00E+04	113	6.00E+06	129
Max	5.41E+02	78	2.00E+03	87	9.00E+04	112	3.00E+03	98	1.00E+03	85

* unit is (1/s.atm)
** unit is kJ/mol

A much better agreement in these two approaches is anticipated, if a "purging effect" in the system during rate measurement could be alleviated. Comparison of the activation energy estimated using a maximum rate and average rate (X=40-80%) show a deviation in the estimated activation energy by about 38 kJ/mol. This result indicates that part of the scatter in reported activation energy value for a given coal char in literature is due to use of various methods.

Table **4-4** shows that, for samples prepared in the DTR, activation energy value estimated using average (X=40-80%) increased with the furnace temperature up to 1,673 K and then decreased. An increase in activation energy value with an increase in heat treatment temperature (HTT) is expected because of an increase in structural order [163, 164]. However, a lower activation energy value of the DTR-1873 sample compared to that of DTR-1673 sample is surprising. Generally, a reduction in activation energy of a sample occurs if the reaction is catalyzed by the presence of mineral matter or if a char contains dis-ordered structure. For example, activation energy of a lignite coal is lower than other higher rank coal [167] because of the presence of inherent mineral matter and dis-ordered char structure. (A further investigation to determine the root cause is beyond the scope of the main objective of this current research, and therefore, not included.). Comparison of activation energy value for char sample prepared under different temperature and heat rate conditions shows a scatter of ~30 kJ/mol. This result shows that the time-temperature history of a particle leads to a different char structure for the high volatile (hvCb) coal studied in the present research. A similar observation is made for the char prepared from an lvb coal as shown in Table **4-4**.

Notably, these rate parameters are estimated in the temperature range of 673-748 K. Rate parameters for a sample was also estimated in the temperature range of 573-648 K to determine the effect of operating temperatures on estimated intrinsic activation energy value. The maximum rate in reactivity profile and activation energy values at different operating temperatures is shown in Figure **4-11**.

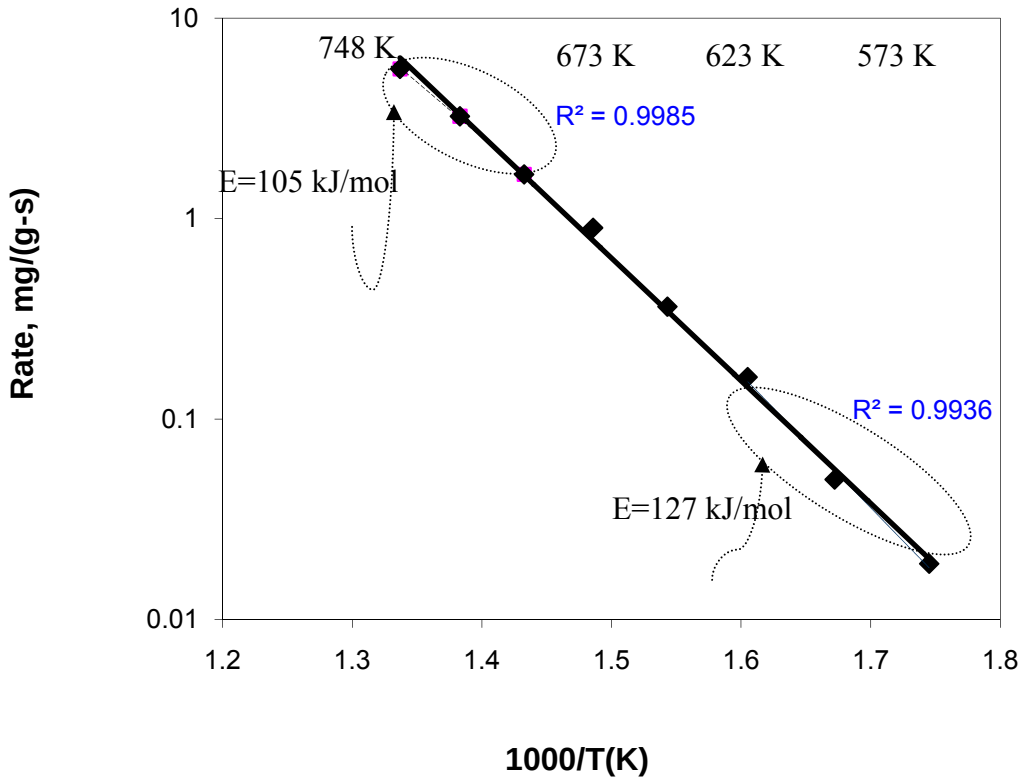

Figure **4-11**: Effect of operating temperatures on estimated activation energy value

This plot indicates that a different temperature range used during the rate measurement alters the estimated activation energy value. Higher activation energy (127kJ/mol) value is estimated at lower operating temperatures in comparison to experiments performed at higher temperatures.

Summary and Conclusions

This research attempts to understand the factors responsible for the occurrence of a maximum in reactivity plots so that accurate intrinsic rate parameters can be determined using an isothermal TGA method. Results obtained for various porous char samples prepared from a high volatile (hvCb) coal, and a pet coke sample indicated that the maximum in reactivity plots occurs irrespective of carbon precursor and their thermal heat treatment histories. A shift in the location of a maximum toward a lower conversion value at lower char oxidation temperatures and intrinsic reactivity of char samples indicated the presence of an intraparticle diffusion limitation even while operating in commonly considered kinetically controlled regime conditions. The presence of an intraparticle diffusion limitation was further established by observation of the estimated activation energy values being low in the initial stages of char conversion which then increased to a maximum and remained constant thereafter. This trend was consistent for the char samples prepared under both low and high heating rate conditions. Occurrence of a maximum during the char-gasification tests for both a low volatile (lvb) and high volatile (hvCb) coal samples rules out the possibility that the maximum appeared because of a balance between mass gain due to stable oxide formation and mass loss due to char oxidation in the reactivity profile obtained in air. However, various tests demonstrated that a maximum was the result of the presence of a “purging effect” (time taken in building partial gas pressure) during the rate measurement. Apparently, the presence of a “purging effect” explains why a change in operating temperature and intrinsic reactivity changed the location of the maximum. Correction for the “purging effect” shows constant

activation energy with conversion in the initial part of rate profile. This suggests that char particles were always under a kinetically controlled regime. Rate parameter estimation based on initial values or on an arbitrary conversion value may be misleading due to the presence of a "purging effect" It is proposed that the activation energy should be estimated from the average rate at the onset of a maximum to 80% conversion values for the reason that in the initial part of a reactivity profile gas partial pressure is non-uniform. The result suggested that, typically assumed, absence of "purging effect" should be demonstrated which would depends upon the volume and flow condition of TGA.

In agreement with the literature, activation energy value was found to depend upon the time-temperature history of char particles prepared from the lvb and hvCb coal. However, for a given coal char, activation energy values are estimated to vary by 38 KJ/mol, depending upon the employed method. It was observed that the range of operating temperature used for rate parameter estimation affects the estimated activation energy. This suggests that the intrinsic activation energy value reported in this chapter may be lower (by about 13 kJ/mol) due to the specified char-oxidation operating temperature range (673-748 K).

Chapter 5

Prediction of Char Burnout from Combustion Conditions Using an Intrinsic Model

Introduction

In a typical boiler environment, temperature of coal particles and surrounding gases varies from ~2,300 K to as low as ~800 K. Due to wide variation in temperature and gas concentration along the boiler length, rate controlling regime changes beginning from mass transfer controlled regime (Zone III), to a pore diffusion controlled regime (Zone II), and finally to a kinetic controlled (Zone I) at lower temperatures [178]. Recent literature also provided ample support that in actual combustion conditions, especially during the later stages of char burnout, particle temperatures are significantly lower and thus accounting for transition from Zone II to Zone I regime is a key for accurately modeling char burnout behaviors [179, 180]. Despite this fact, global rate based combustion model is typically used to predict char burnout from combustion systems [181]. In principle, an intrinsic model, which accounts for such a transition of a rate controlling regime, based on the classical theory of Thiele [100] can be used for the prediction of char burnout. The intrinsic approach is also attractive because the contribution of char-CO_2 reaction can be included in the rate of char burnout which is usually excluded in the global based combustion model. Surprisingly, very few studies attempted to use Thermogravimetric Analyzer (TGA) based, low temperature intrinsic rate parameters for the prediction of the

char burnout from combustion conditions [74]. A brief discussion of this approach and relevant studies are described below.

The reaction rate in pore diffusion controlled regime (Zone II) is expressed as:

$$\left(R_g\right) = \eta R_i , \qquad \textbf{5.1}$$

where, R_i is an intrinsic rate, and η is a effectiveness factor which is a function of K_i / D_e. Here, K_i is an intrinsic rate constant, and D_e is an effective diffusivity of oxidizing gas in a porous network of char particles. In most of the previous research that use the Thiele approach, an intrinsic rate was computed by the global measurement of char reactivity, R_g, [71, 145, 182] and not vice versa. Uncertainty in determining true intrinsic kinetic constant (K_i) for a gas-solid (Char-O_2) reaction using TGA apparatus has been described in detail in Chapter 4. The fact that a participating coal structure at lower temperatures is quite different compared to that at higher temperatures complicates estimation of effective diffusivity (D_e) in combustion. For example, Mitchell et al. [183] observed that the diffusion coefficient through a porous char particle decreases over the course of a high temperature combustion process. On the other hand, Valix et al. [184] observed that the activation energy for the diffusion is approximately constant over the course of combustion. Hurt et al. [185] suggested that this constancy may likely to be due to the net effect of oxidation (which would widen the pore structure) and thermal annealing that may inhibit microporous diffusion. While the significant complexity of pore structure of coal, having sizes varying from Angstrom (A^o) to micron (μm), is well known, various studies have considered uniform size pores for modeling purposes. For example, Hurt et

al. [186] considered that larger sized feeder pore provide the largest diffusion resistance, and thus, was used in estimation of effective diffusivity. Smith, used Wheeler's correlation [187] to estimate the average pore radius [80]. Walker [188], from theoretical analysis, demonstrated that the larger size pores enter a pore diffusion controlled regime first during combustion conditions.

Solomon et al. [74] predicted char reactivity in Zone II using intrinsic rate parameters obtained in a TGA and estimated effective diffusivity using a single adjustable parameter (pore radius [r_p] correlated to rank of coal). The study was very limited in scope and failed to justify the use of some of the parameters employed. For example, a correlation indicating a maximum in surface area with conversion was used while it has been shown that the surface area decreases with conversion at high temperature combustion condition [80, 142]. B. A. Morgan [189] suggested that the actual rate in combustion conditions is much higher than the rate extrapolated from Zone I data. This is attributed to the fact that a two-step procedure employed during the Zone I rate measurement utilizes a char of different pore structure and active sites than the char in actual combustion conditions. Accurate knowledge and accounting of both K_i and D_e is very important for reliable predictions of char burnout in actual combustion conditions.

Objectives

The main objective of this part of the research is to demonstrate the use of intrinsic rate model for the prediction of char burnouts from actual combustion situations (high particle heating rate). This objective is met by performing various tests to:

1. Quantify the effect of two-step procedure on measured char reactivity, and

2. Establish the accuracy of the intrinsic model for prediction of char burnout from combustion conditions.

Methodology

To accomplish the objectives, a series of combustion experiments is conducted in a drop tube reactor (DTR) at different furnace wall temperatures ranging from 1,173-1,573 K for a high-volatile bituminous coal of two particle size classes. At each operating condition, overall char burnout is calculated using ash as the tracer technique. In order to accurately predict gas and particle temperatures, and char burnout in combustion conditions, rate parameters for coal pyrolysis and char oxidation reaction are needed. The rate parameters (pre-exponential factor and activation energy) for coal pyrolysis are determined by conducting tests in the DTR and are shown in Appendix 2-2. Intrinsic rate parameters for the char-oxidation reaction of the pyrolyzed char and partially burnt char samples are determined in a TGA using air in the temperature range of 673-748 K and are shown in Table **5-1**. Textural characterization of the chars was accomplished by N_2 and CO_2 adsorption isotherms at 77 and 273 K, respectively. From the N_2 adsorption isotherms, the apparent surface areas of the samples were obtained using the BET equation. The Dubinin–Polanyi (DP) method was applied to the CO_2 adsorption isotherms in order to obtain the corresponding micropore volumes and surface areas of the chars studied.

Table **5-1**: Intrinsic rate parameters for the char samples pyrolyzed in different thermal treatment conditions and combusted to different extent of conversion in DTR

		DTR-1373	DTR-1473	DTR-1673	DTR-1873	TGA-1123
Pyrolysis	A(1/s.atm)	1.00E+04	1.08E+04	1.33E+06	3.50E+04	1.70E+06
	E (KJ/mol)	92	93	123	108	123
	Rate (1/s.atm)	0.0007825	0.0006807	0.0003937	0.0001332	0.000504
		X-28	X-51	X-67	X-75	
Combustion	A(1/s.atm)	7.50E+04	1.12E+05	6.75E+04	1.23E+03	
	E (KJ/mol)	104	109	108	85	
	Rate (1/s.atm)	0.000602	0.0004096	0.0002941	0.0002881	

Rate in this table is computed at 673 K for comparison of the resultant char samples

Combustion is done in DTR at 1373 K

X denotes the % char burnout of a sample (char as a initial basis)

Results and Discussion

In this research, first of all, a theoretical analysis is conducted using intrinsic model by varying the intrinsic activation energy values (E) and pore radius (r_p) value to predict the Zone II rate values. A sample calculation for the Zone II rate using E=123 kJ/mol and r_p=100 A^o is shown in Appendix 5-1. In the theoretical calculations, E and r_p values are varied in the range (E:104-170 kJ/mol, r_p : 10-200 A^o) keeping the same value of rate constant in Zone I. This is done by adjusting the pre-exponential factor of rate of oxidation reaction. Predicted rates as a function of temperature are shown in Figure **5-1** and compared against well established rate data (obtained in rapid heating rate, lab-scale combustion conditions) from previously published studies [182, 190, 191]. Several interesting points can be noted from Figure **5-1**. First and foremost, it demonstrates that an intrinsic

model can be used to match the rate measured in high temperature combustion conditions *only if* an accurate knowledge of both *E* and r_p is available. The figure also demonstrates that despite having the same reactivity value in Zone I, the predicted reactivity value in Zone II can differ by as much as a factor of ~75, depending upon the chosen *E* and r_p value in model.

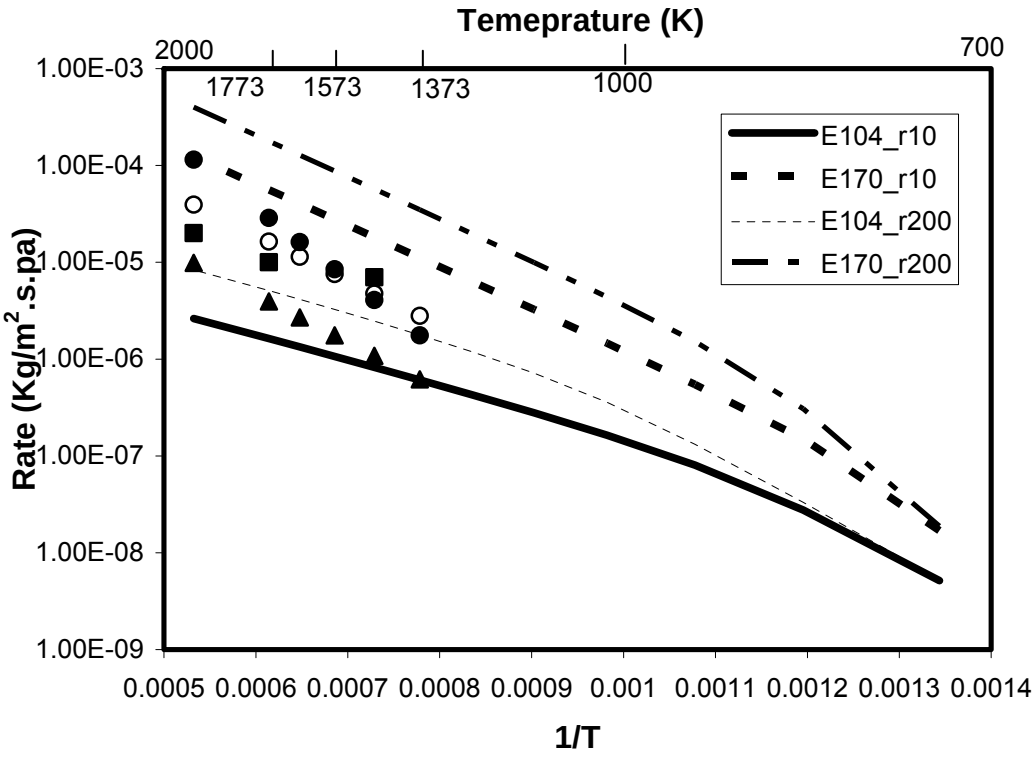

Figure **5-1**: Comparison of theoretically calculated rate (lines) using intrinsic model with experimentally measured rate (symbols) in literature for bituminous coal sample. (○) Smith (Non-Swelling), (•) Smith (Swelling), (▲) Hurt (hvC), (□) Smoot, wide rank. *E*: activation energy in kJ/mol, and r_p: pore radius in A^o

Figure **5-1** also shows the combinations of *E* and r_p that can be used to predict the Zone II rate if the measurement for *E* and r_p is not available. For example, a

combination of smaller r_p (<10 A^o) and E value (110 kJ/mol) or larger r_p (200 A^o) and E value (180 kJ/mol) in the model predicts a Zone II rate that falls outside the measured values. Since the accurate time-temperature history of particles in actual combustion conditions are very difficult to predict or measure, an intrinsic model was first tested in conditions where both of these are accurately measured. To do so, oxidation rates for two DTR prepared char samples are measured over a wide range of temperatures (623- 873 K) in a TGA such that the char oxidation rates span both Zone I and Zone II conditions. Intrinsic rate parameters for these char samples (X-28, X-75)[‡‡] are calculated using the rate data of three low operating temperatures (623 K, 648 K, and 673 K). Rates at higher temperatures are calculated by applying an intrinsic model using the intrinsic char oxidation reaction rate parameters of these two samples. The pores of varying sizes exist in the porous structure of these char samples, as shown in Figure **5-2** . Most of the pore volume lies in the pore diameter range of 10-50 A^0. Average pore size computed from the Barrett-Joiner-Halenda (BJH) method for sample X-27 is 22 A^o and for sample X-75 is 15 A^o. Average micropore size, calculated using CO_2 adsorption isotherm for both samples, is 11 A^o. Since accounting for the pore size distribution was not possible in the model, an average pore size of these samples is used for prediction in the model. Smith et al.[80] adopted a similar strategy and concluded that the assumption of a uniform pore size compared to bimodal distribution does not significantly affect the rate. Predicted rates at higher temperatures are compared against experimentally measured rates in Figure **5-3.**

[‡‡] X denotes prior conversion (%) on a char basis.

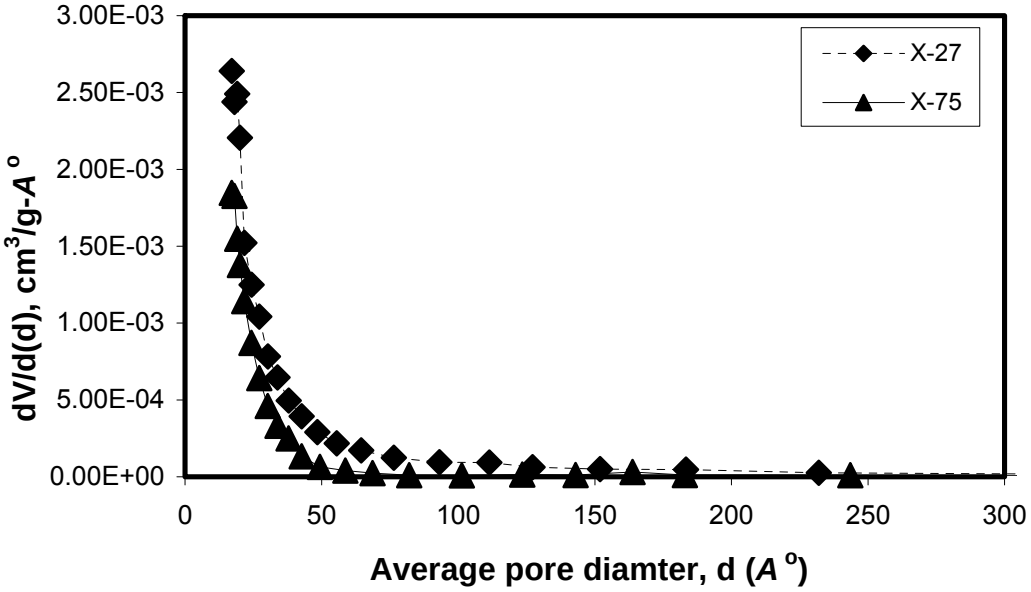

Figure **5-2**: Pore size distribution measured using N_2 adsorption isotherm at 77 K. X refer to prior burnout on a char basis.

The results indicate that the use of $r_p = 20\ A^o$ matches the measured rates for both of these samples. However, a significant deviation between the predicted and measured rate occurs at higher temperature, if $r_p = 150\ A^o$ (computed from the Wheeler model[§§]) is used. The pore radius from Wheeler model is used here for comparison purpose because in a few modeling studies to predict char burnout this correlation has been suggested [192]. The result demonstrates that at lower temperature of TGA, micropore control the char-oxidation process.

[§§] Calculation of pore radius is shown in Appendix 5-2

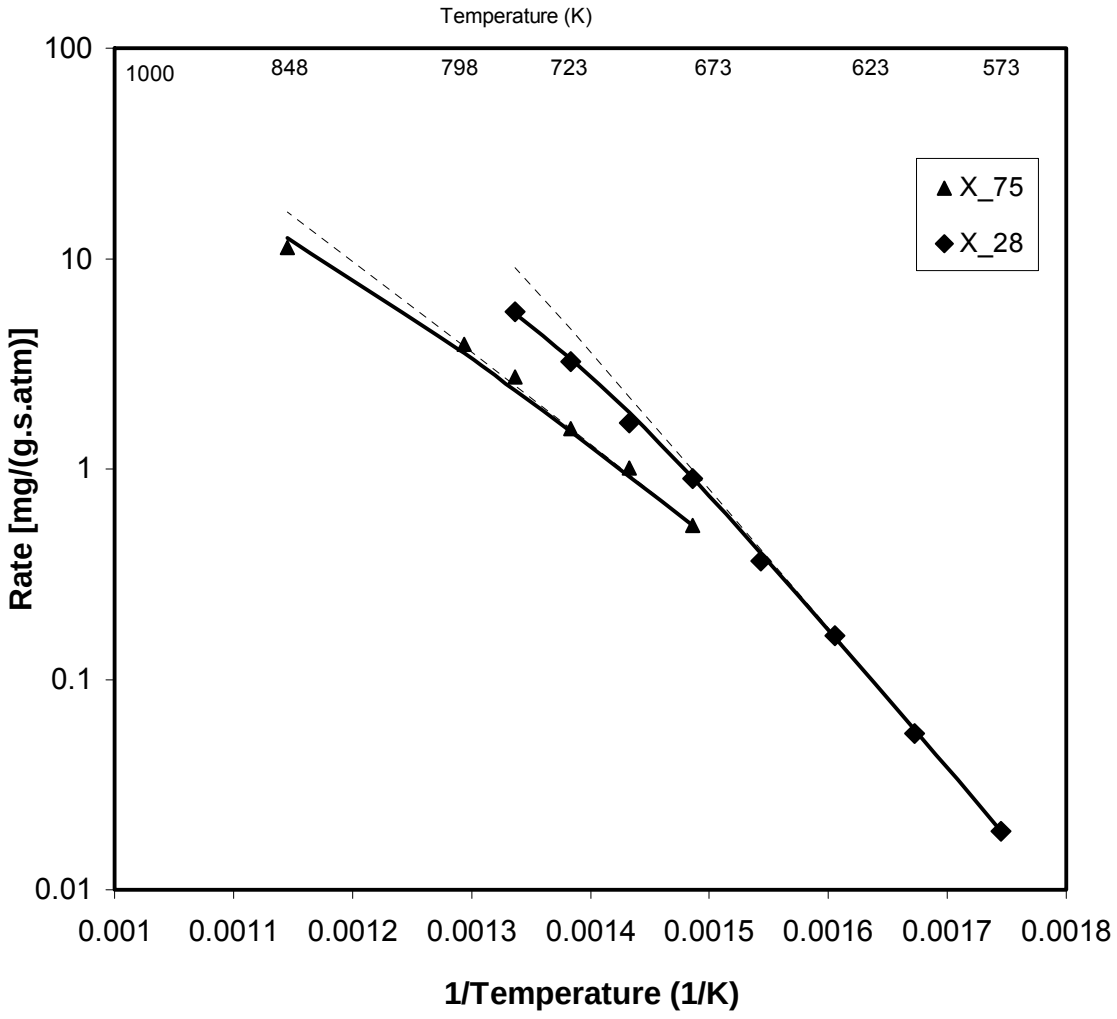

Figure **5-3**: Sensitivity of pore radius (r_p) in prediction of Zone I to Zone II transition rate. Symbols represent measured data. Solid lines are for r_p=20 A^o and dashed line are for r_p=150 A^o

Generally, another concern in using TGA derived rate parameters to predict char burnout under DTR conditions is that coal particles experience different time and temperature histories in the two systems. For example, particles are exposed to a low heating rate (10-50 K/s), a long exposure time (3,600 s) and uniform temperatures in a

TGA compared to a high heating rate (10^5 K/s), a short exposure time (0.5 s) and non-uniform temperatures during the DTR. In Chapter 4, hvCb and lvb rank coal particles were pyrolyzed in the DTR at different furnace temperatures (1,373 K-1,873 K), and in the TGA at 1,123 K for 7 min. and the rate parameters on resulting char particles were measured. The measured activation energy value of the char samples indicated a significant differences (by 30 kJ/mol) based on the experienced temperature history. Clearly, for accurate prediction of char burnout, a model should be able to account for such changes in intrinsic activation energy and reactivity based on their pyrolysis temperature histories. However, this integration is not possible currently for the combustion model available in commercial CFD tools.

Therefore, initial predictions of time-temperature during combustion are accomplished based on the rate parameter data obtained for the char sample generated in the TGA. The particle temperature history during combustion at the centerline of the DTR is predicted, using CFD, at each furnace temperature and is shown in Figure **5-4** for the furnace wall temperatures of 1,173 K and 1,573 K for illustration purpose. It can be observed from the predicted particle temperatures along the furnace length that the particles go through significant variations in temperatures (as much as 400 K) at both furnace temperatures. It should also be noted from the Figure **5-4,** that particle temperatures are significantly higher than the furnace temperatures. The differences between peak particle temperature and furnace temperature are comparatively much higher (~500 K) at a lower furnace temperature (1,173 K). Levendis et al. [193, 194] has summarized past few studies where particle temperature for different rank of coal are measured at different furnace temperature and gas environment. An increase in coal

particle temperature by > 300 K has been consistently reported by various studies [46, 195, 196] for particle undergoing combustion. A similar increase in particle temperature has been theoretically calculated by Smith et al. [197] .

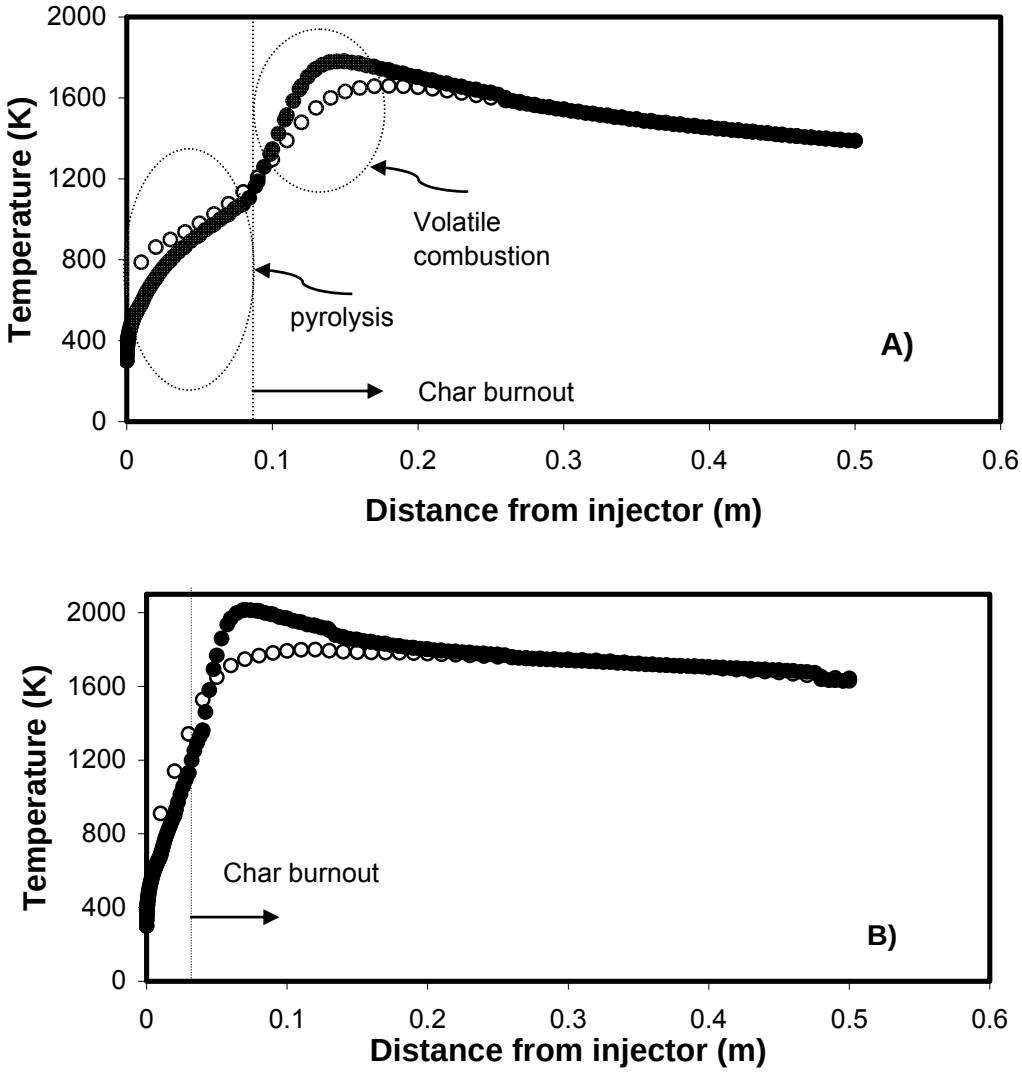

Figure **5-4**: Predicted gas and particle temperatures at DTR furnace temperatures A) 1,173 K; B) 1,573 K. Gas temperature (○), Particle Temperature (●)

Non-consideration of such high particle temperatures in actual combustion conditions is neglected in Morgan's work [189] when a comparison was made, and may be one of the other reason that the extrapolated rate from TGA conditions to DTR conditions yielded a much lower (~20 times) rate than the measured rate.

Since, coal particles would have been pyrolyzed at the predicted peak temperature (1,600 K-1800 K) during the combustion test, rate parameters for further char burnout prediction is taken for the DTR-1673 sample. It should be, noted that the reported reactivity for char samples generated in DTR (in Table **5-1)** is shown for samples that were further heat- treated during rate measurement. Therefore, the reactivity of "as is" chars is compared against reactivity of further heat treated chars and is shown in Figure **5-5**.

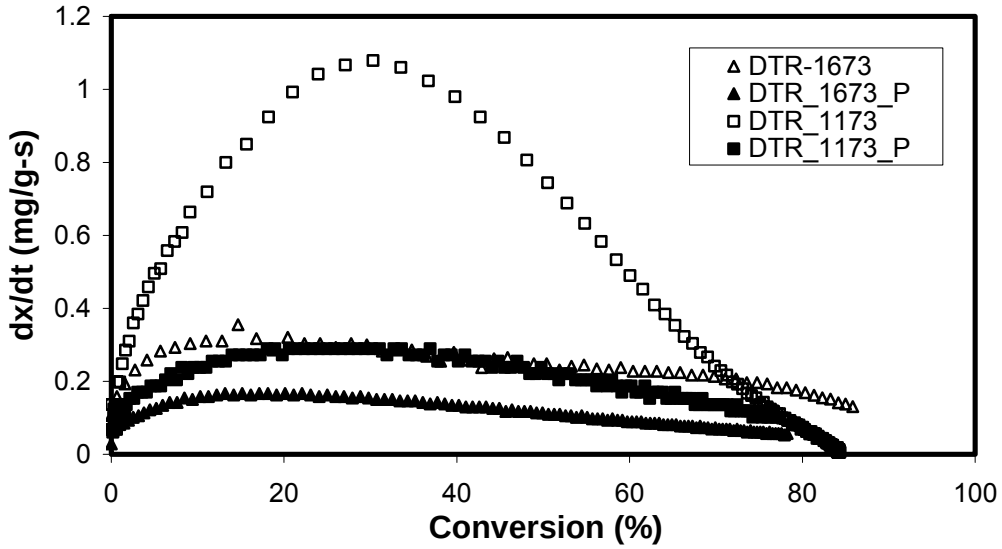

Figure **5-5**: Effect of thermal treatment on measured rate at 673 K. "As is" chars are shown in open symbols. Further treated (1,123 K for 7 min) chars are in closed symbol.

The Figure shows that "as is" DTR-1673 char is ~2 times, and DTR-1173 char is ~4 times, more reactive than their corresponding additionally heat treated samples. Since, actual rate of "as is" DTR-1673 char sample is ~2 times higher than the reported rate in Table **5-1**, the pre-exponential factor is multiplied by 2 to reflect this change in the rate for char burnout prediction. Figure **5-6** compares measured and predicted char burnout at different DTR temperatures ranging from 1,173 to 1,573 K. Char burnouts are calculated using ash tracer technique and are reported on char as initial sample basis (explained in Chapter 2).

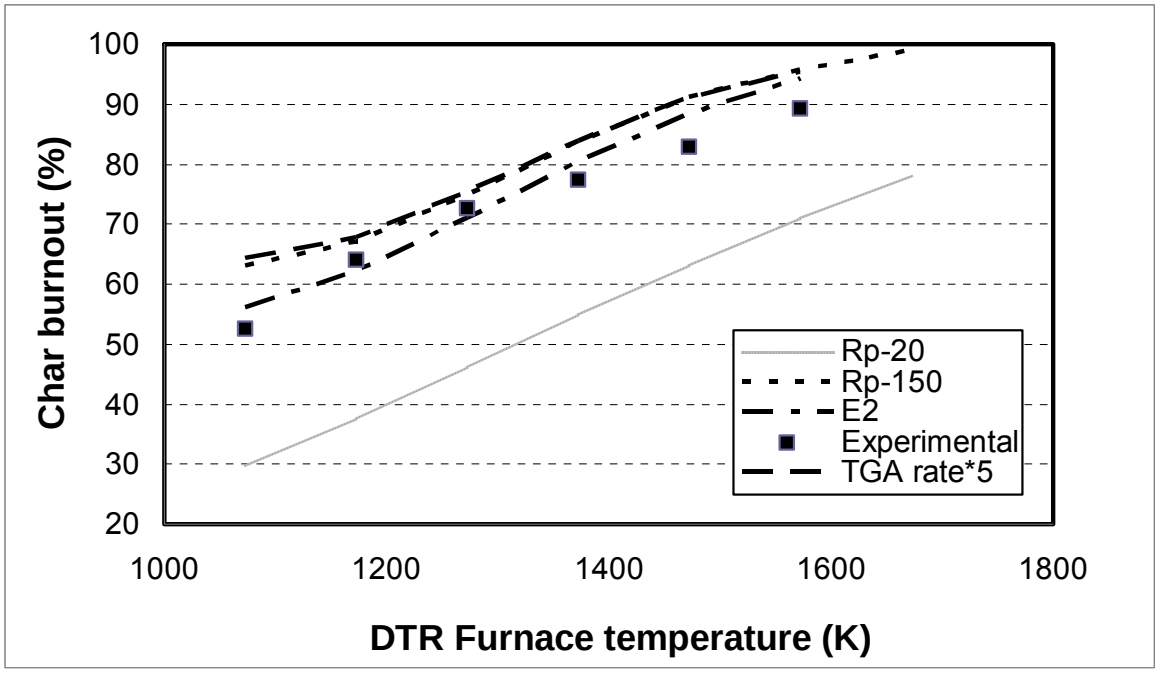

Figure **5-6**: Comparison of experimentally measured (■) and numerically predicted (dotted lines) char burnout: E2: refers to activation energy is increased to 136 kJ/mol. In other predictions, activation energy is 123 kJ/mol. Rp refers to pore radius in A^0

The Figure shows that when r_p = 20, A^o is used to predict char burnout from the DTR; significantly lower burnout values are predicted than the measured values for the

wide range of temperature conditions used. Prediction of lower char burnout using a TGA data may arise for the following reasons: 1) The rate in actual combustion condition is controlled by larger sized feeder pores as opposed to micropores at lower temperatures [198]. 2) A char in actual combustion conditions is more reactive than the char generated in a two-step procedure [136]. 3) Activation energy measured in the TGA is lower than its true value (as shown in Chapter 4). And/or, 4) particle temperatures are under-predicted. The fourth possibility that particle temperatures are calculated incorrectly is ruled out on the grounds that particle temperatures are already predicted to be much higher than the furnace temperature. In order to investigate the other possible reasons, further predictions were made by changing the model parameters. The results indicate that the use of average r_p, computed using Wheeler's correlation (150 A^o) or when the rate is arbitrarily increased by a factor of five or an increase in activation energy by 13 kJ/mol, yield a remarkable agreement between the predicted and measured char burnout values for such wide range of temperature conditions. An attempt is made, in the current study, to determine if the two-step procedure used during char particle collection changed the rate by a factor of 5. For this purpose, a "quenching" step for the DTR was simulated in the TGA. In first case, referred to as in-situ, coal particles are pyrolyzed in the TGA at 1,173 K for 7 min., and then the furnace temperature is decreased to 633 K for rate measurement in air. In the second case, referred as ex-situ, coal particles are pyrolyzed at 1,173 K for 7 min. but then suddenly quenched to room temperature. The rate is then measured on the quenched sample at 633 K in air. The measured rate profile for these two cases is shown in Figure **5-7**. A very minor difference between the rate profiles of *in-situ* and *ex-situ* chars implies that the rate in actual combustion conditions may be

controlled by larger-sized feeder pores, or used activation energy is lower than the true value for a char-oxidation reaction.

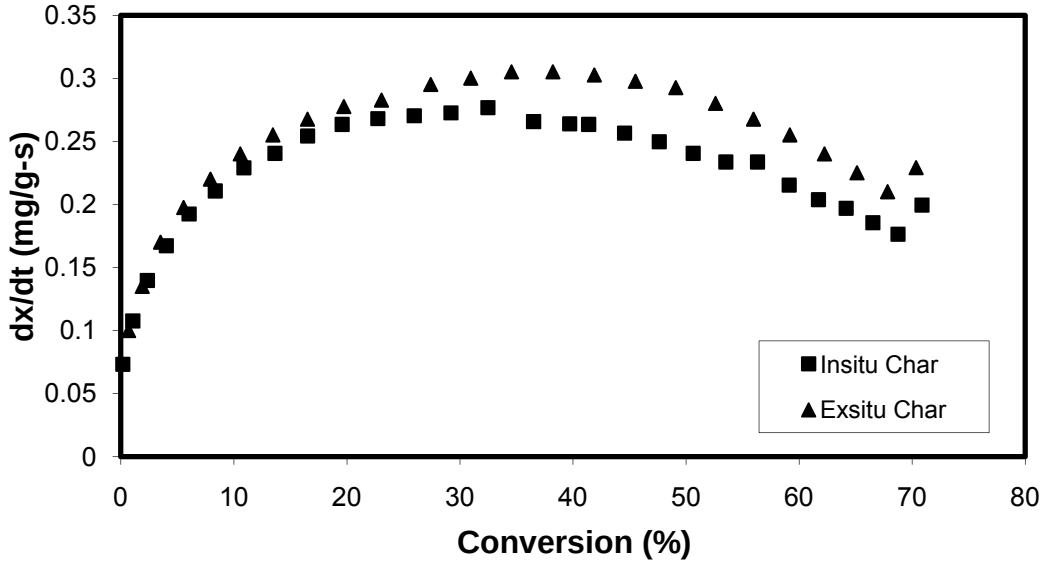

Figure **5-7**: Effect of two-step procedure on measured rate at 633 K

From Figure **5-6**, it was noted that as furnace temperature is increased, the slope (dX/dT) decreased faster, as compared to predicted values. A decrease in slope with an increase in temperature is expected for the following reasons: 1) At lower temperatures, char particles are expected to burn in a pore diffusion controlled regime (Zone II) where temperature sensitivity to reaction is higher compared to a mass transfer controlled regime (Zone III) at high temperatures. 2) A decrease in the intrinsic reactivity of char particles at higher burnout (due to preferential consumption of reactive carbon as observed in Table **5-1),** and 3) an increase in ash diffusion layer with burnout which is neglected in model.

The first possibility is already accounted for in the intrinsic model. In order to account for second possibility, rate parameters are measured for char samples that underwent to different extents of weight loss at 1,373 K during combustion. A different extent of conversion is achieved by changing the amount of excess air and maintaining a similar residence time (0.5 s). The reactivity (or rate parameter for char-oxidation) of the resultant samples is measured in the TGA using air in an isothermal process. The rate parameters for the combusted char samples, as shown in Table **5-1**, are incorporated in FLUENT^{TM} and revised predictions of char burnout are made. These revised predictions are shown in Figure **5-8** for two particle sized classes.

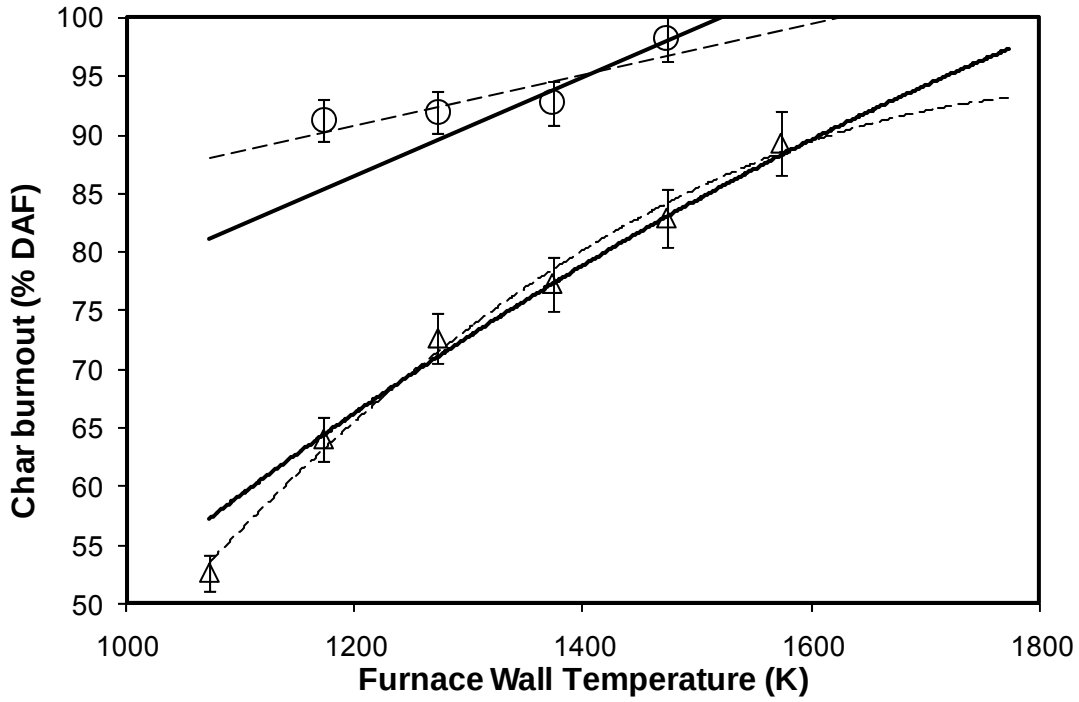

Figure **5-8**: Comparison of experimentally measured (symbols) and numerically predicted (lines) char burnout for a hvCb rank coal of different particle size from the DTR: 74-112 μm (Δ) , 112-150 μm

Figure **5-8** shows that accounting for conversion history in the combustion model truly reflects the nature of carbon burnout. A slightly higher difference between the measured and predicted char burnout values for small particle sizes may be because of relatively higher char burnout values. At such a high conversion, a measured char burnout rate is observed to be less sensitive to temperature than the predicted char burnout values. This is anticipated to be caused by the effect of gas diffusion through ash layer being neglected in model.

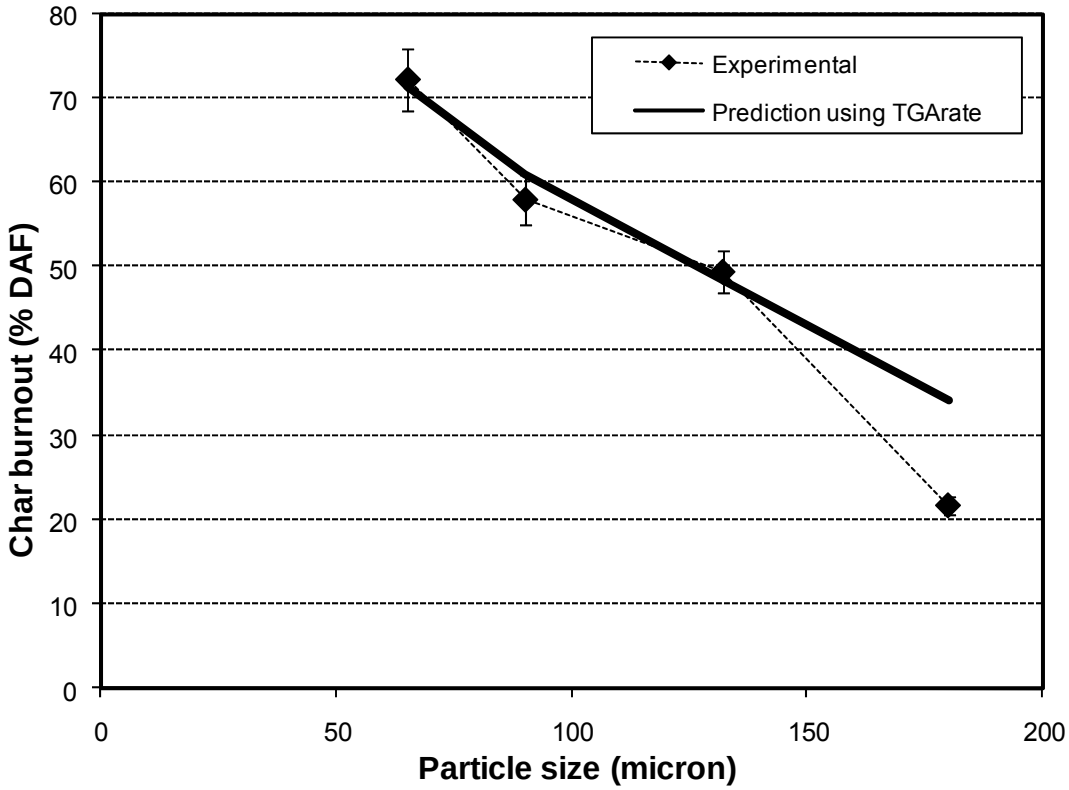

Figure **5-9**: Comparison of experimentally measured and predicted char burnout of different particle size class from a pilot-scale boiler

This intrinsic model is then employed to predict char burnout from an actual pilot scale boiler. The char burnout predictions were made for four particle size classes and are compared against experimental measurements in Figure 5-9. A remarkable agreement is observed between the experimental and predicted char burnout values when 136 kJ/mol as an activation energy (E_A) value of char-O_2 reaction (in place of 123 kJ/mol measured in TGA) is used.

Summary and Conclusions

The main objective behind this research is to determine whether or not intrinsic rate parameters determined in a TGA at low temperatures can be used for reliable predictions of char burnout from actual combustion conditions. Theoretical analysis suggests that accurate knowledge of both the activation energy of char oxidation reaction and the pore structure of char particles are necessary for reliable predictions. The results show that the rate in a low heat-rate condition can be accurately captured using an intrinsic model. However, at a high-heat rate condition of a DTR (furnace temperatures ranging from 1,173-1,573 K), rates were predicted to be ~5 times lower than the measured values. A marginally higher rate of a quenched sample than the rate of a char prepared in a TGA suggests that a two-step procedure used in a TGA is not the reason behind these lower burnout predictions. Good agreement is observed between the predicted and char burnout values if the estimated activation energy is increased (by ~13 kJ/mol) or if the reaction rate is assumed to be controlled by a larger sized feeder pores than the micro-pore size of the samples. The experiments indicate that as temperature is

increased, the slope of char burnout decreased faster than the prediction. This was shown to be caused by a decrease in the char reactivity and activation energy values with conversion. Clearly, for an accurate prediction of char burnout, the model should account for the change in rate and activation energy of a sample based on particle thermal annealing and conversion. Although the effect of conversion on rate can be easily integrated into the commercial CFD modeling tool, the challenging task remains to develop and integrate thermal annealing correlation in the commercially available CFD codes.

Chapter 6

Comparison of Char Burnout and CO and NO_x Formation Behavior in O_2/CO_2 and O_2/N_2 Gas Medium

Introduction

Recently (as evident from the number of papers presented at coal conferences in past 2-3 years) oxy-coal combustion has received considerable attention as one of the potential technologies which can achieve a sequestration ready CO_2 gas stream. Since the costs involved in obtaining a pure oxygen stream and compressing flue gas are a significant barrier for the application of this approach, a few studies have explored the apparent advantages of this approach in terns of NO_x levels [57] and un-burnt carbon (UBC) [40] to minimize the costs. These studies have been conducted at both lab-scale and pilot-scale levels. In the experimental studies for char burnout on both the scales, the trend for char burnout was observed to be on the order of 21 O_2/79% CO_2 < Air < 30 O_2/70% CO_2, as expected. However, what remains unclear is whether or not higher partial pressure of CO_2 in the gas medium causes an increase in the rate of char burnout and CO emissions. Apparently, compared to combustion in air, char burnout in oxy-coal combustion was higher for lower ranks of coal [40]. In the experimental studies for NO_x emissions, a reduction of up to 70% has been measured in various pilot-scale studies [15, 47]. This reduction has been mainly proposed to be the result of the reaction between recycled NO_x and hydrocarbon radicals present in the flame [55]. However, an experimental study on a lab-scale and a pilot-scale suggested that the reduction in NO_x emissions depends upon the coal type [28]. A numerical study also showed that the potential in NO_x reduction

depends upon the burner design [57]. Chapter 3 established that the reactivity of char, and distribution of coal-N between volatile and char phase is not influenced by the presence of higher amounts of CO_2. In Chapter 4, a method to determine intrinsic rate parameters, using a thermogravimetric analyzer, was established. In Chapter 5, validity of a commercially available Computational Fluid Dynamics (CFD) tool, for a wide range of temperature conditions using the measured parameters, for the prediction of the char burnout was shown. The main objectives of this chapter are to test the hypothesis of the current research that some coal are more suitable for oxy-coal combustion and predict the char burnout, NO_x and CO emissions from oxy-coal combustion on a pilot-scale. These specific objectives are described below:

Objectives

1. Experimentally test if some coals are more suitable for use in oxy-coal combustion in terms of char burnout and NO_x emissions, and
2. Use the developed tool to explain the experimentally measured char burnout, NO_x and CO emissions, and predict these parameters for a pilot-scale facility.

Methodology

In order to address these questions, combustion experiments are conducted in a drop tube reactor (DTR) for low volatile (lvb) and high volatile coal (hvCb) samples in air and in a 21% O_2/79% CO_2 mixture at furnace temperatures between 1,173 to 1,773 K.

Although, a 30% O_2/70% CO_2 mixture, as an oxidizer, represents the oxy-coal combustion condition, a 21% O_2/79% CO_2 mixture is used in this study so that the role of CO_2 can be comprehensively understood.

An intrinsic model available to simulate char-oxidation reaction in the Computational Fluid Dynamics (CFD) tool is modified to account for char-CO_2 reaction using User Defined Functions (UDFs). Details of the experimental facilities, testing procedure, and computational model are provided in Chapter 2. Gas species measurement and char burnout at the exit of the DTR are used to compare the model predictions for combustion in air with combustion in a 21% O_2/79% CO_2 mixture. Composition of the coals and their particle size distribution are described in Chapter 2.

Results and Discussion

First, the experimentally measured and computationally predicted char burnout, NO_x and CO emissions from the DTR during combustion in air and in a 21% O_2/ 79% CO_2 mixture are discussed. Afterwards, results of a pilot-scale combustion test conducted in air are compared against the numerical prediction. Finally, pilot-scale model predictions were extended for oxy-coal combustion and compared with combustion in air for different ranks of coal to determine which coal is more suitable for oxy-coal combustion.

Lab-Scale

In order to ascertain whether char-CO_2 reaction will have any noteworthy effect on overall char burnout, a conceptual diagram is constructed using an intrinsic model to compare the combustion rates of coal during conventional combustion in air to the oxy-coal combustion environment. Comparison of combustion rates were made using activation energy (E_A) values of 189 and 256 kJ/mol for char-CO_2 reaction at an activation energy value of 123 kJ/mol for char-O_2 reaction. These values of E_A for char-CO_2 reaction were chosen to represent the typical values reported in the literature for wide ranks of coal char samples. Rate of combustion in air is calculated assuming an O_2 partial pressure of 0.21, and ignoring the contribution from char-CO_2 reaction. For rate of combustion in an O_2/CO_2 media, an additional contribution from rate of char-CO_2 reaction is considered using CO_2 partial pressure of 0.79. A decrease in O_2 diffusivity by 20% due to higher partial pressure of CO_2 was considered in these calculations for oxy-coal combustion.

Figure **6-1** shows the comparison of the rate of char burnout in the two combustion approaches against temperatures ranging from Zone I to Zone III conditions. The Figure shows that in a pilot-scale or industrial-scale facility, where temperatures in the near burner zone are expected to be ~2,300 K, a higher combustion rate in oxy-coal combustion than combustion in air is predicted due to higher levels of CO_2. The increase in rate depends upon the activation energy value of gasification reactions of a particular char. In order to simulate the late stages of char burnout, similar calculations are done using O_2 partial pressure of 5% and a resultant rate of char burnout as a function of

temperature is shown in Figure **6-2**. Since, in the late stages of burnout, particle temperatures are expected to be in the range of 1,400 to 1,600 K, therefore, the Figure shows that the rate in oxy-coal combustion can be higher than that of combustion in air *only if* activation energy for char-CO_2 reaction is in the higher end of reported values (≥250 KJ/mol).

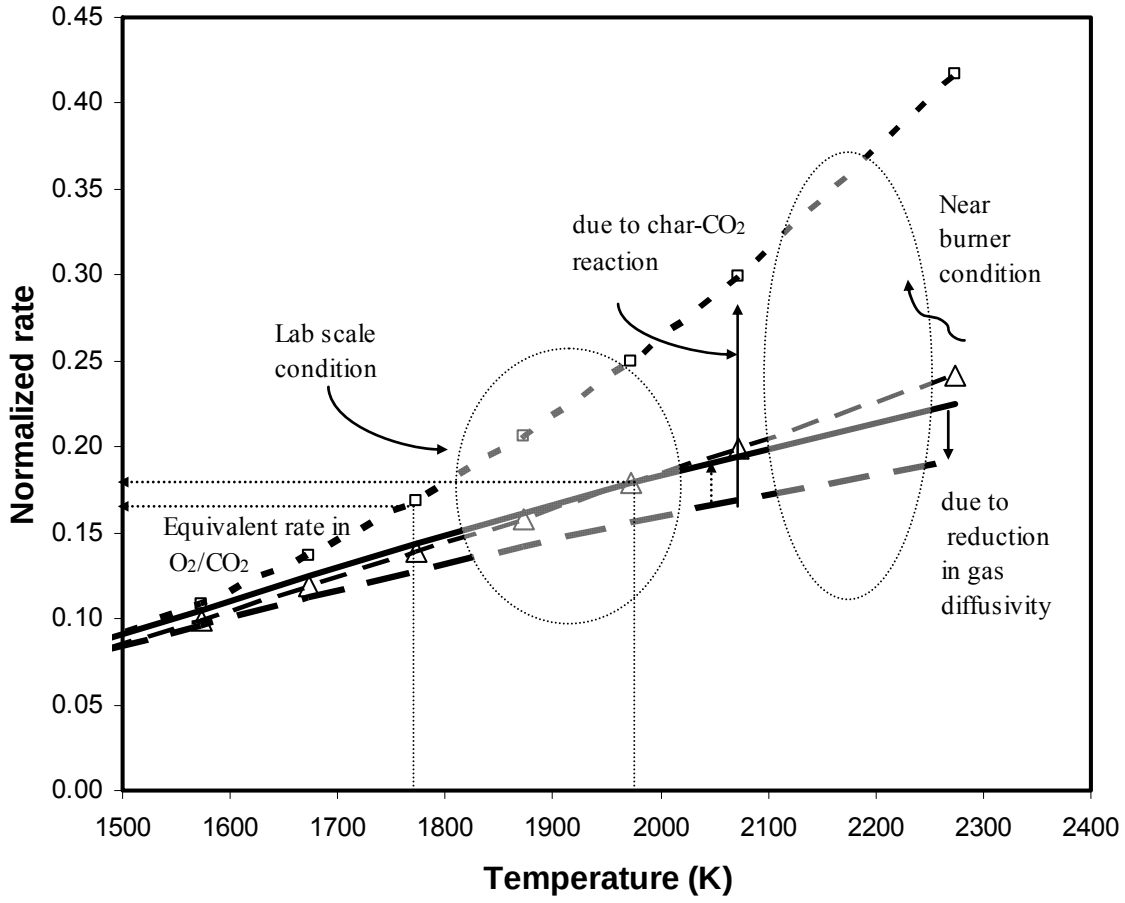

Figure **6-1**: Theoretical calculation for the effect of surrounding CO_2 levels on char combustion rate simulating late stages of combustion (**—**) normalized rate for combustion in 20% O_2; (---) lower $_{O2}$ diffusivity in CO_2 rich combustion media; Symbols account for char-CO_2 reaction. (Δ) *E*=189 kJ/mol; (□) *E*=256 kJ/mol

It must be noted that the comparison of computed rate of char burnout in oxy-coal combustion to combustion in air in Figure **6-1** and Figure **6-2** was done at the same levels of particle temperature. Since gas/particle temperature in actual combustion condition of the DTR was not measured in this study, they were predicted using the CFD model.

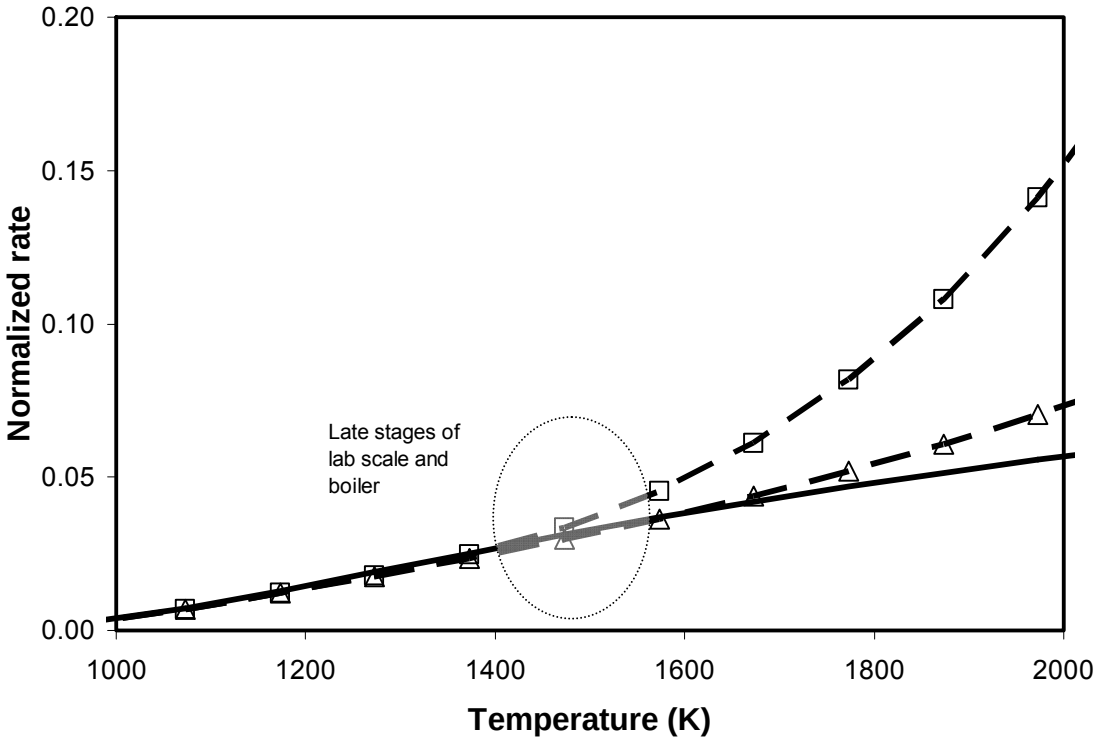

Figure **6-2**: Theoretical calculation for the effect of surrounding CO_2 level on char combustion rate simulating late stages of combustion.(**—**) normalized rate for combustion in 5% O_2; Symbols account for char-CO_2 reaction. (Δ) E=189 kJ/mol; (□) E=256 kJ/mol

The predicted results of the particle temperature at the centerline of the DTR (shown in Figure **6-3**) indicate that the peak particle temperatures in the early stages of combustion are ~200 K lower during combustion in the 21% O_2/79% CO_2 mixture

compared to those of combustion in air. However, in the late stages of burnout, no such difference exists.

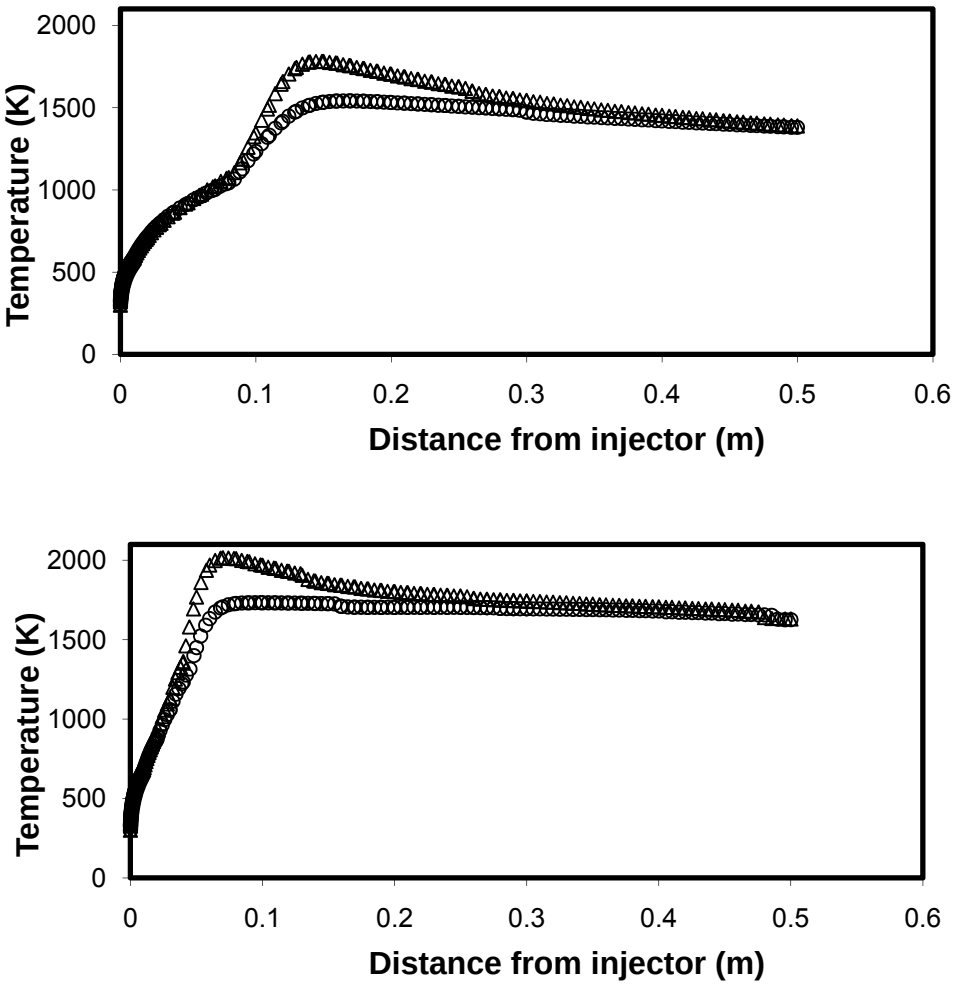

Figure **6-3**: Comparison of predicted particle temperatures during combustion in air (Δ) and in 21% O_2/79% CO_2 mixture (○). A) 1,173 K; B) 1,573 K

The reduction of ~200 K in the peak particle temperature between the two combustion media arises because of the reduction in gas temperature during use of the 21% O_2/79% CO_2 (as shown in Figure **6-4**) due to higher specific heat of CO_2. This reduction in peak temperature in the early stages and similar particle temperature for the

most part of the carbon burnout process for oxy-coal combustion compared to combustion in air indicate that overall char burnout will be higher only for particles whose activation energy value of char-CO_2 reaction is > 250 kJ/mol.

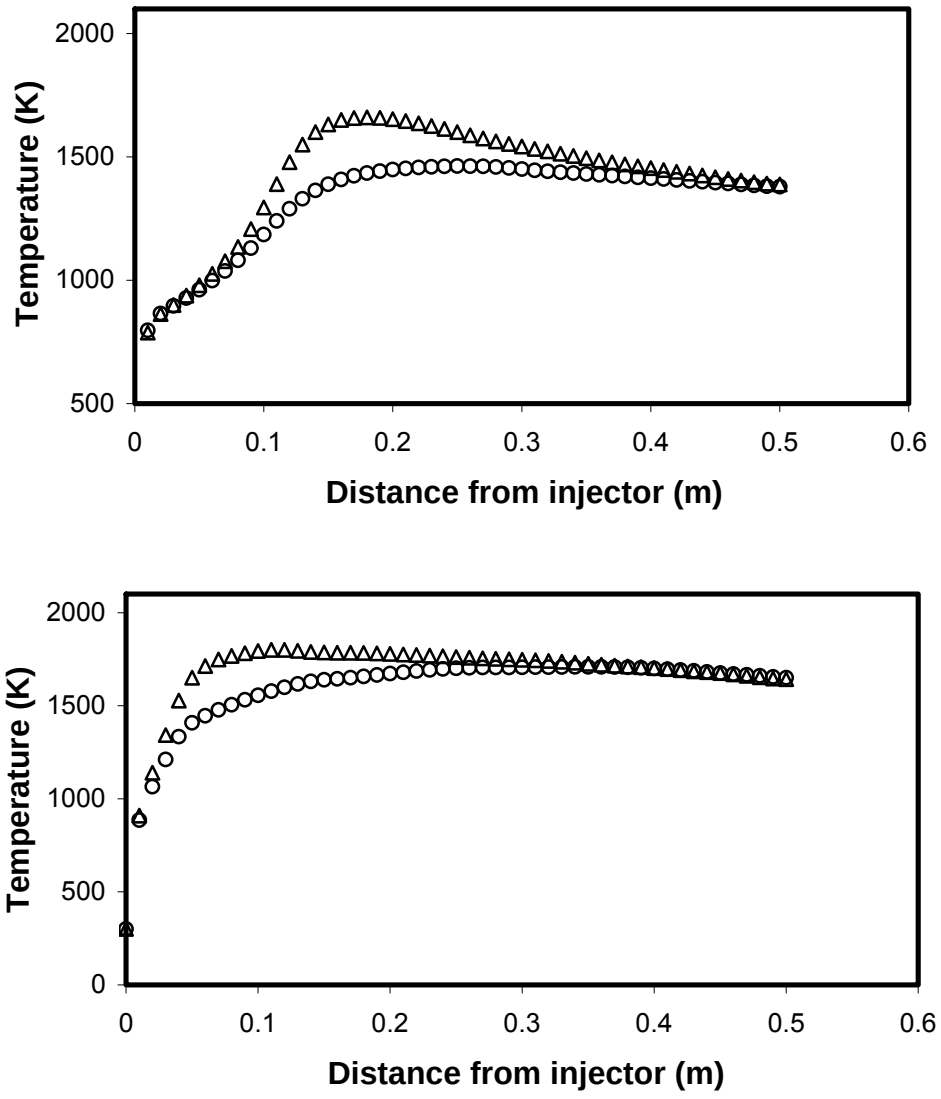

Figure **6-4**: Comparison of predicted gas temperatures during combustion in air (Δ) and in 21% O_2/79% CO_2 mixture (○). A) 1,173 K; B) 1,573 K

Figure **6-5** shows the comparison of experimentally measured char burnout during combustion in air to that of combustion in a 21% O_2/79% CO_2 gas medium for the hvCb and the lvb ranks of coal at furnace wall temperatures ranging from 1,173 K to 1,673 K. Several trends can be observed from the plots shown in Figure **6-5**. First, char burnouts are lower during combustion in a 21% O_2/79% CO_2 mixture compared to that of combustion in air for both ranks of coal, and the difference in char burnouts diminishes as furnace temperature is increased. Lower char burnout during combustion in a 21% O_2/79% CO_2 mixture, as compared to that of combustion in air, is expected due to lower O_2 availability to the particle surface and lower particle temperatures as described earlier.

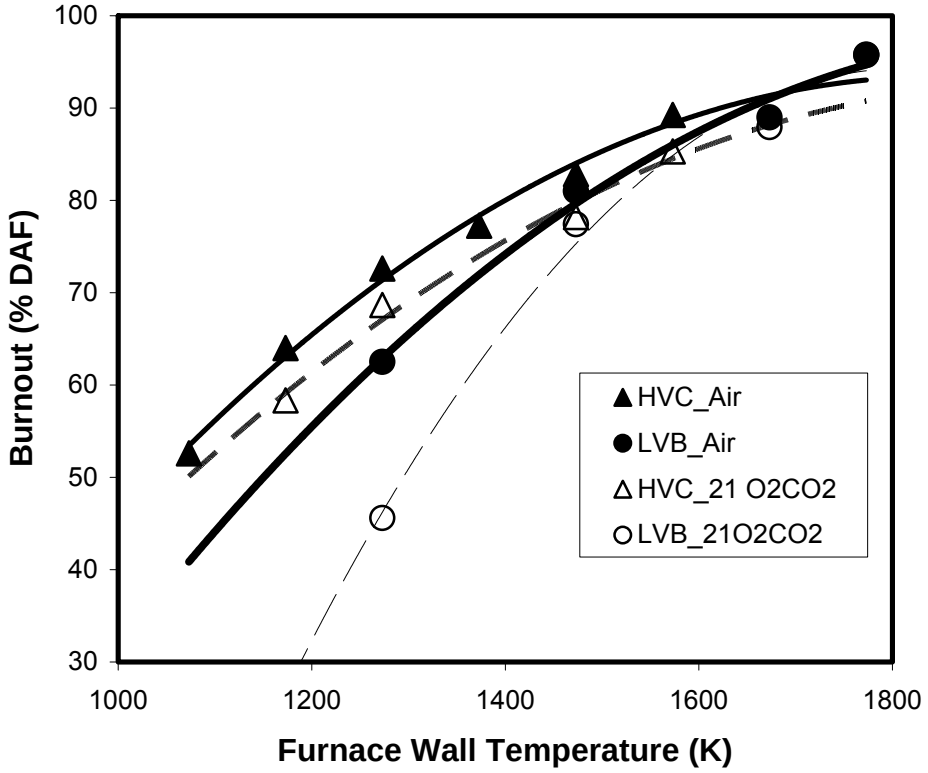

Figure **6-5**: Comparison of char burnout in air and in 21% O_2/79% CO_2 gas medium. Open symbols (21% O_2/79% CO_2); closed symbol (air). (▲,Δ) hvC coal; (•,○) LV coal

However, at higher temperatures, an increase in the rate caused by char-CO_2 reaction possibly compensates for such a decrease of O_2 availability and lower particle surface temperatures for both the coal types. Second, the difference in char burnout from combustion in air and combustion in the 21% O_2/79% CO_2 mixture at higher temperatures is lower for the lvb coal compared to that of the hvCb coal. In order to explain the possible cause, a rate parameter for the chars from hvCb and lvb rank coal is estimated from the reactivity measurement in the TGA using an O_2 and a CO_2 gas. The rate parameter values are calculated as an average value from the onset of a maximum to 80% conversion value in the reactivity plot. The measured rate parameters (shown in Table **6-1**) shows higher activation of char-CO_2 reaction for the lvb coal (E_A-256 kJ/mol) compared to that of the hvCb coal (E_A-189 kJ/mol) and same activation energy of char-O_2 reaction for both the coals. These values of activation energy suggest that the overall rate will increase more for the lvb coal than the hvCb coal upon an increase to higher temperature during oxy-coal combustion. Ratio of char reactivity towards O_2 and CO_2 is extrapolated (using the rate parameter shown in Table **6-1**) at a higher temperature for these two ranks of coal and is shown in Figure **6-6.**

Table **6-1**: Comparison of char oxidation and gasification rate parameters between a hvCb and lvb rank coals

	hvCb-1673		lvb-1673	
	A (g/(g.s.atm air))	E (kJ/mol)	A (g/(g.s.atm air))	E (kJ/mol)
char-CO_2	3.50R+05	189	1.07E+09	269
char-O_2	1.33E+05	123	4.54E+02	94

Figure **6-6** shows that, due to higher activation energy of the char-CO_2 reaction for lvb coal, an increase in rate due to char-CO_2 reaction is higher for the lvb coal than for the hvCb coal above 1,050 K.

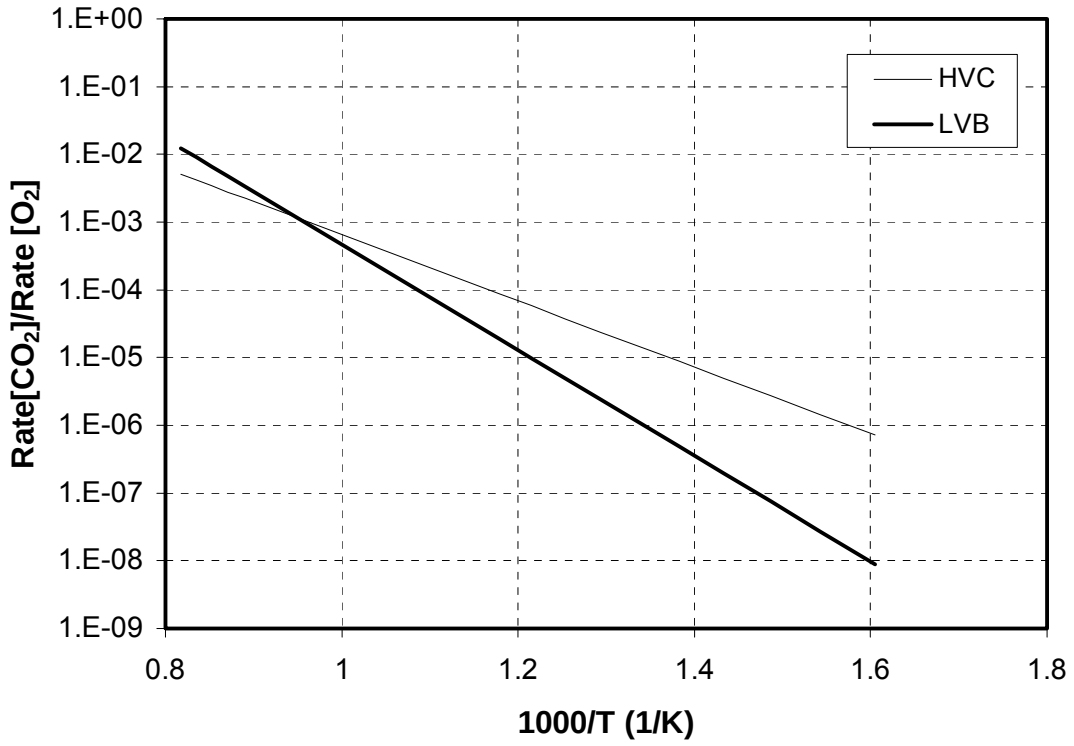

Figure **6-6**: Ratio of char reactivity towards different gases for lvb and hvC rank coal

A comparison of experimentally measured NO_x emissions in these two combustion media for the hvCb and the lvb ranks of coal are shown in Figure **6-7**. Several observations can be made from Figure **6-7**: First, as furnace temperature increases, NO_x emissions increase for both the combustion media, and for both ranks of coal. In conventional combustion in air, an increase in NO_x formation with an increase in temperature is expected because of an increase in contribution of thermal-NO_x and an

increase in conversion of coal-N into NO_x. Second, the NO_x emissions are always lower during combustion in a 21% O_2/79% CO_2 mixture compared to that of combustion in air. A lower NO_x emission from combustion in a 21% O_2/79% CO_2 mixture is expected due to a decrease in gas/particle temperatures (by ~200 K) compared to that of combustion in air. The decrease in gas temperature decreases the conversion of intermediate NO_x precursor species such as HCN and NH_3 into NO_x. The decrease in particle temperature causes a reduction in char burnout which may cause more retention of coal-N in the char.

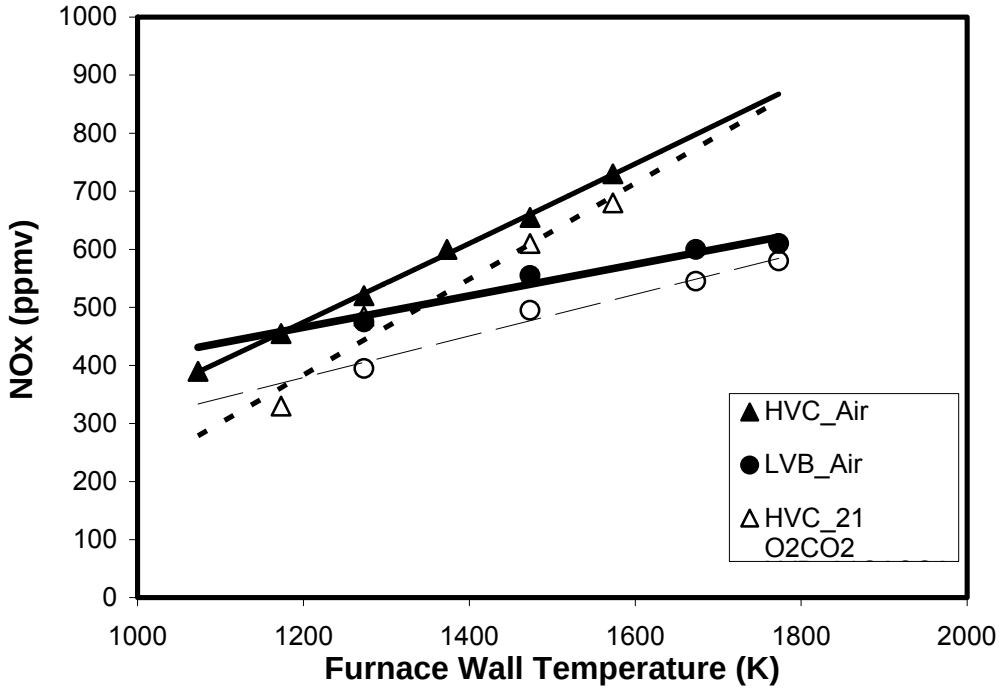

Figure **6-7**: Comparison of NO_x emission during combustion in air in 21% O_2/79% CO_2. Open symbols (21% O_2/79% CO_2); closed symbol (air). (▲,Δ) hvCb coal; (●,○) lvb coal

In order to determine, which of the two factors is dominant, NO_x formation in the DTR was modeled using FLUENT^{TM}. In one case, for combustion in 21% O_2/79% CO_2,

the fraction of coal-N retained in the char was assumed to be same as that of combustion in air. In another case, the fraction of coal-N retained in the char was estimated from the weight loss during combustion in 21% O_2/CO_2 mixture. The predicted NO_x formation for these cases is shown in Figure **6-8** . Notably, the dominant factor responsible for NO_x formation is a reduction in gas phase conversion of N-containing NO_x-precursor species due to lower temperatures in the 21 % O_2/CO_2 medium.

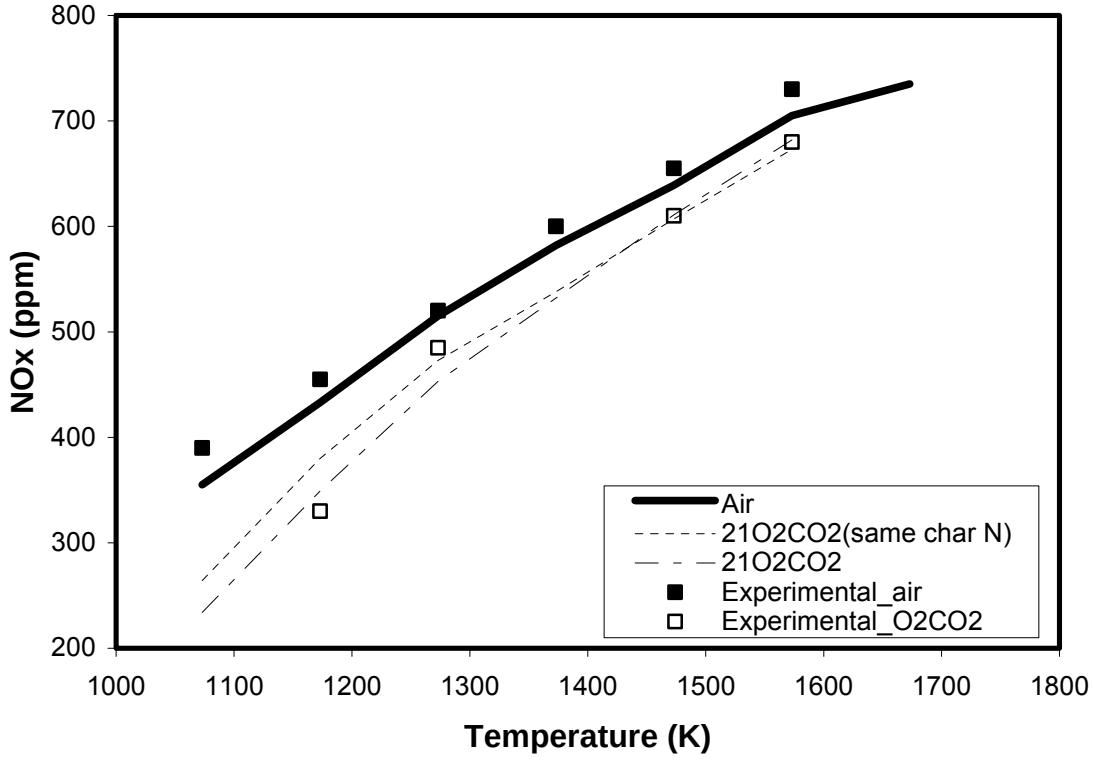

Figure **6-8**: Predicted effect of coal-N retention during 21% O_2/ 79% CO_2 on NO_x formation: Line shows CFD predicted NO_x and symbols shows experimental measurements

Also seen from Figure **6-7** is that for both ranks of coal, the ratio of NO_x formation during combustion in air to that of combustion in the 21% O_2/79% CO_2 mixture is similar. This result suggests that NO_x formation in the two media is not

affected by the rank of coal. The difference in NO_x formation between the two combustion media is found to decrease with an increase in temperature. If the NO_x formation through the thermal route were to take place, the difference should have increased with an increase in temperature. This observation indicates that, during combustion in a lab-scale facility, where gas phase temperatures are lower than ~1,800 K, contribution from thermal NO_x is negligible.

Figure **6-9** shows the comparison of measured CO emission from the DTR during the two combustion media.

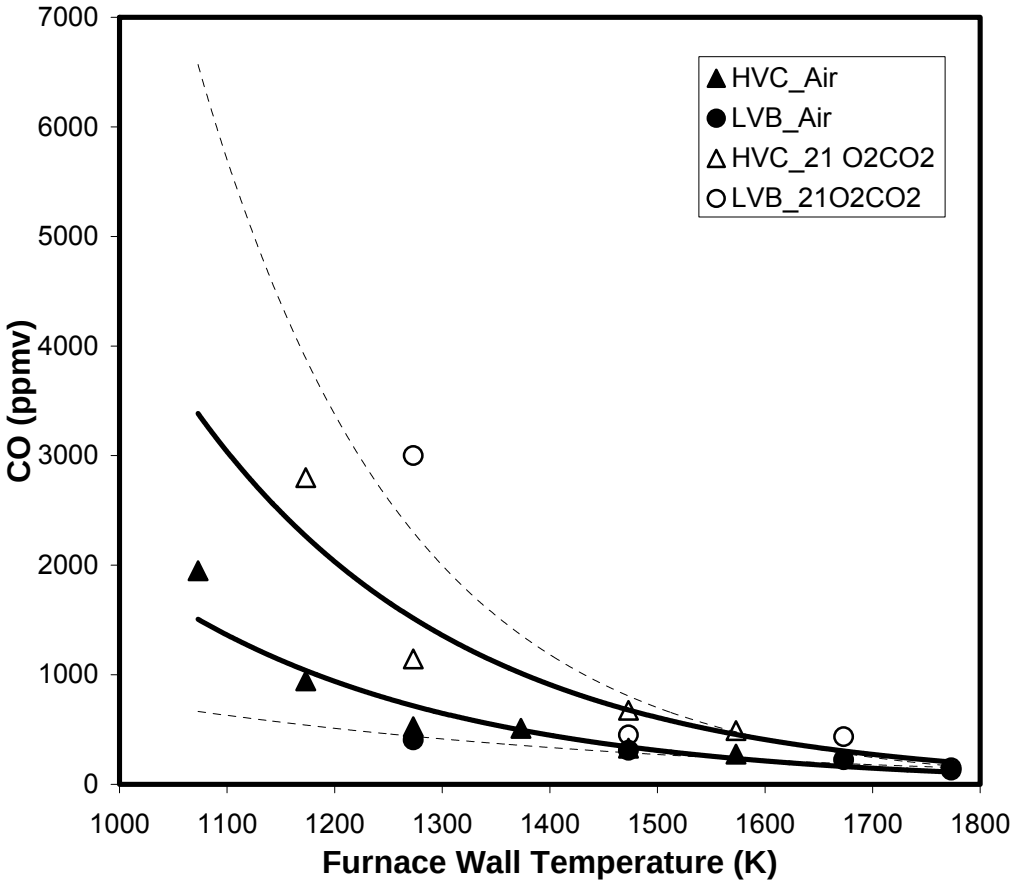

Figure **6-9**: Comparison of CO emissions between combustion in air and in 21% O_2/79% CO_2. Open symbols (21% O_2/79% CO_2); closed symbol (air). (▲,Δ) hvCb ; (●,○) lvb coal

The Figure shows that as furnace temperature increases, the CO emissions decrease and that the CO emissions are always higher during combustion in a 21% O_2/79% CO_2 mixture compared to that of combustion in air. For both ranks of coal, the ratio of CO formation in a 21% O_2/79% CO_2 medium to that of combustion in air is higher at lower furnace temperatures and the ratio decreases as furnace temperatures increase. Importantly, the observed CO concentration values are much higher than the estimated equilibrium CO values at all temperatures (refer to Figure **1-2**). This result highlights that the gas phase chemical composition is not under equilibrium in the laminar flow conditions of a DTR. A decrease in CO emissions with an increase in temperature cannot be explained on the basis of char oxidation surface product (CO/CO_2) ratio which is expected to increase with temperature. Thus, a decrease in CO emissions with an increase in temperature means that upon an increase in temperature the rate of CO formation is slower compared to the rate of CO oxidation. This observation is also consistent with the typical E_A values of CO formation reaction (E=50-100 kJ/mol for pyrolysis) and CO oxidation reaction (E=125-200 kJ/mol). However, the observation of a decrease in CO emission with an increase in DTR furnace temperature could also occur *if* an increase in temperature causes an increase in mixing between O_2 and CO.

Which of the two factors is controlling the overall CO emission is evaluated using the CFD model by conducting a parametric sensitivity analysis. A significant uncertainty remains in the literature regarding the fraction of carbon that goes through CO or CO_2 [96]. Therefore, CO emission is predicted in one case assuming CO as a product and in other case assuming CO_2 as a product. The rate parameter for volatile oxidation is taken from the literature [199]. The mixing parameter between the reactant and product is taken as a

default value in FLUENT^{TM} for the gas phase reaction. Char oxidation product ratio [CO/CO_2] is taken as 1. The predicted CO emissions for these two cases (representing reaction is controlled by kinetics) are shown as solid lines in Figure **6-10**. Another set of simulations was completed by keeping CO as a volatile product but changing the mixing rate parameter as a function of temperature to represent that the reaction is controlled by mixing. This set of predictions is shown as a dotted line in Figure **6-10**. Excellent agreement of experimentally measured CO concentration occurs with the prediction when reaction is assumed to be controlled by mixing. Data in Figure **6-9** indicated higher CO emissions during combustion in a 21% O_2/79% CO_2 mixture than combustion in air.

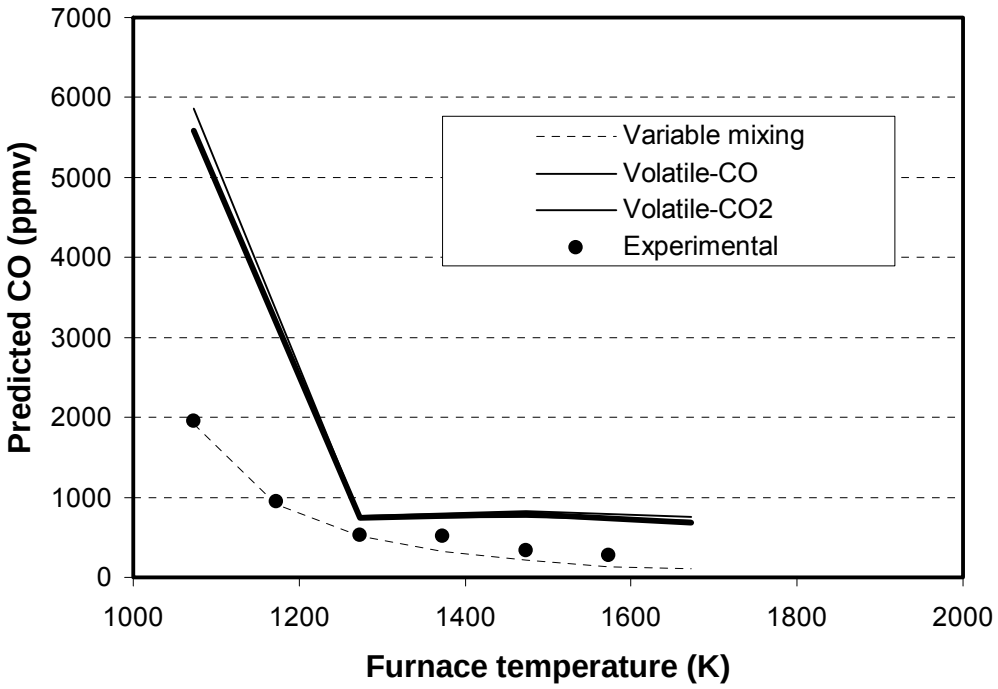

Figure **6-10**: Determination of dominant factor that controls overall CO formation during combustion in a lab-scale DTR: Symbols represent experimental, Solid line represent the case when reaction is controlled by kinetic, dotted line represent when CO formation is controlled by mixing

In order to determine, whether or not this is caused because of char-CO_2 reaction, numerical predictions of CO emission were made with and without char-CO_2 reaction. The CO emissions in Figure **6-11** show that agreement between predictions and experimentally measured values occurs when char-CO_2 reaction is considered in the model. An under prediction in CO emission by ~15 to 20% occurs if the char-CO_2 reaction is not considered in the model.

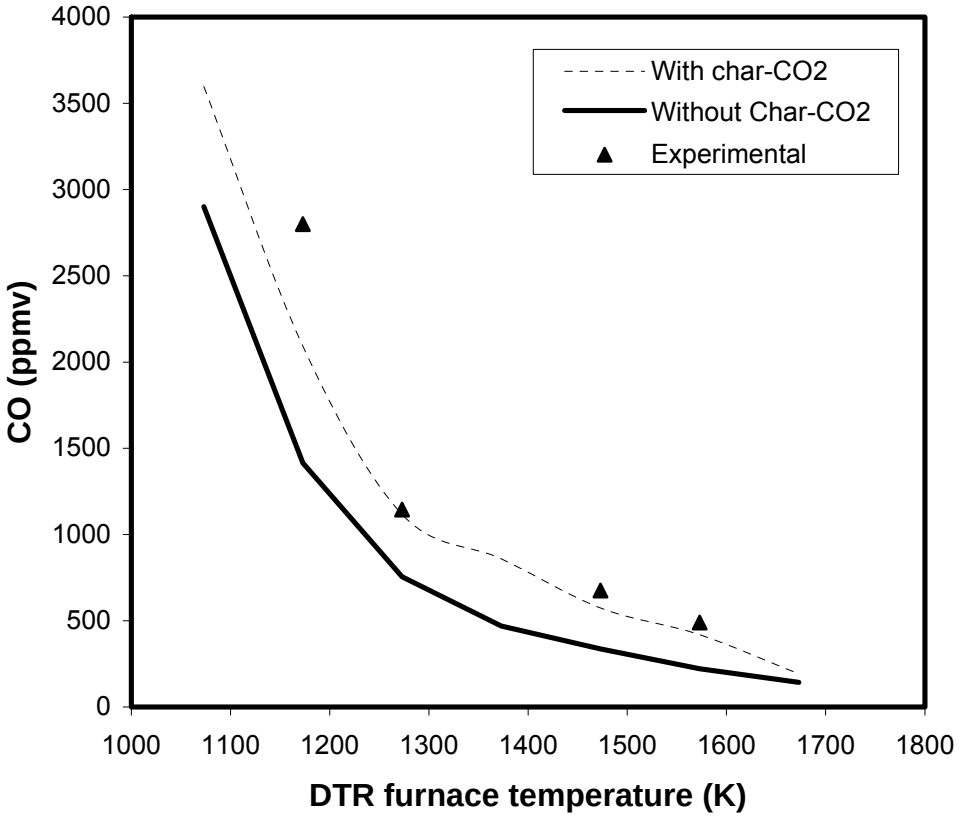

Figure **6-11**: Determination of role of char-CO_2 reaction on CO formation. Lines represent prediction, symbol represents experimental data

Pilot-Scale

The lab-scale data of experimentally measured and CFD predicted values for char burnout and CO emissions suggested that the inclusion of char-CO_2 reaction in the model is necessary. This reaction model was used to predict the char burnout, gas species (CO, NO_x, CO_2 and O_2), and temperature inside the pilot scale boiler and compared against measurements during combustion in air. The location of the experimental measurements of gas species are shown in Figure **6-12.**

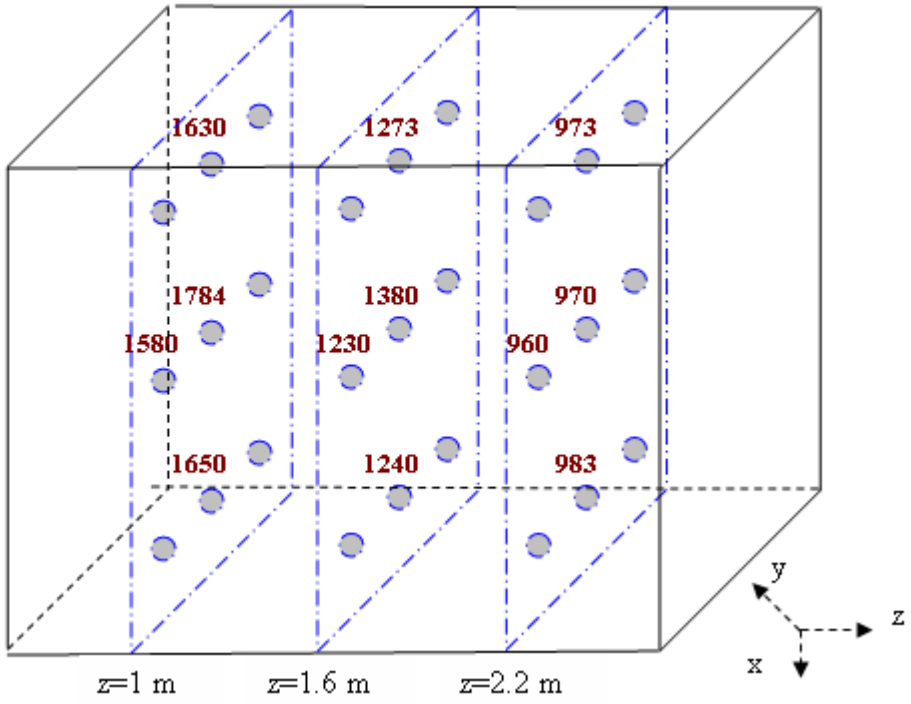

Figure **6-12**: Locations where gas species and temperatures were measured during combustion test in air in the Research Boiler. Actual measured temperatures (K) are included.

The comparison of experimental and predicted results for O_2 (in Figure **6-13**), CO_2 (in Figure **6-14**), CO (in Figure **6-15**), NOx (in Figure **6-16**) and temperature (in Figure **6-17**) is shown. Apparent from these profiles is that most of the carbon conversion and NO_x formation is taking place within the quarl (0.75 m from burner) zone while the measurements ports are located away from the quarl. These profiles show that the model is capturing the trend reasonably well. However, the CFD model is over-predicting the CO formation and under-predicting the CO_2 formation. This is because of the assumption, in the model, that all the carbon converts into CO during coal pyrolysis and volatile oxidation.

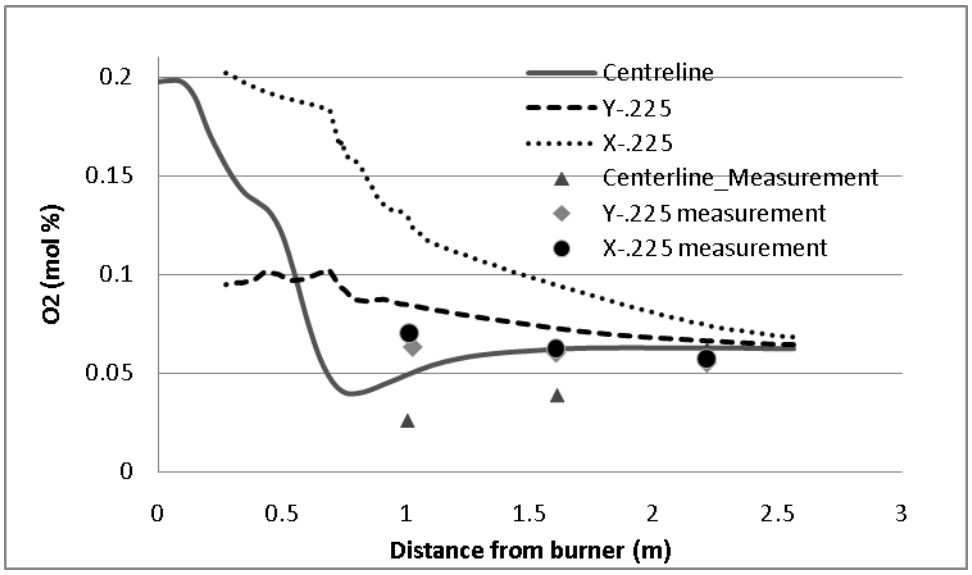

Figure **6-13**: Comparison of predicted and measured O_2 concentration in the pilot-scale boiler

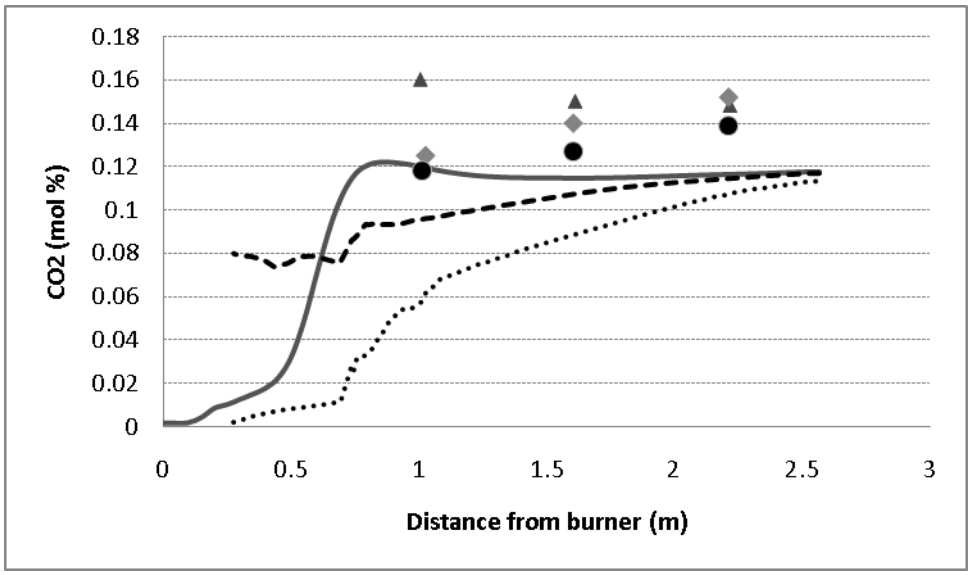

Figure **6-14**: Comparison of predicted and measured CO_2 concentration in the pilot-scale boiler

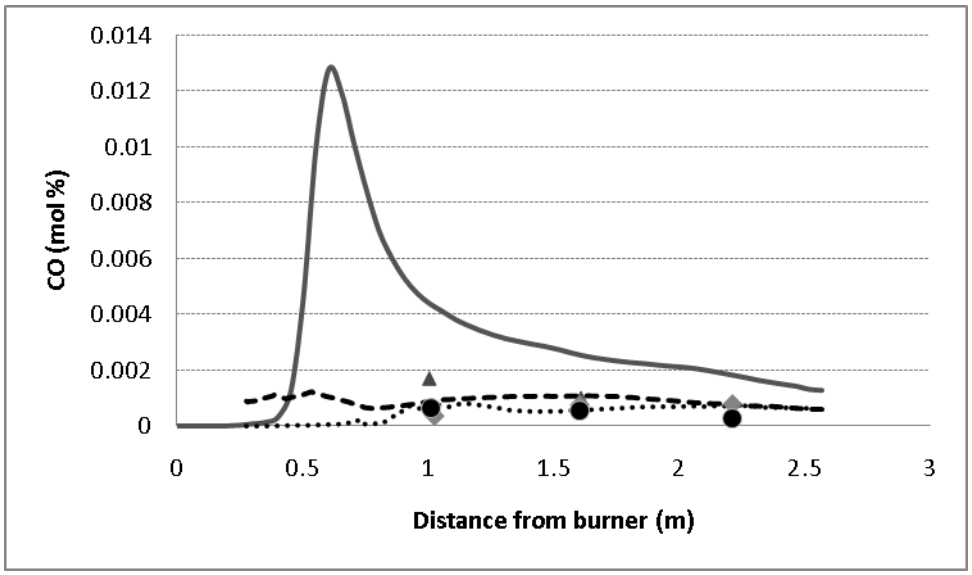

Figure **6-15**: Comparison of predicted and measured CO concentration in the pilot-scale boiler

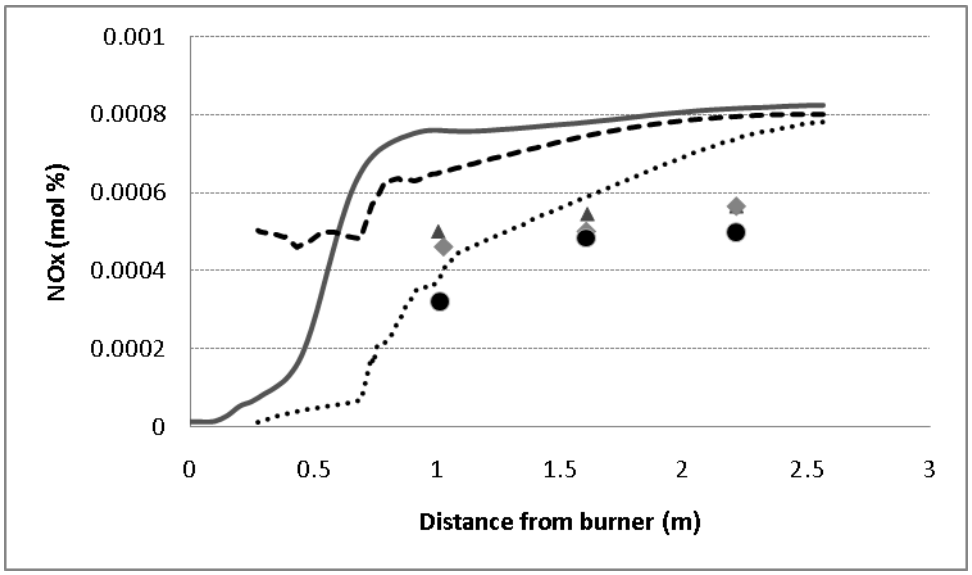

Figure **6-16**: Comparison of predicted and measured NO_x concentration in the pilot-scale boiler

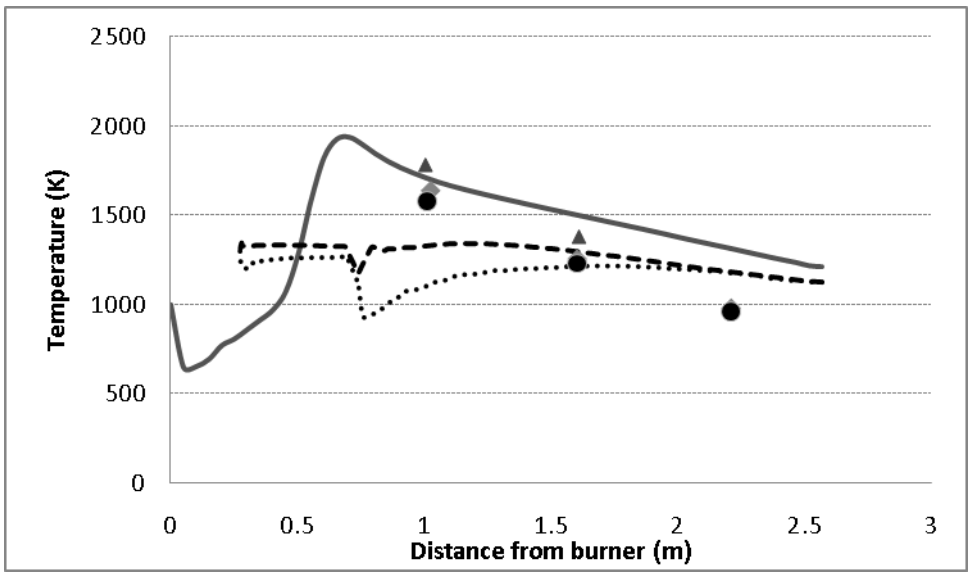

Figure **6-17**: Comparison of predicted and measured gas temperatures in the pilot-scale boiler

This model is then extended to predict the char burnout and NO_x & CO formation from combustion in a 30% O_2/CO_2 medium so that a comparison can be made with combustion in air. Char burnouts were predicted for two different ranks of coal (lvb and hvCb) for different case scenarios to identify the contribution of an increase in O_2 and CO_2 partial pressure during combustion in a 30 %O_2/ 70% CO_2 medium on char burnout. These are shown in Figure **6-18.**

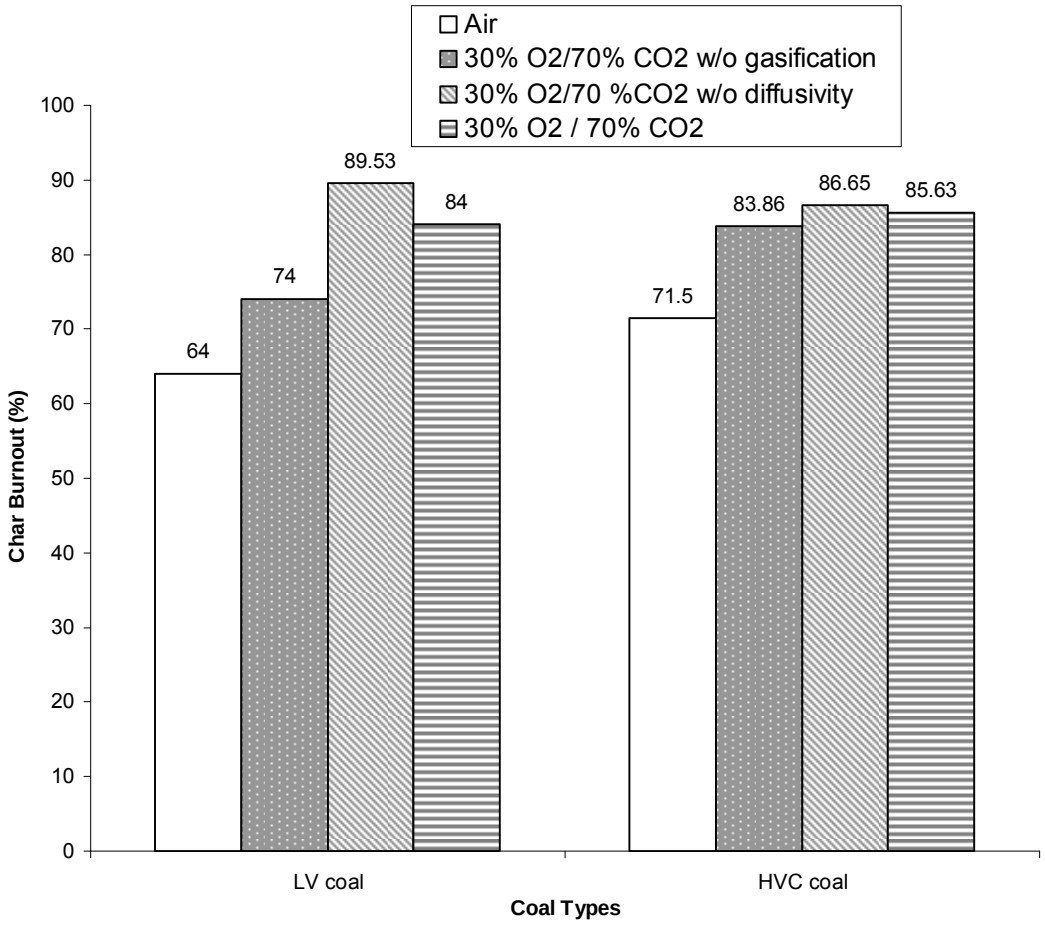

Figure **6-18**: Comparison of predicted char burnout during combustion in air with 30% O_2/70% CO_2 medium for different ranks of coal from a pilot-scale boiler

Notably, char burnout increased from 64% to 84% for an lvb coal and 71% to 86.5% for an hvCb coal when the combustion medium is changed from air to a 30% O_2/ 70% CO_2. Also the char burnout is decreased from 84% to 74% for an lvb coal and from 86.5% to 83.8% if the char-CO_2 reaction were not considered. This also implies that the majority of increase in char burnout occurs because of an increase in O_2 partial pressure during oxy-coal combustion. If a decrease in O_2 diffusivity during CO_2 rich medium is not accounted for then a char burnout is slightly over-predicted. Another simulation was carried out for oxy-coal combustion to determine if the amount of excess air can be reduced. The determination was that up to 15% excess oxidizer can be reduced and still maintaining the same char burnout that existed during combustion in air.

Comparison of predicted NO_x emissions between the two combustion approaches is shown in Figure **6-19** for three different ranks of coal. The predicted NO_x emission is shown as a function of fuel ratio (fixed carbon/ volatile matter)*coal-N of a low volatile, medium volatile and a high volatile bituminous coal. An increase in NO_x emission is observed to increase with the fuel ratio* coal-N in the literature [200]. A similar trend is captured in the prediction as shown in Figure **6-19**.

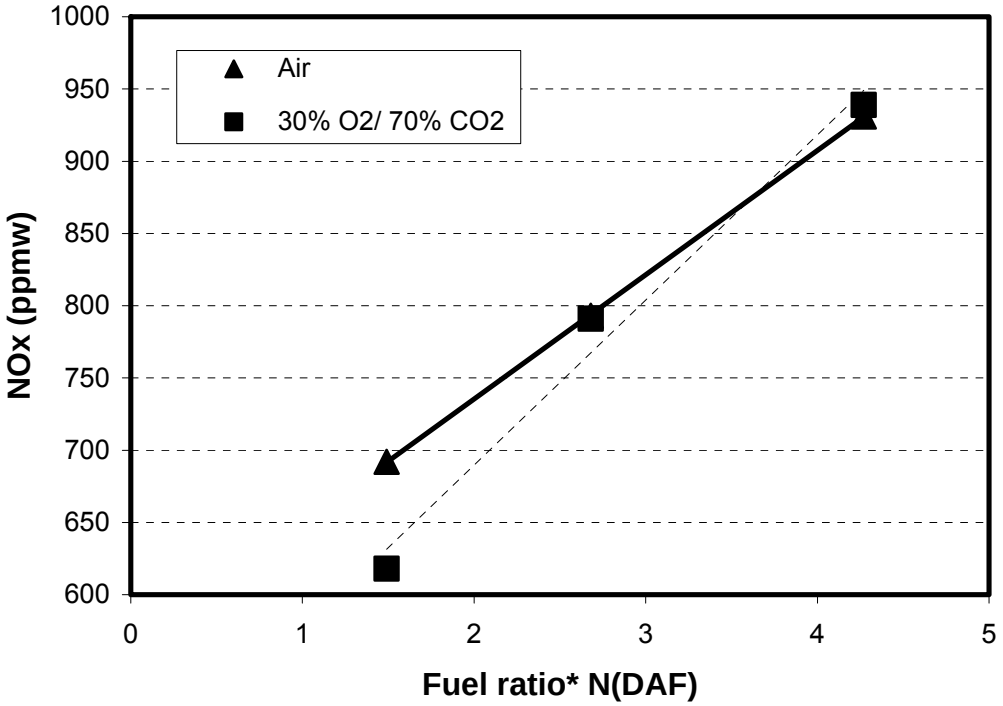

Figure **6-19**: Comparison of predicted NO_x emissions during combustion in air with 30% O_2/ 70% CO_2 medium for different ranks of coal from a pilot-scale boiler

From the comparison of NO_x prediction from the two combustion approaches, the majority of NO_x formation takes place from coal-N. A reduction of ~ 10% in NO_x emissions is predicted for a hvCb coal, while an increase in NO_x is predicted for a lvb coal during combustion in 30% O_2/ 70% CO_2 medium compared to combustion in air. This is because peak gas temperature for high volatile bituminous coal is ~2,100 K while for a low volatile bituminous coal it is 1,940 K. Therefore, thermal NO_x formed during combustion in air for an hvCb coal is minimized when the gas medium is changed to 30% O_2/ 70% CO_2.

Summary and Conclusions

This research was carried out to achieve a better understanding of the quantitative effect on char burnout of $NO_{x,}$ and CO emissions when N_2 in the combustion medium is replaced with $CO_{2.}$ A comparison of experimental results obtained in the DTR at furnace temperatures of 1,173 to 1,773 K in the two combustion media showed lower char burnouts in a 21% O_2/79% CO_2 medium compared to that of combustion in air for the two ranks of coal, and the difference was observed to diminish at higher furnace temperatures.

Difference in char burnout in the two combustion media was also found to depend upon the coal used. Higher activation energy value of C-CO_2 reaction for an lvb bituminous coal was believed to cause a more rapid increase in the rate of char burnout compared to that of an hvCb coal. This result implies that some ranks or types of coal are more suitable for an oxy-coal combustion approach in terms of char burnout. The prediction from a pilot-scale research boiler suggested that char burnout increased from 71.5 % to 85.6% for an hvCb coal and 64.1% to 86% for an lvb coal when the combustion medium is changed from air to 30% O_2/70% CO_2. This increase in char burnout was mainly caused from higher oxygen partial pressure during combustion in a 30% O_2/70% CO_2 mixture compared to that of combustion in air. A ~2% and a 10% increase in char burnout was predicted to be caused from char-CO_2 reaction for hvCb and lvb coal types, respectively during oxy-coal combustion. Pilot-scale prediction also suggested that up to a 15% oxidizer can be reduced during combustion in 30 % O_2/ 70%

CO_2 medium and still obtain the same char burnout that is achieved from combustion in air

Lower NO_x emissions were observed during combustion in a 21% O_2/79% CO_2 medium compared to those of combustion in air, and the difference in emissions was observed to decrease with an increase in the furnace temperature for both ranks of coal. A decrease in the difference in NO_x emissions of the two combustion media with an increase in furnace temperatures indicates that the contribution of thermal-NO_x was insignificant compared to the contribution from fuel-NO_x in overall NO_x formation. Pilot-scale prediction suggested that NO_x will be lower for a high volatile bituminous coal during combustion in a 30% O_2/70% CO_2 medium compared to combustion in air, owing to existence of higher peak temperatures (2,100 K).

CO emissions during combustion in a 21% O_2/79% CO_2 medium was observed to be higher compared to those of combustion in air, and the ratio of CO emissions during combustion in a 21% O_2/79% CO_2 medium to those of combustion in air was observed to decrease with an increase in temperature. Observation of higher CO emissions during combustion in a 21% O_2/79% CO_2 mixture provide supporting evidence that additional char-CO_2 reaction does takes place compared to combustion in air. A decrease in CO emissions with an increase in temperature indicates that equilibrium between the gas species is not established in the combustion time scales of a DTR.

Chapter 7

Summary, Conclusions and Recommendations

Summary and Conclusions

The overall goal of this research is to modify the existing char-oxidation kinetic sub-model in FLUENT^{TM} and use more accurate activation energy values to accurately account for the higher partial pressure of CO_2 in oxy-coal combustion. This model then can be used to exploit the operational flexibility in oxy-coal combustion to minimize NO_x emissions or oxygen consumption requirements, or reduce the furnace size in newer designs. A principal hypothesis for this study was that some coals are more suitable than others for oxy-coal combustion in terms of a) higher char burnout because of char-CO_2 reaction and, b) lower NO_x emissions because of differences in volatile matter content.

1. Modifying the char oxidation model required experimental determination of whether or not elevated levels of CO_2 during coal pyrolysis cause any change in the reactivity of the resultant char particles, or coal-N distribution between the volatile and char phases. Lab-scale experiments conducted in a drop tube reactor for two ranks of coal showed that pyrolyzing coals in a CO_2 medium, compared to an inert medium, changes the pore structure and reactivity of the char, and split the coal-N between volatile and char fractions. However, the differences occurred because of the additional weight loss due to char-CO_2 reaction during pyrolysis. This result implies

that, for purposes of predicting char burnout, the existing knowledge of coal pyrolysis behavior compiled over the years can be used for oxy-coal combustion.

2. For accurately capturing the combustion characteristics of coal chars in an O_2/CO_2 environment, a more appropriate intrinsic approach was used in the model. However, two challenges were identified when employing this approach. First, during intrinsic rate measurement, the rate goes through a maximum (as is well known) which causes an uncertainty in extracting reliable intrinsic rate parameters. From the activation energy estimated in the intervals of 10% conversion, apparently, the activation energy increases with conversion and plateaus after the conversion, where the maximum in rate occurs. This apparently implies the presence of an intra-particle diffusion limitation in the initial part of the reactivity profile. However, further investigations suggested the presence of a "purging effect" is responsible for observing a maximum in rate. Correction for the purging effect showed constant activation energy in the entire conversion range indicating that the rate measured in the TGA was in the kinetically controlled regime. For modeling purposes, activation energy was taken as an average of activation energy from the onset of a maximum to 80% conversion.

3. The second challenge concerns the use of intrinsic parameters in the model. Often, it has been argued that even if the intrinsic rate parameters are accurate , nascent char particles in actual combustion conditions (such as in DTR) are much more reactive than quenched char or char prepared in a TGA because of the difference in particle heating rate and temperature conditions of the two systems. A comparison of the char burnouts obtained from experiments and modeling suggested that the burnout

predicted using rate parameters of a char sample collected from DTR was about 5 times lower than the measured char burnout in DTR. The reactivity of a quenched and unquenched sample in TGA showed negligible differences, indicating that quenching during particle collection in a DTR does not alter the reactivity. Therefore, under-prediction of char burnout was attributed to the uncertainty in estimating effective diffusivity by a factor of 5, or an uncertainty in estimating activation energy by 13 kJ/mol. The TGA results show that during the rate parameter estimation a significant uncertainty in activation energy value arises depending on the operating temperature and the rate parameter method employed. In the current research, an activation energy for a char-O_2 reaction was estimated to be 127 kJ/mol and 105 kJ/mol in temperature range of 573 to 623 K and 673 to 748 K, respectively

4. Research shows that the use of CO_2 in place of N_2 in an oxidizer during combustion causes a reduction in gas/particle temperature (by ~250 K) during the volatile combustion and early stages of char burnout. This reduction in gas/particle temperature explains the decrease in NO_x formation and char burnout, and also an increase in the CO emissions observed during combustion in a 21% O_2/79% CO_2 medium. It was also shown numerically that an increase in CO emissions was partly caused by char-CO_2 reaction during combustion in a 21% O_2/79% CO_2 medium. However, the CO formation was observed to decrease with temperature, suggesting that at higher temperatures, any CO formed due to char-O_2 or char-CO_2 reaction rapidly converts into CO_2. For this reason, approximately the same CO emissions

were predicted from a pilot-scale boiler during combustion in air and in 30 % O_2/ 70% CO_2 media.

5. Lab-scale experimental results of exit NO_x emissions for a low volatile (lvb) and a high volatile (hvCb) coal from combustion in air and in 21% O_2/CO_2 showed that NO_x formation in the two combustion media was insensitive to the rank of coals studied in the current research. However, on a pilot-scale, a 10% reduction in NO_x emissions is predicted during combustion in a simulated 30% O_2/70% CO_2 mixture for the hvCb coal due to higher flame temperature as compared to the lvb coal.

6. Numerical results show that higher char burnout during oxy-coal combustion can be expected from existing boilers for burning coals that are more reactive towards CO_2. In the present study, lvb coal was found to be more suitable (in terms of char burnout) for oxy-coal combustion due to its higher reactivity towards CO_2 and the activation energy of a char-CO_2 reaction.

Overall, in this research, application and challenges of TGA derived rate parameters for prediction of char burnout from actual combustion condition was shown. However, the model captured the trends for CO and NO_x emissions only by adjusting some of the variables in the model. In this research, a low-volatile coal was found to yield higher char burnout and a high-volatile coal was found to yield lower NO_x emission during oxy-coal combustion in comparison to combustion in air.

Recommendations for Future Work

1. In the present research, a foundation was laid to establish rate parameters needed to model oxy-coal combustion. However, quantitative evaluation of NO_x reduction potential in this approach was not conducted. A few studies have clearly revealed that NO_x reduction due to recycling of flue gas is significantly lower than the use of a simulated O_2/CO_2 mixture [15]. Since the exact potential is not clearly understood yet [49], conceivably, the NO_x reduction would depend upon where the recycled stream is injected in the burner. Therefore, a burner optimization study with different partitioning of the RFG stream within the burner should be conducted.

2. This study shows that CO_2 does contribute to char burnout, and significant improvement in char burnout can be achieved in existing systems by use of oxy-coal combustion technology. Theoretically, this suggests that lower excess amounts of oxygen can be used compared to the typically used 3% v/v excess O_2 in existing coal-fired systems. The decrease in oxygen requirement will reduce the oxygen penalty in this technology. However, a few studies have shown that the same amount of oxygen (as used during combustion in air) is needed to maintain flame stability [12, 32, 33]. Therefore, either co-firing of coal and biomass should be evaluated to enhance flame ignition, or further numerical studies should be conducted to identify the burner design that can exploit the operational flexibility from maintaining flame stability for a O_2/CO_2 mixture with lower oxygen levels. Biomass is proposed because it is more reactive compared to coal, and is anticipated to increase the overall heat release rate and thus reduce the ignition temperature of the coal-biomass particle cloud [40].

3. Experimental results obtained in this study suggest that coal samples more reactive towards CO_2 will be more suitable for the oxy-coal combustion technology in achieving higher char burnout. Various studies in the literature have suggested that lignite rank coal is more reactive towards CO_2 because of the presence of inherent catalytic mineral matter [201]. This coal can be further evaluated in the drop tube reactor for its combustion characteristics in an O_2/CO_2 atmosphere.

4. The present study evaluated oxy-coal combustion technology for retrofitting existing boilers. However, new coal-fired units can be designed to operate at higher furnace temperatures [202]. Therefore, effect of different partial pressures of O_2 in CO_2 on the potential reduction in boiler size and heat transfer to boiler wall should be numerically or experimentally investigated.

References

1. Steinberg, M., Cheng, H.C., Horn, F., A System Study for the Removal, Recovery and Disposal of the Carbon Dioxide from Fossil Fuel Power Plants in the US. *Brookhaven National Lab, NY,* **1984**.
2. Watson, R. T. *Third Assesment report of the intergovernmental panel on climate change: Climate change 2001: synthesis report*; Maldives, 2001; p 34.
3. *Information on Global Warming Potential*; FCCC-TP-2004-3; United Nations Framework Convention Climate Change: 15 June, 2004; p 12.
4. Metz, B.; Davidson, O.; Coninck, H.; Loos, M.; Meyer, L. *Carbon Dioxide Capture and Storage*; IPCC: Sep, 2005; pp 1-62.
5. *Inventory of U.S. Greenhouse Gas Emissions and Sinks: 1990-2005*; U.S. Environmental Protection Agency: 2007.
6. Bounaceur, R.; Lape, N.; Roizard, D.; Vallieres, C.; Favre, E., Membrane processes for post-combustion carbon dioxide capture: A parametric study. *Energy* **2006,** 31, (14), 2556-2570.
7. Horn, F. L.; Steinberg, M., Control of carbon dioxide emissions from a power plant (and use in enhanced oil recovery). *Fuel* **1982,** 61, 415-422.
8. Payne, R.; Chen, S. L.; Wolsky, A. M.; Richter, W. F., CO2 Recovery Via Coal Combustion in Mixtures of Oxygen and Recycled Flue-Gas. *Combustion Science and Technology* **1989,** 67, (1-3), 1-16.
9. Buhre, B. J. P.; Elliott, L. K.; Sheng, C. D.; Gupta, R. P.; Wall, T. F., Oxy-fuel combustion technology for coal-fired power generation. *Progress in Energy and Combustion Science* **2005,** 31, (4), 283-307.
10. Weller, A. E.; Rising, B. W.; Boiarski, A. A.; Nordstrom, R. J.; Barrett, R. E.; Luce, R. J. *Experimental evaluation of firing pulverized coal in a CO2/O2 atmosphere*; ANL/CNSV-TM-168; Argonne National Laboratory: 1985.
11. Nakayama, S.; Noguchi, Y.; Kiga, T.; Miyamae, S.; Maeda, U.; Kawai, M.; Tanaka, T.; Koyata, K.; Makino, H., Pulverized Coal Combustion in O-2 CO2 Mixtures on a Power-Plant for CO2 Recovery. *Energy Conversion and Management* **1992,** 33, (5-8), 379-386.
12. Kiga, T.; Takano, S.; Kimura, N.; Omata, K.; Okawa, M.; Mori, T.; Kato, M., Characteristics of pulverized-coal combustion in the system of oxygen recycled flue gas combustion. *Energy Conversion and Management* **1997,** 38, S129-S134.
13. Chui, E. H.; Croiset, E.; Thambimuthu, K. V., Simulation of coal combustion in high CO2 and O2 environements. In *The Fifth International Conference on GreenHouse Gas Technologies*, Cairns, Australia, 2000.
14. Croiset, E.; Thambimuthu, K.; Palmer, A., Coal combustion in O-2/CO2 mixtures compared with air. *Canadian Journal of Chemical Engineering* **2000,** 78, (2), 402-407.
15. Miura, T., Advanced Coal Combustion. *Nova Science Publishers* **2001**, 185-241.

16. Singh, D.; Croiset, E.; Douglas, P. L.; Douglas, M. A., Techno-economic study of CO2 capture from an existing coal-fired power plant: MEA scrubbing vs. O-2/CO2 recycle combustion. *Energy Conversion and Management* **2003,** 44, (19), 3073-3091.
17. Jared, C. *Pulverized coal oxycombustion power plants*; DOE/NETL-2007/1291; National Energy Technology Laboratory: August, 2007; p 305.
18. Bonaquist, D.; Victor, R.; Shah, M., Oxy-Coal Combustion Demonstration Project. In *The 33rd International Technical Conference on Coal Utilization & Fuel Systems*, Clearwater, 2008; p 2.
19. Gaffney, T. R., Porous solids for air separation *Current Opinion in Solid State and Materials Science* **1996,** 1, (1), 69-75.
20. Yamada, T.; Kiga, T.; Okawa, M.; Omata, K.; Kimura, N.; Arai, K.; Mori, T.; Kato, M., Characteristics of pulverized-coal combustion in CO2-recovery power plant applied to O-2/CO2 combustion. *JSME International Journal Series B-Fluids and Thermal Engineering* **1998,** 41, (4), 1017-1022.
21. Herzog, H., What future for carbon capture and sequestration? *Environ Sci Technol* **2001,** 35, (7), 148-153.
22. Okawa, M.; Kimura, N.; Kiga, T.; Takano, S.; Arai, K.; Kato, M., Trial design for a CO2 recovery power plant by burning pulverized coal in O-2/CO2. *Energy Conversion and Management* **1997,** 38, S123-S127.
23. Horn, F. L.; Steinberg, M., Contro of carbon dioxide emissions from a power plant (and use in enhanced oil recovery). *Fuel* **1982,** 61, 415-422.
24. Sander, M. T.; Mariz, C. L., The Fluor Daniel® econamine FG process: Past experience and present day focus *Energy Conversion and Management* **1992,** 33, 341-348
25. Wilson, M. A.; R.M. Wrubesk, R. M.; Yarborough, L., Recovery of CO2 from power plant flue gases using amines. *Energy Conver Manage* **1992,** 33, 325-331.
26. Yagi, T.; Shibuya, H.; Sasaki, T., Application of chemical absorption process to CO2 recovery from flue gas generated in power plants. *Energy Conver Manage* **1992,** 33, 349-355.
27. Shao, Y.; Golomb, D.; Brown, G., Natural Gas Fired Combined Cycle power plant with CO2 capture. *Energy Conversion and Management* **1995,** 36, (12), 1115-1128.
28. Liu, H.; Zailani, R.; Gibbs, B. A., Pulverized coal combustion in air and in O-2/CO2 mixtures with NOx recycle. *Fuel* **2005,** 84, (16), 2109-2115.
29. Hu, Y.; Naito, S.; Kobayashi, N.; Hasatani, M., CO2, NOx and SO2 emissions from the combustion of coal with high oxygen concentration gases. *Fuel* **2000,** 79, (15), 1925-1932.
30. Tan, Y.; Douglas, M. A.; Thambimuthu, K. V., CO2 capture using oxygen enhanced combustion strategies for natural gas power plants. *Fuel* **2002,** 81, (8), 1007-1016.
31. Habib, M. A.; Elshafei, M.; Dajani, M., Influence of combustion parameters on NOx production in an industrial boiler *Computers and Fluids* **2008,** 37, (1), 12-23.
32. Molina, A.; Shaddix, C. R., Ignition and devolatilization of pulverized bituminous coal particles during oxygen/carbon dioxide coal combustion. In *Proceedings of the Combustion Institute*, Germany, 2007; Vol. 31, pp 1905-1912.

33. Man, C. K.; Gibbins, J. R.; Cashdollar, K. L., Effect of coal type and oxy-fuel combustion parameters on pulverized coal ignition. In *International Coal Conference on Science and Technology*, Nottingham, 2007; p 5A1.
34. USEPA, http://www.epa.gov/air/clearskies. In 2004.
35. Maier, J.; Dhungel, B.; Mönckert, P.; Kull, R.; Scheffknecht, G., Impact of recycled gas species (so2, no) on emission behaviour and fly ash quality during oxy-coal combustion. In *33rd International Technical Conference on Coal Utilization & Fuel Systems*, Florida, USA, 2008.
36. Santos, S.; Haines, M.; Davison, J.; Roberts, P., Challenges in the development of oxy-fuel combustion technology for coal fired power plant. In *The proceedings of the 31st technical conference on coal utilization and fuel systems*, Clearwater, Florida, 2006.
37. Sethi, V.; Omar, K.; Martin, P.; Barton, T., Oxy-Combustion versus Air-Blown Combustion of Coals. In *32nd International Technical Conference on Coal Utilization & Fuel Systems*, Florida, USA, 2007.
38. Wang, C. S.; Berry, G. F.; Chang, K. C.; Wolsky, A. M., Combustion of Pulverized Coal Using Waste Carbon-Dioxide and Oxygen. *Combustion and Flame* **1988,** 72, (3), 301-310.
39. Liu, H.; Zailani, R.; Gibbs, B. M., Comparisons of pulverized coal combustion in air and in mixtures of O-2/CO2. *Fuel* **2005,** 84, (7-8), 833-840.
40. Arias, B.; Pevida, C.; Rubiera, F.; Pis, J. J., Effect of biomass blending on coal ignition and burnout during oxy-fuel combustion. *Fuel* **2008,** 87, (12), 2753-2759.
41. Mitchell, R. E.; Madsen, O. H., Experimentally Determined Overall Burning Rates of Pulverized Coal Chars in Specified O_2 and CO_2 Environment. *21st Sym on Comb,* **1986**, 173-181.
42. Saastamoinen, J. J.; Aho, M. J.; Hamalainen, J. P.; Hernberg, R.; Joutsenoja, T., Pressurized pulverized fuel combustion in different concentrations of oxygen and carbon dioxide. *Energy & Fuels* **1996,** 10, (1), 121-133.
43. Shaddix, C. R.; Murphy, J. J., Coal char combustion reactivity in oxy-fuel applications. In *20th Pittsburgh Coal Conference*, Pittsburgh, PA, 2003.
44. Hampartsoumian, E.; Murdoch, P. L.; Pourkashanian, M.; Trangmar, D. T.; Williams, A., The reactivity of coal chars gasified in carbon dioxide environemnts. *Combustion Science and Technologies* **1993,** 92, 105-121.
45. Varhegyi, G.; Till, F., Comparision of Temperature Programmed Char Combustion in CO2-O2 and Ar-O2 Mixtures at Elevated Pressures. *Energy & Fuels* **1999,** 13, 539-540.
46. Murphy, J. J.; Shaddix, C. R., Combustion kinetics of coal chars in oxygen-enriched environments. *Combustion and Flame* **2006,** 144, (4), 710-729.
47. Farzan, H.; Vecci, S. J.; Pelage, F. C.; Pranda, P.; Bose, A. C., Pilot-scale evaluation of coal combustion in an oxygen-enriched recylced flue gas. In *22nd Int Pittsburgh Coal Conference*, Pittsburgh, PA, 2005.
48. Croiset, E.; Thambimuthu, K. V., NOx and SO2 emissions from O-2/CO2 recycle coal combustion. *Fuel* **2001,** 80, (14), 2117-2121.
49. Tan, Y. W.; Croiset, E.; Douglas, M. A.; Thambimuthu, K. V., Combustion characteristics of coal in a mixture of oxygen and recycled flue gas. *Fuel* **2006,** 85, (4), 507-512.

50. Abbas, T.; Costen, P.; Lockwood, F. C., The Influence of near Burner Region Aerodynamics on the Formation and Emission of Nitrogen-Oxides in a Pulverized Coal-Fired Furnace. *Combustion and Flame* **1992,** 91, (3-4), 346-363.
51. Kimura, N.; Omata, K.; Kiga, T.; Takano, S.; Shikisima, S., The Characteristics of Pulverized Coal Combustion in O2/CO2 Mixtures for CO2 Recovery. *Energy Conversion and Management* **1995,** 36, (6-9), 805-808.
52. Mackrory, A. J.; Lokare, S.; Baxter, L. L.; Tree, D. R., An Investigation of Nitrogen Evolution in Oxy-fuel Combustion. In *32nd International Technical Conference on Coal Utilization & Fuel Systems*, Florida, USA, 2007.
53. Pershing, D. W.; Wendt, J. O. L., Pulverized coal combustion: The influence of flame temeprature and coal composition on thermal NOx and fuel NOx. In *16th Sym (Int) on Combustion*, 1976; pp 389-399.
54. Okazaki, K.; Ando, T., NOx reduction mechanism in coal combustion with recycled CO2. *Energy* **1997,** 22, (2-3), 207-215.
55. Nozaki, T.; Takano, S.; Kiga, T.; Omata, K.; Kimura, N., Analysis of the flame formed during oxidation of pulverized coal by an O-2-CO2 mixture. *Energy* **1997,** 22, (2-3), 199-205.
56. Chui, E. H.; Douglas, M. A.; Tan, Y. W., Modeling of oxy-fuel combustion for a western Canadian sub-bituminous coal. *Fuel* **2003,** 82, (10), 1201-1210.
57. Chui, E. H.; Majeski, A. J.; Douglas, M. A.; Tan, Y.; Thambimuthu, K. V., Numerical investigation of oxy-coal combustion to evaluate burner and combustor design concepts. *Energy* **2004,** 29, (9-10), 1285-1296.
58. Khare, S. P.; Wall, T.; Farida, A. Z.; Liu, Y.; Moghtaderi, B.; Gupta, R. P., Factor influencing the ignition of flames from air-fired swirl pf burners retrofitted to oxy-fuel. *Fuel* **2007,** in press.
59. Fry, A.; Davis, K.; Wang, D., CFD Modeling of Single Burner Oxy-Coal Combustion Retrofit Concepts. In *33rd International Technical Conference on Coal Utilization & Fuel Systems*, Florida, USA, 2008.
60. Mclean, W. J.; Hardesty, D. R.; Pohl, J. H., Direct Observations Of Devolatilizing Pulverized Coal Particles In A Combustion Environment. In *Eighteenth Symposium (International) on Combustion*, 1981; pp 1239-1248.
61. Roberts, D. G.; Harris, D. J.; Wall, T. F., Total pressure effects on chemical reaction rates of chars with O-2, CO2 and H2O. *Fuel* **2000,** 79, (15), 1997-1998.
62. Roberts, D. G.; Harris, D. J., Char gasification with O-2, CO2, and H2O: Effects of pressure on intrinsic reaction kinetics. *Energy & Fuels* **2000,** 14, (2), 483-489.
63. Shaddix, C. R.; Molina, A., Effect of O2 and High CO2 Concentrations on PC Char Burning Rates during Oxy-Fuel Combustion. In *33rd International Technical Conference on Coal Utilization & Fuel Systems*, Florida, USA, 2008.
64. Stanmore, B. R.; Visona, S. P., The contribution to char burnout from gasification by H2O and CO2 during pulverized-coal flame combustion. *Combustion and Flame* **1998,** 113, (1-2), 274-276.
65. Haynes, R. J., Reclamation and revegetation of fly ash disposal sites - Challenges and research needs. *Journal of Environmental Management* **2009,** 90, (1), 43-53.

66. Gautier, F.; Ghani, M. U.; Châtel-Pélage, F., Optimization of Oxygen Injection into an Air-Coal Stream using CFD. In *30th International Technical Conference on Coal Utilization & Fuel Systems*, Florida, USA, 2005.
67. Pershing, D. W.; Wendt, J. O. L., Relative contributions of volatile nitrogen and char nitrogen to NOx emissions fom pulverized coal flames. *Industrial & Engineering Chemistry Process Design and Development* **1979,** 18, (1), 60-67.
68. Chang, L.; Xie, Z.; Xie, K. C.; Pratt, K. C.; Hayashi, J.; Tadatoshi, C.; Li, C. Z., Formation of NO_x Precursors during the Pyrolysis of Coal and Biomass Part IV. Effects of Gas Atmosphere on the Formation of NH_3 and HCN. *Fuel* **2003,** 82, 1159-1166.
69. Thakur, S. C.; Brown, L. F., The Pyrolysis of a Wyoming Coal in Different Non-Reactive Atmospheres. *Carbon* **1982,** 20, (1), 17-24.
70. Russell, N. V.; Beeley, T. J.; Man, C. K.; Gibbins, J. R.; Williamson, J., Development of TG measurements of intrinsic char combustion reactivity for industrial and research purposes. *Fuel Processing Technology* **1998,** 57, (2), 113-130.
71. Smith, I. W., Intrinsic Reactivity of Carbons to Oxygen. *Fuel* **1978,** 57, (7), 409-414.
72. Suuberg, E. M.; Wojtowicz, M.; Calo, J. M., Reaction order for low temperature oxidation of carbons. *Proceedings of the Combustion Institute* **1988,** 22, 79-87.
73. Liu, G.; Benyon, P.; Benfell, K. E.; Bryant, G. W.; Tate, A. G.; Boyd, R. K.; Harris, D. J.; Wall, T. F., The porous structure of bituminous coal chars and its influence on combustion and gasification under chemically controlled conditions. *Fuel* **2000,** 79, (6), 617-626.
74. Charpenay, S.; Serio, M. A.; Solomon, P. R., The prediction of coal char reactivity under combustion conditions. *Symposium (International) on Combustion* **1992,** 24, (1), 1189-1197.
75. Anthony, D. B.; Howard, J. B., Coal Devolatilization and Hydrogasification. *Aiche Journal* **1976,** 22, (4), 625-656.
76. Badzioch, S.; Hawskley, P. G. W., Kinetics of thermal decomposition of pulverized coal particles. *Industrial & Engineering Chemistry Process Design and Development* **1970,** 9, (4), 521-530.
77. Mathews, J. P. Following changes in the constitution of rapidly heated bituminous vitrinites. The Pennsylvania State University, University Park, 1998.
78. Vorres, K. S., The Argonne Premium Coal Sample Program. *Energy & Fuels* **1990,** 4, (5), 420-426.
79. Marsh, H., Surface areas of coal as evaluated from adsorption isotherm of carbon dioxide using Dubinin-Polanyi equation. *Fuel* **1965,** 44, (5), 355-366.
80. Smith, I. W.; Tyler, R. J., Internal Burning of Pulverized Semi-Anthracite - Relation between Particle Structure and Reactivity. *Fuel* **1972,** 51, (4), 312-&.
81. Kobayashi, H.; Howard, J. B.; Sarofim, A., Coal devolatilization at high temperatures. In *Symposium (International) on Combustion* The Combustion Institute: 1976; Vol. 16, p 411.
82. Scaroni, A. W.; Walker, P. L.; Essenhigh, R. H., Kinetics of Lignite Pyrolysis in an Entrained-Flow, Isothermal Furnace. *Fuel* **1981,** 60, (1), 71-76.
83. Hambly, E. M. The Chemical Structure of Coal Tar and Char During Devolatilization. MS, Bringham Young University, 1998.

84. Zarnescu, V. An integrated approach for combustor design to minimize nitrogen oxide emissions using CFD methods. Ph.D, The Pennsylvania State University, 2000.
85. Miller, B. G.; Miller, S. F.; Wincek, R. T.; Wasco, R. S. *Fuel Flexibility in Boilers for Fuel Cost Reduction and Enhanced Food Supply Security*; The Pennsylvania State University: University Park, June 30, 2006; p 509.
86. Price, R. J. Modeling three reacting flow systems with modern computational fluid dynamics. PhD, Bringham Young University, 2007.
87. Eaton, A. M.; Smoot, L. D.; Hill, S. C.; Eatough, C. N., Components, formulations, solutions, evaluation, and application of comprehensive combustion models. *Progress in Energy and Combustion Science* **1999,** 25, (4), 387-436.
88. Visser, B. M.; Smart, J. P.; Van de kamp, W. L.; Weber, R., Measurements And Predictions Of Quarl Zone Properties Of Swirling Pulverised Coal Flames. In *Twenty-Third Symposium (International) on Combustion*, 1991; pp 949-955.
89. FLUENT, User's manual. In Fluent Inc: NH, 2006; Vol. 6.3.26.
90. Anthony, D. B.; Howard, J. B.; Hottel, H. C.; Meissner, H. P., Rapid devolatilization and hydrogasification of bituminous coal. *Fuel* **1976,** 55, 121.
91. Solomon, P. R.; Serio, M. A.; Carangelo, R. M.; Markham, J. R., Very rapid coal pyrolysis. *Fuel* **1986,** 65, 182-194.
92. Field, M. A., Measurements of the Effect of Rank on Combustion Rates of Pulverized Coal. *Combustion and Flame* **1970,** 14, 237-248.
93. Ayling, A. B.; Smith, I. W., Measured Temperatures of Burning Pulverized-Fuel Particles, and Nature of Primary Reaction Product. *Combustion and Flame* **1972,** 18, (2), 173-&.
94. Arthur, J. R., Reactions Between Carbon And Oxygen. *Transactions of the Faraday Society* **1951**, 164-178.
95. Commissaris, F. A. C. M.; Banin, V. E.; Roekaerts, D. J. E. M.; Veefkind, A., The Rates of Production of CO and CO 2 from the Combustion of Pulverized Coal Particles in a Shock Tube. *Combustion and Flame* **1998,** 12, 121-131.
96. Annamalai, K.; Ryan, W., Interactive processes in gasification and combustion--ii. Isolated carbon, coal and porous char particles. *Prog. Energy Combust. Sci.* **1993,** 19, 383-446.
97. Tognotti, L.; longwell, J. P.; Sarofim, A. F., The products of the high temperature oxidation of a Single char particle in an electrodynamic balance. *Proceedings of the Combustion Institute* **1990**, (23), 1207-1213.
98. Mitchell, R. E., On the products of the heterogeneous oxidation reaction at the surfaces of burning coal char particles. *Symposium (International) on Combustion* **1989,** 22, (1), 69-78.
99. Smoot, L. D.; Smith, P. J., *Coal Combustion and Gasification*. Plenum Press: Ny, 1985; p 443.
100. Thiele, E. W., Relation between catalytic activity and size of particle. *Industrial and Engineering Chemistry* **1939,** 31, 916-920.
101. Smith, K. L.; Smoot, L. D.; Fletcher, T. H.; Pugmire, R. J., *The Structure and Reaction Processes of Coal*. Plenum Press: NY, 1994; p 471.

102. Magnussen, B. F.; Hjertager, B. H., On mathematical modeling of turbulent combustion with special emphasis on soot formation and combustion kinetics. In *Sixteenth Symp (Int.) on Combustion*, 1976; pp 719-729.
103. Howard, J. B.; Williams, G. C.; Fine, D. H., Kinetics of carbon monoxide oxidation in postflame gases. *Proceedings of the Combustion Institute* **1973**, 975-986.
104. Hill, S. C.; Smoot, L. D., Modeling of nitrogen oxides formation and destruction in combustion systems. *Progress in Energy and Combustion Science* **2000,** 26, (4-6), 417-458.
105. van der Lans, R. P.; Glarborg, P.; Dam-Johansen, K., Influence of process parameters on nitrogen oxide formation in pulverized coal burners. *Progress in Energy and Combustion Science* **1997,** 23, (4), 349-377.
106. Miller, J. A.; Bowman, C. T., Mechanism and Modeling of Nitrogen Chemistry in Combustion. *Progress in Energy and Combustion Science* **1989,** 15, (4), 287-338.
107. Abbas, T.; Costen, P.; Lockwood, F. C.; Romomillares, C. A., The Effect of Particle-Size on No Formation in a Large-Scale Pulverized Coal-Fired Laboratory Furnace - Measurements and Modeling. *Combustion and Flame* **1993,** 93, (3), 316-326.
108. Chaiklangmuang, S.; Jones, J. M.; Pourkashanian, M.; Williams, A., Conversion of volatile-nitrogen and char-nitrogen to NO during combustion. *Fuel* **2002,** 81, (18), 2363-2369.
109. Wendt, J. O. L., Mechanisms governing the formation and destruction of NOx and other nitrogenous species in low NOx coal combustion systems. *Combustion Science and Technology* **1995,** 108, (4-6), 323-344.
110. Smart, J. P.; Weber, R., Reduction of Nox and Optimization of Burnout with an Aerodynamically Air-Staged Burner and an Air-Staged Precombustor Burner. *Journal of the Institute of Energy* **1989,** 62, (453), 237-245.
111. B.R. Stanmore; Visona, S. P., Prediction of NO emissions from a number of coal-fired power station boilers. *Fuel Processing Technology* **2000,** 64, 25-46.
112. Peters, A. A. F.; Weber, R., Mathematical modeling of a 2.4 MW swirling pulverized coal flame. *Combustion Science and Technology* **1997,** 122, (1-6), 131-182.
113. Beer, J. M.; Chomiak, J.; Smoot, L. D.; Essenhigh, R. H., Fluid-Dynamics of Coal Combustion - a Review. *Progress in Energy and Combustion Science* **1984,** 10, (2), 177-208.
114. Banerjee, N. N.; Murty, G. S.; Rao, H. S.; Lahiri, A., Flash Pyrolysis of Coal - Effect of Nitrogen, Argon and Other Atmospheres in Increasing Olefin Concentration and Its Significance on Mechanism of Coal Pyrolysis. *Fuel* **1973,** 52, (3), 168-170.
115. Eltawil, M. M.; Brown, L. F., Changes in Pore Structure of a Devolatilized Coal Char Upon Further Heating at Lower Temperature. *Carbon* **1976,** 14, (2), 132-133.
116. Hindmarsh, C. J.; Wang, W. X.; M., T. K.; Cai, H. Y.; Guell, A. J.; Dugwell, D. R., Volatile release of coals and reactivity of chars prepared in wire-mesh and entrained flow reactors: The effect of reactor configuration, pressure and heating rate. . In *Int. Conf. Coal Sci.*, 1993; Vol. 7th, pp 31-34.
117. Walker, P. L.; Pentz, L.; Biederman, D. L.; Vastola, F. J., Influence of Inert Diluent Gases on Rate of Carbon Gasification. *Carbon* **1977,** 15, (3), 165-168.

118. Anthony, D. B.; Hottel, H. C.; Howard, J. B.; Meissner, H. P., Rapid Devolatilization and Hydrogasification of Bituminous Coal. *Abstracts of Papers of the American Chemical Society* **1975,** 170, (AUG24), 31-31.
119. Jenkins, R. G.; Morgan, M. E., Pyrolysis of a Lignite in an Entrained Flow Reactor .3. Pyrolysis in Reactive Atmospheres of Air, Carbon-Dioxide and Wet Nitrogen. *Fuel* **1986,** 65, (6), 769-771.
120. Tomita, A.; Oikawa, Y.; Kanai, T.; Tamai, Y., Gasification of coals treated with non-aqueous solvents. 6. Catalytic steam gasification at atmospheric pressure. *Fuel* **1979,** 58, (8), 614-618.
121. Hashimoto, K.; Miura, K.; Ueda, T., Correlation of gasification rates of various coals measured by a rapid heating method in a steam atmosphere at relatively low temperatures. *Fuel* **1986,** 65, (11), 1516-1523.
122. Miura, K.; Hashimoto, K.; Silveston, P. L., Factors affecting the reactivity of coal chars during gasification, and indices representing reactivity. *Fuel* **1989,** 68, (11), 1461-1475.
123. Peng, F. F.; Lee, I. C.; Yang, R. Y. K., Reactivities of in-Situ and Ex-Situ Coal Chars During Gasification in Steam at 1000-1400-Degrees-C. *Fuel Processing Technology* **1995,** 41, (3), 233-251.
124. Messenbock, R.; Dugwell, D. R.; Kandiyoti, R., CO2 and steam-gasification in a high-pressure wire-mesh reactor: the reactivity of Daw Mill coal and combustion reactivity of its chars. *Fuel* **1999,** 78, (7), 781-793.
125. Laurendeau, N. M., Heterogenous Kinetics of Coal Char Gasification and Combustion. *Prog in Energy & Comb Sci* **1978,** 4, 221-270.
126. Hayashi, J. I.; Iwatsuki, M.; Morishita, K.; Tsutsumi, A.; Li, C. Z.; Chiba, T., Roles of inherent metallic species in secondary reactions of tar and char during rapid pyrolysis of brown coals in a drop-tube reactor. *Fuel* **2002,** 81, (15), 1977-1987.
127. Chang, L. P.; Xie, Z. L.; Xie, K. C.; Pratt, K. C.; Hayashi, J.; Chiba, T.; Li, C. Z., Formation of NOx precursors during the pyrolysis of coal and biomass. Part VI. Effects of gas atmosphere on the formation of NH3 and HCN. *Fuel* **2003,** 82, (10), 1159-1166.
128. Jamil, K.; Hayashi, J. I.; Li, C. Z., Pyrolysis of a victorian brown coal and gasification of nascent char in CO2 atmosphere in a wire-mesh reactor. *Fuel* **2004,** 2004, (83), 833-843.
129. Bayarsaikhan, B.; Hayashi, J. I.; Shimada, T.; Sathe, C.; Li, C. Z.; Tsutsumi, A.; Chiba, T., Kinetics of steam gasification of nascent char from rapid pyrolysis of a Victorian brown coal. *Fuel* **2005,** 84, (12-13), 1612-1621.
130. Senneca, O.; Salatino, P., Overlapping of heterogeneous and purely thermally activated solid-state processes in the combustion of a bituminous coal. *Combustion and Flame* **2006,** 144, (3), 578-591.
131. Borrego, A. G.; Alvarez, D., Comparison of chars obtained under oxy-fuel and conventional pulverized coal combustion atmospheres. *Energy & Fuels* **2007,** 21, (6), 3171-3179.
132. Tamhankar, S. S.; Sears, J. T.; Chin-Yung, W., Coal pyrolysis at high temperatures and pressures. *Fuel* **1984,** 63, (9), 1230-1235.

133. Jenkins, R. G.; Morgan, M. E., Pyrolysis of a lignite in entrained flow reactor.3. Pyrolysis in reactive atmospheres of air, carbon dioxide and wet nitrogen. *Fuel* **1986,** 65, 769-771.
134. Coppalle, A.; Vervisch, P., The Total Emissivities of High-Temperature Flames. *Combustion and Flame* **1983,** 49, (1-3), 101-108.
135. Hilsenrath, J., *Tables of thermal properties of gases*. National Bureau of Standards: 1955; p 488.
136. Megaritis, A.; Messenbock, R. C.; Collot, A. G.; Zhuo, Y.; Dugwell, D. R.; Kandiyoti, R., Internal consistency of coal gasification reactivities determined in bench-scale reactors: effect of pyrolysis conditions on char reactivities under high-pressure CO2. *Fuel* **1998,** 77, (13), 1411-1420.
137. Gale, T. K.; Bartholomew, C. H.; Fletcher, T. H., Effects of pyrolysis heating rate on intrinsic reactivities of coal chars. *Energy & Fuels* **1996,** 10, (3), 766-775.
138. Jenkins, R. G.; Nandi, S. P.; Walker, P. L., Reactivity of Heat-Treated Coals in Air at 500 Degrees C. *Fuel* **1973,** 52, (4), 288-293.
139. Gavalas, G. R., A Random Capillary Model with Application to Char Gasification at Chemically Controlled Rates. *Aiche Journal* **1980,** 26, (4), 577-585.
140. Arenillas, A.; Pevida, C.; Rubiera, F.; Pis, J. J., Comparison between the reactivity of coal and synthetic coal models. *Fuel* **2003,** 82, (15-17), 2001-2006.
141. Hurt, R. H.; Sarofim, A. F.; Longwell, J. P., The Role of Microporous Surface-Area in the Gasification of Chars from a Sub-Bituminous Coal. *Fuel* **1991,** 70, (9), 1079-1082.
142. Davis, K. A.; Hurt, R. H.; Yang, N. Y. C.; Headley, T. J., Evolution of char chemistry, crystallinity, and ultrafine structure during pulverized-coal combustion. *Combustion and Flame* **1995,** 100, (1-2), 31-40.
143. Zolin, A.; Jensen, A.; Dam-Johansen, K., Kinetic analysis of char thermal deactivation. *Proceedings of the Combustion Institute* **2000,** 28, 2181-2188.
144. Zolin, A.; Jensen, A.; Pedersen, L. S.; Dam-Johansen, K.; Torslev, P., A comparison of coal char reactivity determined from thermogravimetric and laminar flow reactor experiments. *Energy & Fuels* **1998,** 12, (2), 268-276.
145. Mitchell, R. E.; McLean, W. J., On the temperature and reaction rate of burning pulverized fuels. *Symposium (International) on Combustion* **1982,** 19, (1), 1113-1122.
146. Sorensen, L. H.; Gjernes, E.; Jessen, T.; Fjellerup, J., Determination of reactivity parameters of model carbons, cokes and flame-chars. *Fuel* **1996,** 75, (1), 31-38.
147. Morgan, P. A.; Robertson, S. D.; Unsworth, J. F., Combustion Studies by Thermogravimetric Analysis .2. Char Oxidation. *Fuel* **1987,** 66, (2), 210-215.
148. Norton, G. A., A review of the derivative thermogravimetric technique (burning profile) for fuel combustion studies. *Thermochimica Acta* **1993,** 214, (2), 171-182.
149. Ballal, G.; Zygourakis, K., Evolution of pore surface area during non-catalytic gas-solid reactoins. 2. Experimental results and model validation. *Industrial Engineering Chemical Reseacrh* **1987,** 26, 1787-1796.
150. Lizzio, A. A.; Piotrowski, A.; Radovic, L. R., Effect of Oxygen-Chemisorption on Char Gasification Reactivity Profiles Obtained by Thermogravimetric Analysis. *Fuel* **1988,** 67, (12), 1691-1695.

151. Tsai, C. Y.; Scaroni, A. W., Reactivity of Bituminous Coal Chars During the Initial-Stage of Pulverized-Coal Combustion. *Fuel* **1987,** 66, (10), 1400-1406.
152. Zeng, D.; Clark, M.; Gunderson, T.; Hecker, W. C.; Fletcher, T. H., Swelling properties and intrinsic reactivities of coal chars produced at elevated pressures and high heating rates. *Proceedings of the Combustion Institute* **2005,** 30, 2213-2221.
153. Hecker, W. C.; Madsen, P. M.; Sherman, M. R.; Allen, J. W.; Sawaya, R. J.; Fletcher, T. H., High-pressure intrinsic oxidation kinetics of two coal chars. *Energy & Fuels* **2003,** 17, (2), 427-432.
154. Ashu, J. T.; Nsakala, N. Y.; Mahajan, O. P.; Walker, P. L., Enhancement of Char Reactivity by Rapid Heating of Precursor Coal. *Fuel* **1978,** 57, (4), 250-251.
155. Floess, J. K.; Longwell, J. P.; Sarofim, A. F., Intrinsic Reaction-Kinetics of Microporous Carbons .1. Noncatalyzed Chars. *Energy & Fuels* **1988,** 2, (1), 18-26.
156. McDonald, K. M.; Hyde, W. D.; Hecker, W. C., Low-Temperature Char Oxidation-Kinetics - Effect of Preparation Method. *Fuel* **1992,** 71, (3), 319-323.
157. Zimbardi, F., Evaluation of reaction order and activation energy of char combustion by shift technique. *Combustion Science and Technology* **2000,** 156, 251-269.
158. Kulaots, I.; Aarna, I.; Callejo, M.; Hurt, R. H.; Suuberg, E. M., Development of porosity during coal char combustion. *Proceedings of the Combustion Institute* **2003,** 29, 495-501.
159. Patel, M. M.; Grow, D. T.; Young, B. C., Combustion Rates of Lignite Char by Tga. *Fuel* **1988,** 67, (2), 165-169.
160. de la Puente, G.; Fuente, E.; Pis, J. J., Reactivity of pyrolysis chars related to precursor coal chemistry. *Journal of Analytical and Applied Pyrolysis* **2000,** 53, (1), 81-93.
161. Hecker, W. C.; McDonald, K. M.; Reade, W.; Swensen, M. R.; Cope, R. F., Effects of burnout on char oxidation kinetics. *Symposium (International) on Combustion* **1992,** 24, (1), 1225-1231.
162. Liu, T. F.; Fang, Y. T.; Wang, Y., An experimental investigation into the gasification reactivity of chars prepared at high temperatures. *Fuel* **2008,** 87, (4-5), 460-466.
163. Suuberg, E. M.; Wojtowicz, M.; Calo, J. M., Some Aspects of the Thermal Annealing Process in a Phenol-Formaldehyde Resin Char. *Carbon* **1989,** 27, (3), 431-440.
164. Khan, M. R., Significance of Char Active Surface-Area for Appraising the Reactivity of Low-Temperature and High-Temperature Chars. *Fuel* **1987,** 66, (12), 1626-1634.
165. Kasaoka, S.; Sakata, Y.; Shimada, M., Effects of Coal Carbonization Conditions on Rate of Steam Gasification of Char. *Fuel* **1987,** 66, (5), 697-701.
166. Marsh, H.; Taylor, D. A.; Lander, J. R., Kinetic-Study of Gasification by Oxygen and Carbon-Dioxide of Pure and Doped Graphitizable Carbons of Increasing Heat-Treatment Temperatures. *Carbon* **1981,** 19, (5), 375-381.
167. Kwon, T. W.; Kim, S. D.; Fung, D. P. C., Reaction-Kinetics of Char-Co2 Gasification. *Fuel* **1988,** 67, (4), 530-535.
168. Knight, A. T.; Sergeant, G. D., Reactivity of Australian Coal-Derived Chars to Carbon-Dioxide. *Fuel* **1982,** 61, (2), 145-149.

169. Osafune, K.; Marsh, H., Gasification Kinetics of Coal Chars in Carbon-Dioxide. *Fuel* **1988,** 67, (3), 384-388.
170. Floess, J. K.; Longwell, J. P.; Sarofim, A. F., Intrinsic Reaction-Kinetics of Microporous Carbons .2. Catalyzed Chars. *Energy & Fuels* **1988,** 2, (6), 756-764.
171. Zolin, A.; Jensen, A.; Dam-Johansen, K.; Jensen, L. S., Influence of experimental protocol on activation energy in char gasification: the effect of thermal annealing. *Fuel* **2001,** 80, (7), 1029-1032.
172. Gopalakrishnan, R.; Bartholomew, C. H., Effects of CaO, high-temperature treatment, carbon structure, and coal rank on intrinsic char oxidation rates. *Energy & Fuels* **1996,** 10, (3), 689-695.
173. Everson, R. C.; Neomagus, H. W. J. P.; Kasaini, H.; Njapha, D., Reaction kinetics of pulverized coal-chars derived from inertinite-rich coal discards: Characterisation and combustion. *Fuel* **2006,** 85, 1067-1075.
174. Franklin, R. E., Crystallite growth in graphitizing and non-graphitizing carbons. *Proceedings of the Royal Society of London Series a-Mathematical Physical and Engineering Sciences* **1951,** 209, 196-218.
175. Senneca, O.; Russo, P.; Salatino, P.; Masi, S., The relevance of thermal annealing to the evolution of coal char gasification reactivity. *Carbon* **1997,** 35, (1), 141-151.
176. Tsai, C. Y.; Scaroni, A. W., Pyrolysis and Combustion of Bituminous Coal Fractions in an Entrained-Flow Reactor. *Energy & Fuels* **1987,** 1, (3), 263-269.
177. Cai, H. Y.; Guell, A. J.; Chatzakis, I. N.; Lim, J. Y.; Dugwell, D. R.; Kandiyoti, R., Combustion reactivity and morphological change in coal chars: Effect of pyrolysis temperature, heating rate and pressure. *Fuel* **1996,** 75, (1), 15-24.
178. Walker, P. L.; Rusinko, F.; Austin, L. G., Gas Reactions of Carbon. *Advances in Catalysis* **1959,** 11, 133-221.
179. Essenhigh, R. H.; Fortsch, D.; Klimesh, H. E., Combustion characteristics of carbon: Influence of the Zone I-Zone II transition on burn-out in pulverized coal flames. *Energy & Fuels* **1999,** 13, (5), 955-960.
180. Beeley, T.; Crelling, J.; Gibbins, J.; Hurt, R.; Lunden, M.; Man, C.; Williamson, J.; Yang, N., Transient high-temperature thermal deactivation of monomaceral-rich coal chars. *Symposium (International) on Combustion* **1996,** 26, (2), 3103-3110.
181. Nsakala, N.; Patel, R.; Borio, R., An Advanced methodology for prediction of carbon loss in commercial pulverized coal-fired boilers. In *ASME/IEEE Joint Power Generation Conference*, Portland, OR, 1986.
182. Wells, W. F.; Kramer, S. K.; Smoot, L. D.; Blackham, A. U., Reactivity and combustion of coal chars. In *20th Sym (international) on Combustion*, 1984; pp 1539-1546.
183. Mitchell, R. E.; Tsai, N. K.; Morris, C. I., Experimental determination of effective pore diffusion coefficients of pulverized coal chars. In *International Conference on Coal Science*, Alberta, Canada, 1993.
184. Valix, M. G.; Harris, D. J.; Smith, I. W.; Trimm, D. L., The intrinsic combustion reactivity of pulverised coal chars: The use of experimental pore diffusion coefficients. *Symposium (International) on Combustion* **1992,** 24, (1), 1217-1223.

185. Hurt, R.; Davis, K.; Yang, N.; Hardesty, D. *The origin and properties of unburned carbon from pulverized-coal combustion* TR-105743 Electric power research institute: Sandia National Laboratories, Livermore, 1995.
186. Sun, J. K.; Hurt, R. H., Mechanisms of extinction and near-extinction in pulverized solid fuel combustion. *Proceedings of the Combustion Institute* **2000,** 28, 2205-2213.
187. Wheeler, A., Reaction Rates and Selectivity in Catalyst Pores. *Advances in Catalysis* **1951,** 3, 249-327.
188. Walker, P. L., Pore System in Coal Chars - Implications for Diffusion Parameters and Gasification. *Fuel* **1980,** 59, (11), 809-810.
189. Morgan, B. A. Effects of ion exchangeable cations on the combustion behavior of a pulverized Texas lignite Ph.D., The Pennsylvania State University, University Park, 1985.
190. Hurt, R. H.; Mitchell, R. E., Unified high-temperature char combustion kinetics for a suite of coals of various rank. *Symposium (International) on Combustion* **1992,** 24, (1), 1243-1250.
191. Smith, I. W., The Combustion Rates of Coal Chars: A review. *Prog in Energy & Comb Sci* **1982,** 19, 1045-1065.
192. Williams, A.; Backreedy, R.; Habib, R.; Jones, J. M.; Pourkashanian, M., Modelling coal combustion: the current position. *Fuel* **2002,** 81, (5), 605-618.
193. Bejarano, P. A.; Levendis, Y. A., Combustion of coal chars in oxygen-enriched atmospheres. *Combustion Science and Technology* **2007,** 179, (8), 1569-1587.
194. Levendis, Y. A.; Joshi, K., Combustion of two lignite coals In o2-n2 & o2-co2. In *33rd International Technical Conference on Coal Utilization & Fuel Systems*, Florida, USA, 2008.
195. Timothy, L. D.; Sarofim, A. F.; Beer, J. M., Characteristics of Single Particle of Coal Combustion. *Proceedings of the Combustion Institute* **1982,** 19, 1123.
196. Joutsenoja, T.; Saastamoinen, J.; Aho, M.; Hernberg, R., Effects of the Pressure on Oxygen Concentration on the Combustion of Different Coals. *Energy & Fuels* **1999,** 13, 130-145.
197. Hamor, R. J.; Smith, I. W.; Tyler, R. J., Kinetics of combustion of a pulverized brown coal char between 630 and 2200°K. *Combustion and Flame* **1973,** 21, (2), 153-162.
198. Sun, J.-K.; Hurt, R. H., Mechanisms of extinction and near-extinction in pulverized solid fuel combustion. *Symposium (International) on Combustion* **2000,** 28, (2), 2205-2213.
199. Dryer, F. L.; Glassman, I., High Temperature Oxidation of CO and CH4. In *Sym (International) on Combustion*, 1973; pp 987-1003.
200. Hesselmann, G. J., Optimization of combustion by fuel testing in a NO x reduction test facility. *Fuel* **1997,** 76, 1269-1275.
201. Molina, A.; Mondragon, F., Reactivity of coal gasification with steam and CO2. *Fuel* **1998,** 77, (15), 1831-1839.
202. Zheng, C.; Clements, B.; Zheng, L., The feasibility of decreased furnace size with reduced flue gas recirculation in coal-fired boiler designs. In *30th Int Tech Conf on Coal Utilization & Fuel Systems*, Clearwater, FL, 2005.

203. Liu, Q. R.; Hu, H. Q.; Zhou, Q.; Zhu, S. W.; Chen, G. H., Effect of inorganic matter on reactivity and kinetics of coal pyrolysis. *Fuel* **2004,** 83, (6), 713-718.
204. Lin, S. Y.; Hirato, M.; Horio, M., The Characteristics af Coal Char Gasification at Around Ash Melting Temperature. *Energy & Fuels* **1994,** 8, 598-606.
205. Ye, D. P.; Agnew, J. B.; Zhang, D. K., Gasification of a South Australian low-rank coal with carbon dioxide and steam: kinetics and reactivity studies. *Fuel* **1998,** 77, (11), 1209-1219.
206. Lee, J. M.; Kim, Y. J.; Lee, W. J.; Kim, S. D., Coal-gasification kinetics derived from pyrolysis In a fluidized-bed reactor. *Energy* **1998,** 23, (6), 475-488.
207. Shufen, L.; Ruizheng, S., Kinetic studies of a lignite char pressurized gasification with CO2, H2 and steam. *Fuel* **1994,** 74, (3), 413-416.
208. Raghunathan, K.; Yang, R. Y. K., Unification of Coal Gasification Data and Its Applications. *Ind. Eng. Chem. Res* **1989,** 28, (518-523).
209. Tyler, R. J.; Smith, I. W., Reactivity of Petroleum Coke to Carbon-Dioxide between 1030 and 1180 K. *Fuel* **1975,** 54, (2), 99-104.
210. Dutta, S.; Wen, C. Y., Reactivity of coal and char.1. In carbon dioxide atmospshere. *Industrial & Engineering Chemistry Process Design and Development* **1977,** 16, (1), 20-30.
211. Hurt, R. H.; Dudek, D. R.; Longwell, J. P.; Sarofim, A. F., The Phenomenon of Gasification-Induced Carbon Densification and Its Influence on Pore Structure Evolution. *Carbon* **1988,** 26, (4), 433-449.
212. Ochoa, J.; Cassanello, M. C.; Bonelli, P. R.; Cukierman, A. L., CO2 gasification of Argentinean coal chars: a kinetic characterization. *Fuel Processing Technology* **2001,** 74, (3), 161-176.

Appendix 1.1

Comparison of boiler heat transfer during combustion in air and in O_2/CO_2 medium

When flue gases are recycled back into the inlet of furnace to control the boiler temperature, a change in heat transfer distribution inside the furnace are expected due to different transport properties of the medium. The CO_2 and water vapor, being tri-atomic molecules, absorb and emit more radiation and are expected to enhance the radiant zone heat transfer and thus lower Furnace Exit Gas Temperature (FEGT). The lower FEGT along with difference in physical properties of the system may change heat transfer in convective section. A simple analysis is shown below to demonstrate the possible heat transfer imbalance.

Radiant zone heat transfer

Applying the energy balance across radiant section of boiler for each combustion approach:

Energy input = Energy transferred to boiler wall through radiation + Energy in exit gases

$$\dot{M}_f Q_f = \varepsilon A_w \left(T'_g - T_w\right)^4 + m_g Cp_g (T_{g_i}) \qquad \textbf{A1.1}$$

Where, $T'_g = T_{gi} + 300$ is assumed

$\dot{M}_f$ = mass flow rate of coal

Q_f = heating value of coal

ε = emissivity of system (contribution from particle phase is neglected in the analysis for simplicity)

A_w =heat transfer surface area of boiler wall

m_g = mass flow rate of combustion gas

$C_{p,g}$ = specific heat of combustion mixture

T_w = Temperature of boiler tube wall (typically saturation temperature of steam)

T_g = Furnace exit gas temperature

i = subscript, refers to two different case scenario

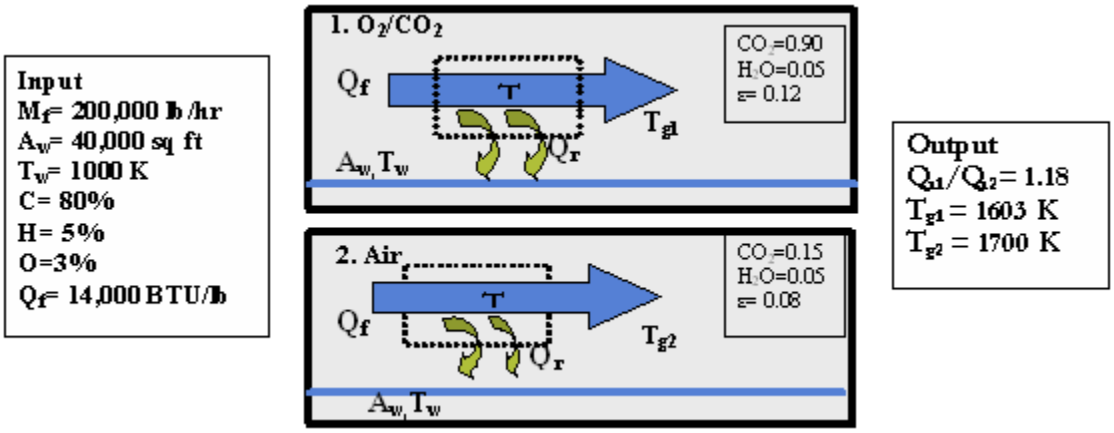

Eq. **A1.1** is solved for T_{gi} (FEGT) in each approach, and relative contribution of radiative heat transfer in the two approaches is compared in the output side of above Figure.

Convective zone heat transfer

In the convective zone of a boiler, main mode of heat transfer is through convection mechanism. This heat transfer (Q_c) is represented as:

$$Q_c = hA(T_g - T_e) \qquad \textbf{A1.2}$$

Where, T_e is exit flue gas temperature from convective zone.

Heat transfer co-efficient (h) can be approximated by

$$N_U = (\mathrm{Re})^{0.6} * (\mathrm{Pr})^{1/3}$$

A further simplification suggests that, $Q_c \propto \left(K_g / (\mu_g)^{0.6} \right) * (\mathrm{Pr})^{1/3} * (T_g - T_e)$

Where, K_g is thermal conductivity of flue gas, μ_g is viscosity of flue gas

An analysis is conducted, using the gas properties data for each constituents (CO_2, N_2) taken from the literature [135], and is given in Table below. Properties of gas mixture in the two cases are calculated as weighted average of each constituent.

Convective heat transfer comparison for combustion in O_2/CO_2 and air

	N_2	CO_2	Air (0.12*CO_2+0.78N_2)	O_2/RFG (0.9 CO_2)
Pr	0.686	0.668	0.615	0.601
K_g (mW/m-k) @ 300 K	45.70	71.5-	44.22	64.35
μ (kg/m-s) @ 300 K	1.752	1.958	1.601	1.762
T_g (K)			1700	1600
T_e (K)			450	450
Q_c (arbit. Unit)			35502	44533
$Qc_{(O2/RFG)}/Qc_{(air)}$			1.25	

Computed values, shown in the Figure suggest that there is approximately 18% increase in radiation heat transfer in the furnace, and a temperature decrease of approximately 100 K for retrofitting an existing boiler to oxy-coal combustion technology. Data in the Table suggest that despite a decrease in FEGT during oxy-coal combustion, an increase of up to 25% heat transfer in convective section of boiler can be

expected during oxy-coal combustion. Despite lower FEGT, the higher convective heat transfer during oxy-coal combustion appears to be due to higher thermal conductivity and lower viscosity of the CO_2 compared to that of N_2. This analysis suggests that heat transfer during oxy-coal combustion system will not be an issue for retrofitting the existing system, assuming that the heat release rate of the two combustion media remains same.

Appendix 1.2

Comparison of equilibrium CO concentration during combustion in air and in O_2/CO_2 medium

It can be considered for the coal flames that the carbon conversion takes place due to the reactions listed below. Both reactions (I) & (II) take place at the particle surface, and the resultant CO is oxidized in the gas phase into CO_2 according to reaction (III).

$$C+CO_2 \text{—} CO \qquad \text{(reaction I)}$$

$$C+1/2\ O_2 \text{—} CO \qquad \text{(reaction II)}$$

$$CO+1/2\ O_2 \text{—} CO_2 \qquad \text{(reaction III)}$$

Reaction (III) has also been shown to be catalytically enhanced by the presence of water vapor[14]. The equilibrium rate constants for these reactions as a function of temperature are calculated using Gibbs free energy.

The equilibrium concentration of CO in the gas phase can be approximately calculated by

$$CO = K\ [CO_2]/[O_2]^{1/2} \qquad \textbf{1.2.1}$$

It is apparent from Equation 1.2.1 that equilibrium concentration of CO depends upon the temperature and partial pressure of CO_2 and O_2. An increase in temperature and CO_2 concentration and a decrease in O_2 concentration cause an increase in CO formation. The plot was calculated considering 10% CO_2 and 5% O_2 in gas mixture to represent combustion in air and -80%, -89% CO_2 and 5% O_2 in gas mixture to represent typical concentration in oxy-coal combustion.

Appendix 2.1

An example char burnout calculation

Let's say proximate analysis of coal is:

Moisture	2.7
Ash (%dry)	4.83
Volatile (% dry)	31.06
Fixed carbon (% dry)	64.11

Therefore, initial ash in char = Ash (%) dry / (100- Volatile (%) dry)➔ 7.00

Let's assume, that average ash content in collected sample is 50 % (dry)

Char Burnout (%) = (1- 7/50)*100 ➔ 85.98 %

Weight loss (%) = [1- 4.83*(100-50)/(50*(100-4.83))]*100 ➔ 94.92%

Appendix 2.2

Coal pyrolysis parameters for studied coal

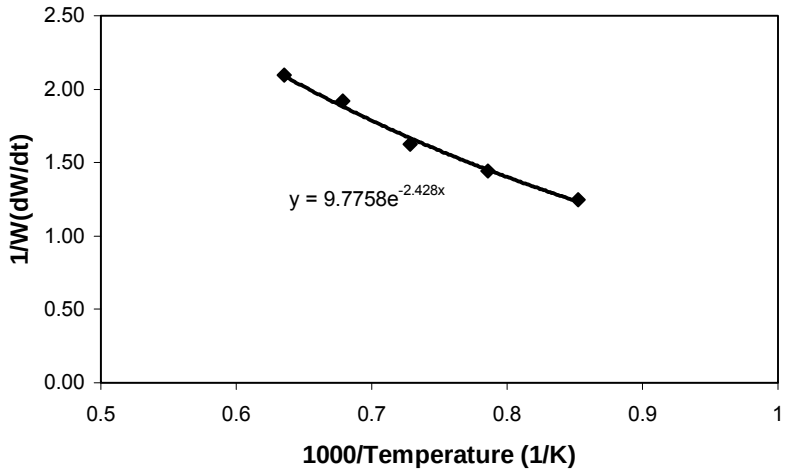

Coal pyrolysis parameter determined in the DTR for a hvCb coal

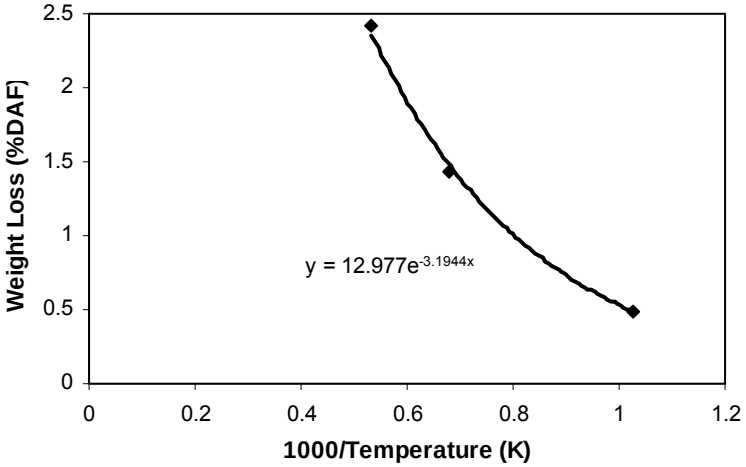

Coal pyrolysis parameter determined in the DTR for a lvb coal

Appendix 2.3

Calculation for volatile matter composition

C	0.8519
H	0.0377
N	0.0096
S	0
Moisture	0.0083
Ash	0.0544
O	0.0381
Volatile Matter	0.1716
Fixed Carbon	0.7657

Let's consider N exists as HCN in the coal. So revised coal composition would be

C	0.8437
H	0.0370
HCN	0.0184

This HCN will be distributed into volatile and char fraction according to the respective char and volatile fraction

Volatile-HCN	0.0035
char-HCN	0.0150

So N-free volatile matter = 0.1716-0.0035

N-free Fixed Carbon = 0.7657-.01496 ➔ 0.7507

Therefore, volatile carbon= .8437-0.7507 ➔ 0.0930

All H and O in the coal is considered as volatile component

Volatile formula: $C_{0.775}H_{3.7}O_{0.3175}$

Based on the composition of volatile product gas composition can be calculated. Heating value of volatile matter is estimated from the heating value of coal and char as follows:.

Volatile HHV = [Coal HHV – Fixed C* (ΔH)]/ Volatile matter

Fuel reference enthalpy then can be calculated from product composition and assigned into FLUENT™.

Appendix 3.1

Coal particle heat-up rate during pyrolysis

Applying the energy balance around the coal particles

Energy gained by the particles = Energy transferred from gases due to convection + Energy transferred from gases due to radiation

Eq. **A3.1**

$$m_p Cp_p \left(dT/dt\right) = hA_p \Delta T + \sigma \varepsilon A\left(T_g^4 - T_p^4\right) \qquad \textbf{A3.1}$$

In a DTR environment, where $(T_g - T_p) < 1000$, heat transfer due to radiation will be negligible compare to convective heat transfer.

Assuming a stagnant gas flow, h can be estimated from

$$h = K_g d_p / 2$$

Therefore,

$$\text{Particle heat up rate} \left(dT/dt\right) \propto K_g, \varepsilon$$

The properties of thermal conductivities are taken from the literature[135] as shown in Table **3-2** (Chapter 3).

Appendix 4.1

Survey of char-CO_2 reaction activation energy value

Rate measurement	Method	Reference	Coal Rank	Operating Temperature	Activation Energy (kJ/mol)
Isothermal	E computed at all conversion	[162]	SB	1273-1573 K	175-155
Fluidized reactor	E taken from X=0	[203]	hvC	1273-1473 K	175
				1473-1873	95
Isothermal	X=0.1	[204]	hvC	1173-1773 K	212
isothermal	X=0.5	[205]	Lignite	987-1165 K	91
Isothermal	Shrinking core	[206]	SB	1023-1173 K	168
Isothermal	Shrinking core	[207]	Lignite	1073-1223 K	150
Isothermal	T0.5	[208]	Lignite	1073-1473 K	64.5
			SB		165
			SB		250
			brown char		148
Isothermal	shrinking core	[169]	wide ranks	1143-1573 K	175-195
isothermal	Maximum	[168]	wide ranks	1073-1411 K	219-233
Isothermal	Average	[209]	pet coke	1022-1178 K	203-237
			graphite		293
Isothermal	X=0.2	[210]	hvC/HVA	1113-1373 K	250
Isothermal	….nm…	[158]	hvC	948-1118 K	230
Isothermal	X=0.5	[211]	Sucrose char	1240-1405 K	300
			Spherocarb		275
Isothermal	X=0.1	[62]	HV	1123-1213 K	209
			Anthracite		223
Isothermal	X=0, X=0.5	[123]	Bituminous	1273-1673 C	62
			SB		82
			Lignite		98
Isothermal	Random pore model	[212]	SB	1173-1333 K	147
			HVB		180
Isothermal	Entire range	[150]	HVA	1090-1148 K	240
Isothermal	Shrinking core	[167]	Lignite	973-1173 K	146
			SB		151
			HVB		155
			Lignite		79

Appendix 4.2

Presence of maximum in TGA for various char samples oxidized in air

Rate profiles are measured isothermally at different TGA furnace temperature for char sample prepared under different pyrolysis condition.

A) DTR_1373

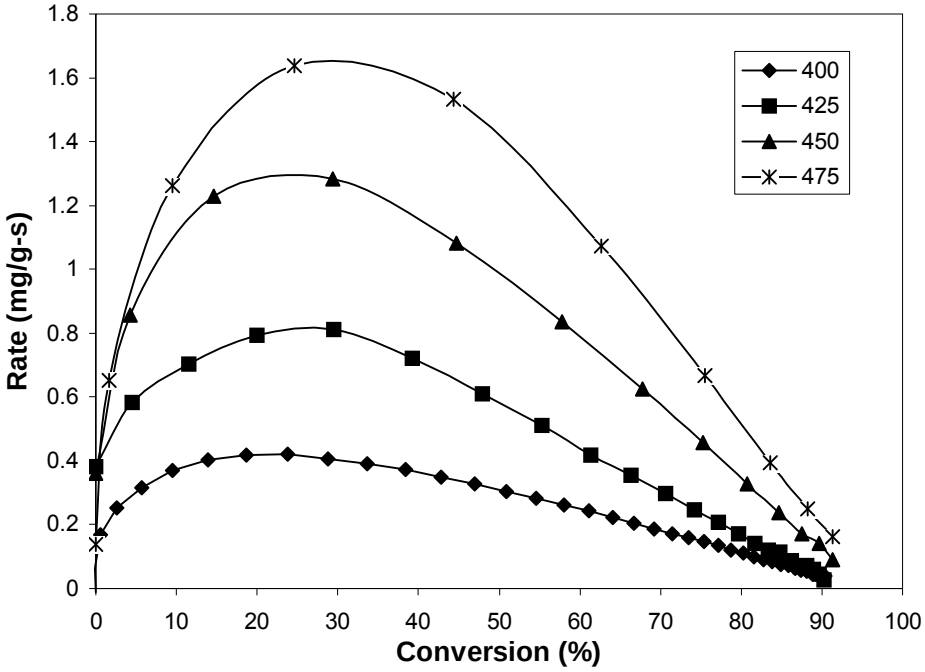

B) DTR_1573

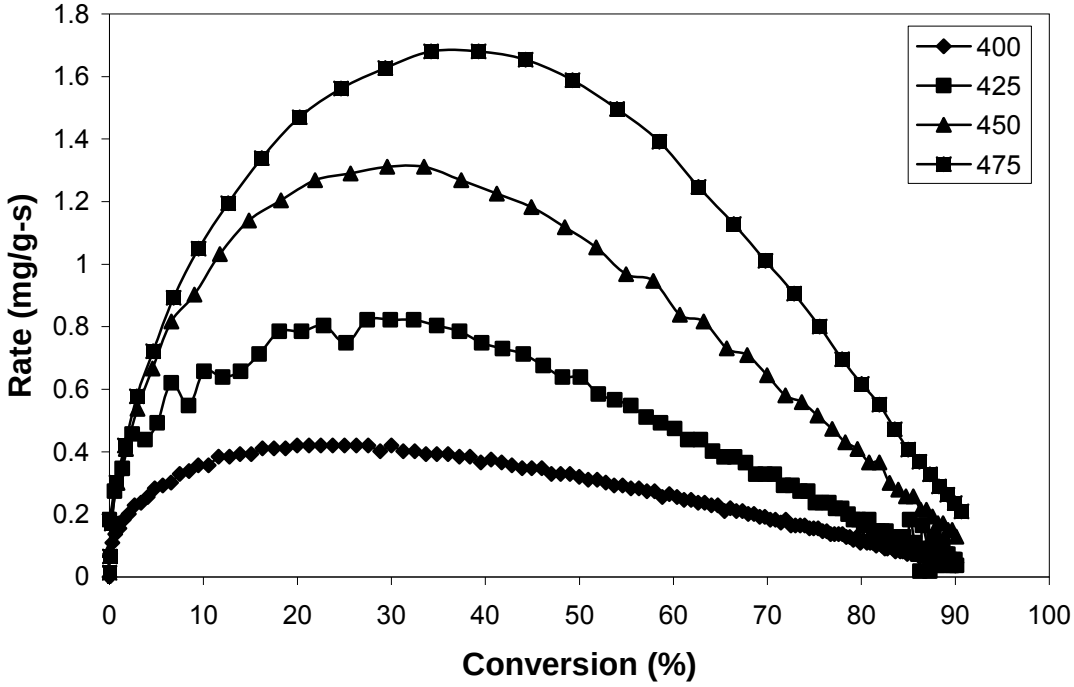

C) DTR_1673

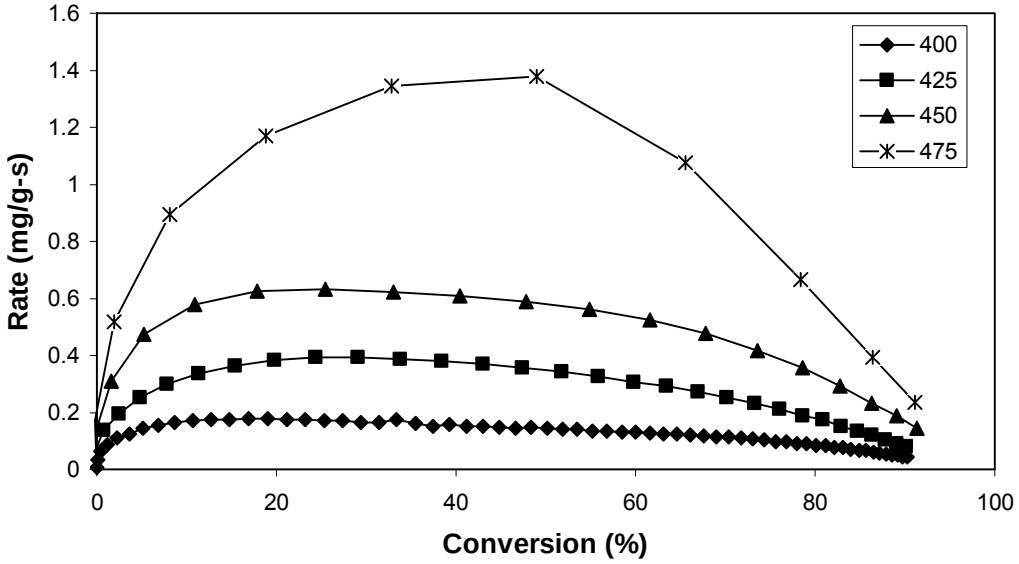

D) DTR_1873

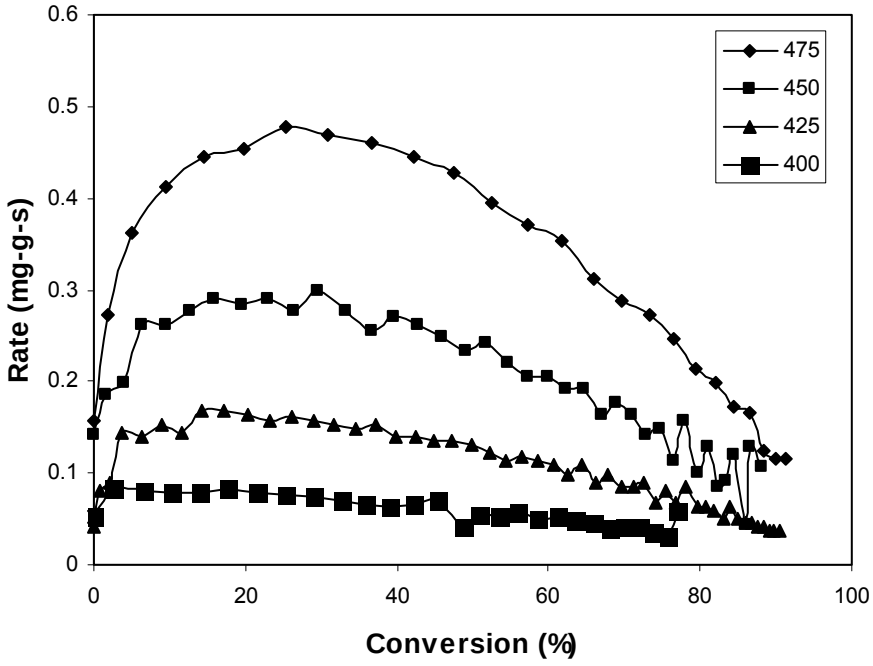

E) TGA_1123

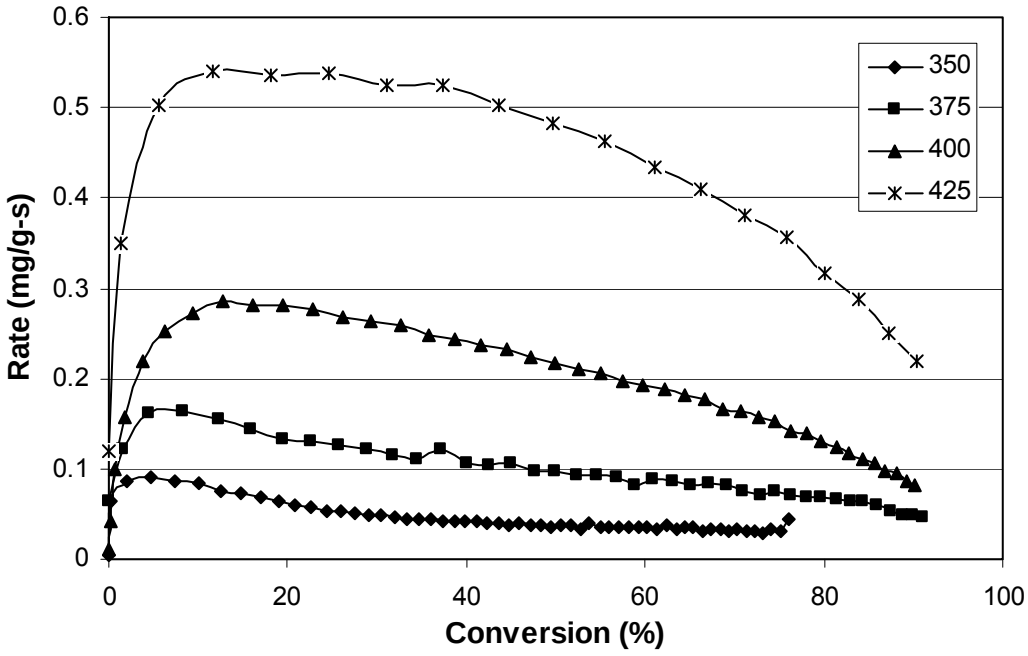

Appendix 4.3

Presence of maximum in TGA for a char sample gasified in CO_2

DTR-1373

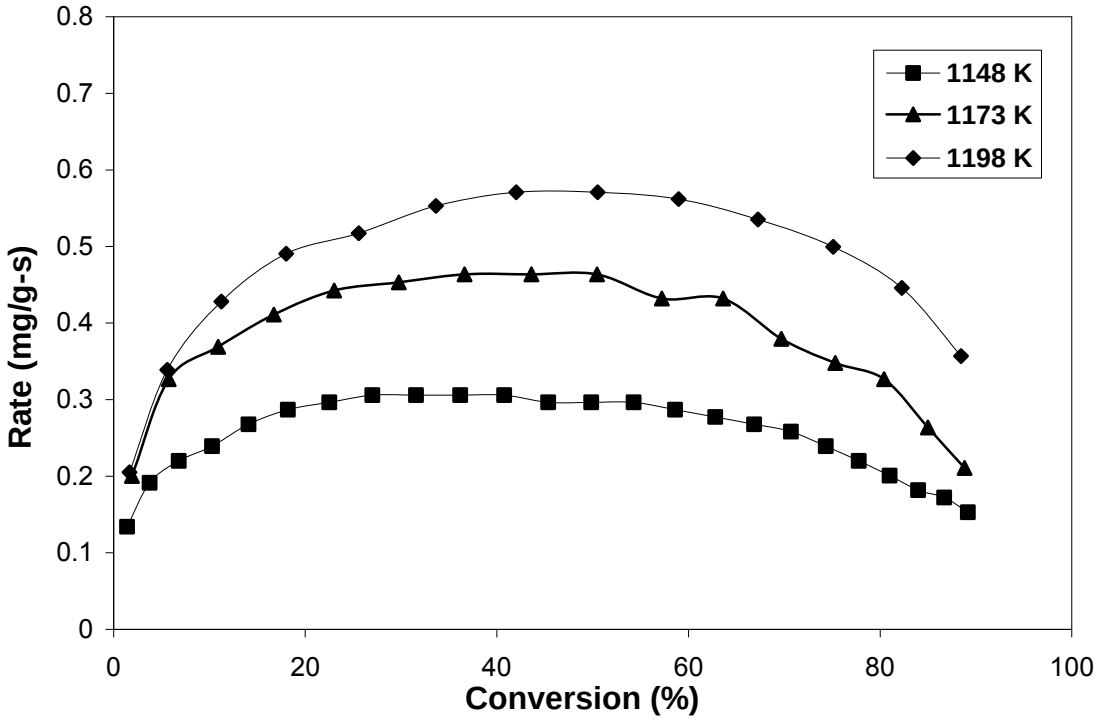

Appendix 4.4

Change in shape of reactivity profile after correction for "purging effect"

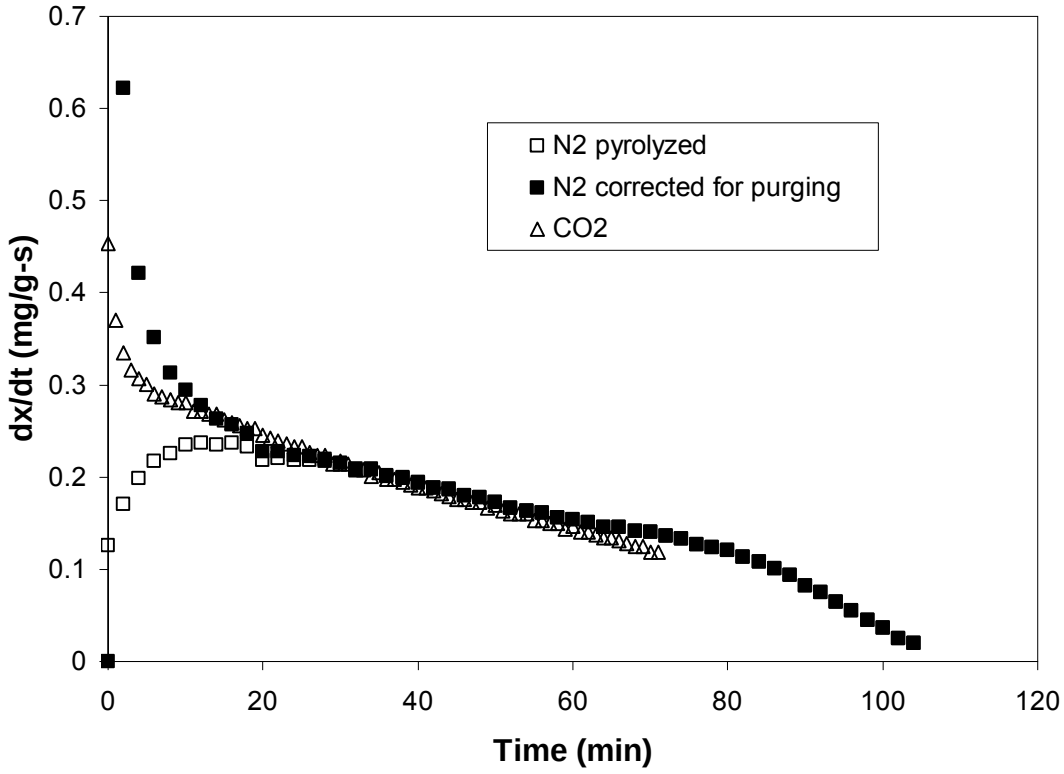

Appendix 4.5

Change in estimated activation energy value after correction for "purging effect"

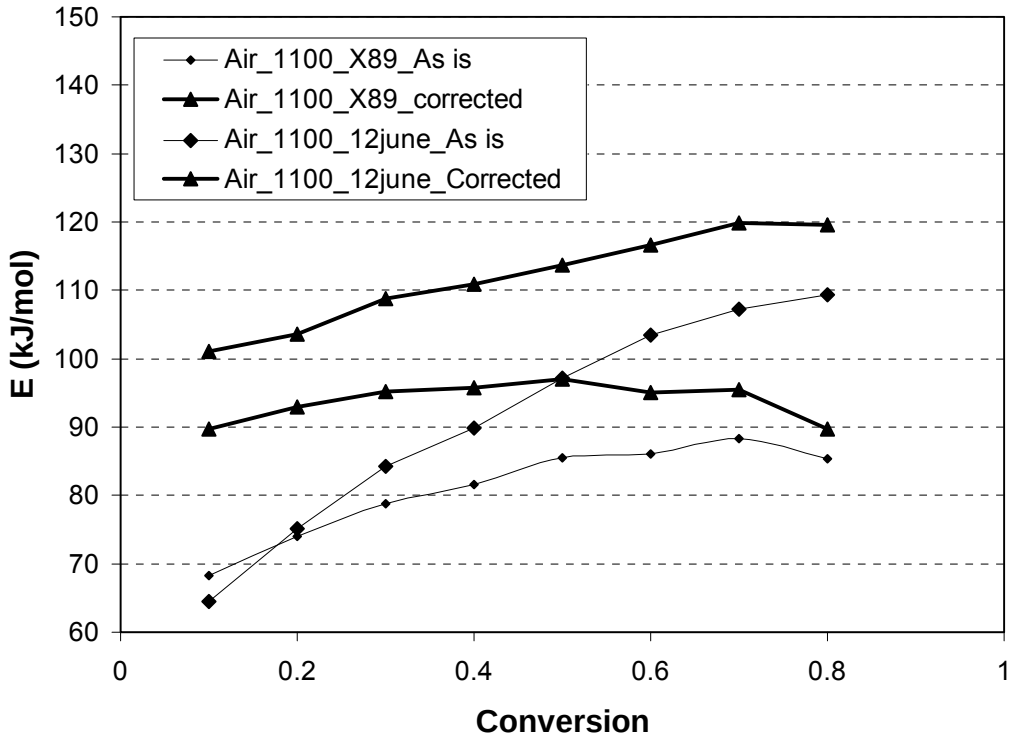

Appendix 5.1

Calculation of extrapolated rate at combustion condition using intrinsic model

Overall rate of char consumption, R per unit *external* area in kg/m^{2}s is calculated from

$$R = \left(1/R_{ac} + 1/R_d \right)^{-1} P_g \qquad \textbf{A5.1.1}$$

Where, R_{ac} = rate of reaction expressed per unit *external* area of solid in Kg.m^2.s/P$_a$ is given by

$$R_{ac} = \left(\eta d_p A_g R_s\right)/6 \qquad \textbf{A5.1.2}$$

and, R_d = Rate of gas diffusion ((Kg.m^2.s)/P$_a$) and is calculated from

$$R_d = C\left(T_p\right)^{0.75}/d_p \qquad \textbf{A5.1.3}$$

In Equation A5.1.2. R_s is the intrinsic reactivity of solid per unit *total* surface area in (Kg.m^2.s)/P$_a$ and is given as

$$R_s = A\exp\left(-E/RT\right) \qquad \textbf{A5.1.4}$$

d_p = diameter of the particle, m

A_g = Total surface area of solid, m^2/Kg

A = Preexponential factor of intrinsic gas-solid reaction

E = Intrinsic activation energy

η = effectiveness factor, ratio of actual rate to the rate in absence of pore diffusion and is calculated from the Thiele modulus using following correlation

$$\eta = \left(3/\phi^2 \right)\left(\frac{\phi}{\tanh\phi} - 1 \right) \qquad \textbf{A5.1.5}$$

Thiele modulus (ϕ) is estimated using the following correlation

$$\phi = \frac{d_p}{2}\left(\sqrt{S_b \rho_p A_g R_s P_g / D_e \rho_g} \right) \qquad \textbf{A5.1.6}$$

Where,

S_b = Stoicheometry factor

ρ_p = Density of particle, Kg/m^3

P_g = Partial pressure of oxidizer in the bulk gas stream, Pa

D_e = Effective diffusion coefficient though pore structure, m^2/s

ρ_g = Density of the oxidizer gas, Kg/m^3

In using Thiele modulus, effective diffusivity (D_e) in m^2/s is estimated from

$$D_e = \left(\theta/\tau^2 \right)\left(1/D_{kn} + 1/D_A \right)^{-1} \qquad \textbf{A5.1.7}$$

Where, Knudsen diffusion coefficient (D_{kn}) is estimated from

$$D_{kn} = 97 r_p \left(\sqrt{T_p / M_g} \right) \qquad \textbf{A5.1.8}$$

And molecular diffusion coefficient (D_A) is estimated from

$$D_A = D_{A,0}(T_g)^{1.75} \qquad \textbf{A5.1.9}$$

In Equation A5.1.8,

T_p = Temperature of particle, K

M_g = Molecular weight of the diffusing gas

r_p = Mean pore radius of the particle

DATA:

Assuming $T_p = T_g$ =1473 K and following property data

d_p =100 μm, ρ_p = 1300 Kg/m^3, A_g =100,000 m^2/Kg, θ=0.5, τ =2,

A = 0.00133 Kg/(m^2.s.Pa), E = 123 kJ/mol, C =5e-12, r_p =100 A^o

S_b = 2.67, P_g = 20,000 Pa, M_g =32, $D_{A,0}$ (at 273 K)= 1.53e-05 m^2/s

CALCULATIONS:

R_s = 5.96e-08 Kg/(m^2.s.Pa)

D_A = 2.5e-04 m^2/s

D_{kn} = 16.58 e-06 m^2/s

D_e = 8.01e-07 m^2/s

ϕ =70.3

η =0.042

R_d =1.188e-05 Kg/(m^2.s.Pa)

R_{ac} = 5.44e-06 Kg/(m^2.s.Pa)

R=7.46e-02 Kg/(m^2.s)

Appendix 5.2

Average pore radius calculated using Wheeler model

r_p = Mean pore radius of the particle, is estimated using wheeler model and is given as

$$r_p = 2\theta\tau \Big/ \left(A_g \rho_p\right) \qquad \textbf{A5.2.1}$$

Where,

θ = total porosity of the solid

τ = Tortuosity of the pores

DATA:

Data is taken of a hvCb char prepared in Ar at 1,673 K (refer to Table 4-3 of Chapter 4 for A_g and ρ_s data.

ρ_p = 900 Kg/m^3, A_g =10,000 m^2/Kg, τ =2, ρ_s = 1.59 Kg/m^3

θ =1- ρ_p / ρ_s = 0.43

r_p =2*.43*2/(900*10,000) = 136 A^0

VITA

Prabhat Naredi attended the Malaviya National Institute of Technology, Jaipur, India, where he obtained his B.E. degree in Chemical Engineering in 2000. He obtained his M.S. degree in Process Engineering and Design from Institute of Technology, Delhi, India in 2001. In 2001 he worked for Energy Resources and Generations Pvt. Ltd. as a process engineer for a period of six months, before going for PhD degree at the Pennsylvania State University in 2002. Currently, he is working for Creative Power Solutions, Fountain hills, AZ in USA as an engineer.